Hartree-Fock-Bogoliubov treatment of the two-dimensional trapped Bose gas

Christopher Gies

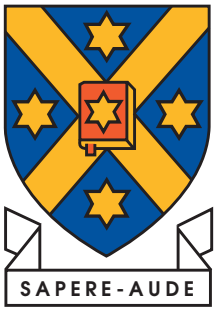

a thesis submitted for the degree of

Master of Science

at the University of Otago, Dunedin,

New Zealand.

May 2004

Supervisor:
Dr. David Hutchinson

First examiner:
Professor Rob Ballagh

Second examiner:
Dr. Matthew Davis

Abstract

In this thesis we present a finite temperature Hartree-Fock-Bogoliubov (HFB) treatment of the weakly interacting Bose gas which is confined to a two-dimensional geometry. It is well-known that the phenomenon of BEC cannot occur in a two-dimensional ideal Bose gas at finite temperatures. Phase fluctuation destroy long range order and make the formation of a BEC impossible. In two and one dimensions, phase fluctuations become enhanced and persist even at temperatures well below the critical temperature. We investigate the phase fluctuating regime by calculating the correlation function and find that a true BEC exists up to about $0.5\,T_c$. Above this temperature, the superfluid is best described as a quasicondensate.

We present numerical solutions to the HFB equations in the whole temperature regime below T_c, such as density profiles of both condensate and non-condensate, as well as the spectrum of the low-lying excitations. We find the breathing mode to lie, independent of temperature, at a frequency of twice the trap frequency, as is predicted for a genuine 2D system where interactions are modelled via a contact potential.

The semi-classical approximation contains difficulties if applied in the two-dimensional case. This has previously led to the question of whether BEC can occur in a two-dimensional condensate or if long wavelength fluctuations destroy long range order. With our treatment we show that the trap stabilizes the condensate against long wavelength fluctuations and that the issues are related to a failure of the semi-classical approximation.

The reduced dimensionality fundamentally influences scattering events with atoms in the condensate and requires a more accurate treatment of collisions. Many-body effects on collisions must be included to first order, since the two-body transition (T-)matrix vanishes in the zero energy limit which is used to describe collisions with the condensate atoms. We calculate the many-body T-matrix using two independent approaches, the gapless HFB and an off-shell two-body T-matrix evaluated at a shifted collision energy. We find agreement between these two in the quasi-2D regime at zero temperature and, finally, also discuss an extension of the latter approach to finite temperatures.

Acknowledgements

I would like to thank many people for supporting me during this time, work fellows as well as my friends and my family.
My supervisor Dr. David Hutchinson, whom working together with was a lot of fun. I would also like to thank him for making it possible for me to go to the ICOLS conference in Australia, which was definitely a highlight of the last year. Thanks also to his fellows from overseas: Especially Dr. Sam Morgan, for his encouragement and for patiently answering all my numerous questions, Dr. Matthew Davis for helping me a lot to get started in the beginning, and Dr. Mark Lee, who I much enjoyed working with. The whole Dunedin BEC group (even if they now prefer to call themselves UCO group) was a great place for doing my masters degree, and for this I'd like to thank Katharine Challis, Adam Norrie, James Douglas, Nick Thomas, Thomas Müller, Gaël Varoquaux, Gráinne Duffy, Callum McKenzie, Niels Kjaergaard, Reece Geursen, Nicola van Leeuwen, Angela Mellish, Andrew Wilson and Rob Ballagh. Separately I'd like to name Andreas Penckwitt for being always willing to think about physical problems and for being a worthy Carrom opponent, even though his true passion has long been lost to pool, and Tapio Simula just for being as crazy and enthusiastic as he is.
I would also like to thank Dr. Axel Pelster who supported me constantly throughout my physics degree, even in the end when I was beyond reach, and Prof. Bodo Hamprecht, who I owe my fascination in theoretical physics.
Last but not least I name Stefan, who actually belonged to the BEC group, but rather much to my closest friends, as well as Linus and Jana, who made it Dunedin for three months to visit me, Jz for countless hours of distraction, and Stacey of course!
Finally I thank my mother and father for making all this possible, and sorry to them and to the rest of my family for being gone longer than expected.

Contents

List of Figures

Part I.

Foundations

1. Introduction

In 1924 the Indian physicist Satyendranath Nathanel Bose sent a paper to Albert Einstein regarding an alternative derivation of Planck's radiation law. Based on Plank's quantum hypothesis, Bose derived the radiation law by considering, for the first time, light as indistinguishable particles – photons. His revolutionary idea had not found recognition and his article was rejected from publication. Einstein saw the importance of his work and used his influence to have it published it in the "Zeitschrift für Physik". Based on Bose's work, Einstein developed the quantum statistics of indistinguishable, or quantum particles with the same properties as photons [25]. In his theoretical treatment he found that a dilute gas of these quantum particles can undergo a phase transition into a new state of matter if the temperature is lowered sufficiently. These particles were named 'Bosons' to honour Bose and this theoretical curiosity was christened Bose-Einstein condensation (BEC). Fourteen years later the concept was picked up again by London [74, 75] and Tisza [113] to explain the superfluidity of Helium. However, quantitative agreement with experimental results could not be found due to the strong interactions in the superfluid, and Bose-Einstein condensation was not believed to be the underlying phenomenon of superfluidity for many years. Finally, in 1995 it became possible to cool a dilute gas of bosons down to the critical temperature and to achieve Bose-Einstein condensation in the manner envisaged by Einstein [2, 23]. This success, 70 years after the with slight scepticism seen theoretical prediction, was awarded with the Nobel prize in 2001.

Since the experimental realization the research field around Bose-Einstein condensation has rapidly grown and become highly interdisciplinary. Nowadays, about 40 groups worldwide[1] work with Bose-Einstein condensates in atom traps and recently even Bose-Einstein condensation of molecules has been achieved [59].

The fascination of Bose-Einstein condensation is that, being a purely quantum mechanical system, it magnifies the strange effects of the quantum world to a dimension

[1] See http://www.uibk.ac.at/c/c7/c704/ultracold/atomtraps.html for an up-to-date list.

visible to the eye. Not only from an experimentalist's perspective is it an attractive playground for quantum mechanics, but also from a theoretical point of view it offers unique possibilities for the development and testing of the complicated equations of quantum field theory. The 'ab initio' theory this thesis is based on has precisely predicted properties of the Bose-Einstein condensate in three dimensions at finite temperatures [48, 49], without any kind of fitting parameter. The feasibility of working closely together with experimental development and mutual stimulation between experiment and theory has been the driving force in the field during the last years. The advances in quantum atom optics and manipulation of atoms since the creation of Bose-Einstein condensates will be of great importance to applications related to nano-technology and quantum computing.

We do not want to give a general introduction into the exciting field of Bose-Einstein condensation, but rather refer to a talk by Eric Cornell [22], given shortly after the success in 1995, and discuss instead some aspects that are typical for two-dimensional systems and influence the physics of Bose-Einstein condensation in two dimensions.

1.1. Physics of two-dimensional systems

An important and nowadays well-understood phenomenon peculiar to a fermionic two-dimensional system of electrons in a strong external magnetic field, perpendicular to the electron gas, is the Fractional Quantum Hall Effect (FQHE). Originally explained by Laughlin (Nobel Prize in Physics 1998) by means of quasiparticles carrying a fractional charge in an incompressible quantum liquid [71, 95], Jain found a different description of the FQHE by introducing the "composite fermion" [56, 57]. The idea is to attach an even number of magnetic flux quanta to each electron and name the combination of fermion and flux quanta a new particle, the composite fermion. The even number of flux quanta preserves the minus sign associated with an exchange of two fermionic particles. Jain's approach successfully describes the Integer Quantum Hall effect and the FQHE in the same picture of non-interacting quasiparticles.
This idea has also proven successful in the context of BEC [20, 21, 107, 115, 116]. Consider a bosonic gas in the B-field of a magnetic trap. Now if we attach an uneven number of flux quanta to each boson, we lose the symmetry under particle exchange and the composition of boson and flux quanta becomes a fermion, feeling only the residual magnetic field B^* which has been reduced by the number of attached flux quanta. One

can go even further by realizing that the Aharonov-Bohm phase [1], associated with closed paths in the presence of a magnetic vector potential, can formally be obtained by introducing vortices into the system, which can be done by rotating the trap. Then, the magnetic field is replaced by the angular momentum due to the rotating trap. A rotating BEC with vortices has been found to be well described by means of composite particles obeying either bosonic or fermionic statistics. In fact, results obtained for the fermionic Fractional Quantum Hall regime have successfully been applied to a rotating BEC. For small particle numbers, Laughlin states, which are the eigenstates for the FQHE, have been found to describe the wave function of the system very well [20, 115], emphasizing the close relation between the fermionic FQHE system and the bosonic BEC.

Dimensionality fundamentally determines the physics of a system. This becomes apparent in the Mermin-Wagner-Hohenberg theorem that forbids a spontaneously broken symmetry with long range order in a two-dimensional system [45, 77, 78]. In terms of the coherence function $G^{(1)}(\mathbf{x}, \mathbf{x}')$, this means that $\lim_{|\mathbf{x}-\mathbf{x}'|\to\infty} G^{(1)}(\mathbf{x}, \mathbf{x}') \neq 0$, which can be seen as the definition of Bose-Einstein condensation (BEC) [86, 118], is impossible for $T > 0$. Thus, in an ideal two-dimensional Bose gas BEC cannot occur at finite temperatures. What prevents the phase transition that can take place in three dimensions? It is the enhanced importance of phase fluctuations in lower dimensional systems. It was Popov who originally introduced the idea of a *quasicondensate* to explain the superfluidity of a two-dimensional Bose gas [94]. The difference to a true BEC is that phase fluctuations destroy the coherence of the global phase throughout the condensate, and phase coherence governs only regimes of a size smaller than the size of the condensate, characterized by the coherence length.

To understand why phase fluctuations become important in lower dimensions, consider an ideal model of regularly spaced particles with just the property of a spin that can point into any available spatial direction, denoted by $\mathbf{S}_i$. The spins of the particles interact and the Hamiltonian can be modelled by $\hat{H} \propto \sum_{\langle ij \rangle} \mathbf{S}_i \cdot \mathbf{S}_j$, where we sum over nearest neighbours. This model constitutes a good approximation to a superfluid system of neutral particles with an order parameter $\psi_j = \langle \psi \rangle e^{i\delta_j}$, where $\langle \psi \rangle$ is assumed to be constant for all particles and the phase δ_j corresponds to the direction of the spin. If the spin of one particle is flipped around, a neighbouring particle is tempted to flip its spin, too. However, this fluctuation is suppressed the more other neighbours stabilize this particle. Thus, while in a three-dimensional lattice, fluctuations can be

suppressed by the large number of neighbouring particles, in the extreme of one a one-dimensional system the fluctuation in the spin of one particle can travel down the chain of neighbouring atoms and destroy long-range order in the whole system. The two-dimensional system lies between these two cases and can show the intermediate case of algebraically decaying long-range order.

This is a peculiarity of two-dimensional systems, allowing for a different kind of phase transition to a state with algebraically decaying long-range order, even if a macroscopically occupied state with long-range order in the sense of BEC cannot form. This phenomenon was predicted by Kosterlitz and Thouless (and, independently, by Berezinski) [6, 68, 69] and has gained great interest in the study of two-dimensional BECs [109]. Topological defects play the central role in this phase transition. In an ordered system of spins as we considered before, a topological defect corresponds to a vortex, i. e. a point around which the phase of the spin changes by a multiple of $\pm 2\pi$, referred to as the charge or vorticity of the vortex. Below a critical temperature T_{KT} vortices of opposite charge are bound together in pairs. Looking at the order parameter space, given by $\mathbb{S}^1$ in the ideal two-dimensional system we discussed before, suggests that introducing vortex/antivortex pairs into the system should be thermodynamically forbidden because of the topological energy associated with the introduction of a single vortex. However, the state of a vortex/antivortex pair is homotopic to the uniform state, since from a distance the opposite vorticities cancel and, thus, the introduction of vortices bound in pairs is possible. Above this critical temperature, however, it becomes favourable for the vortices to unbind and to become free topological charges. Then phase fluctuations destroy any kind of long-range order in the system and the coherence function decays exponentially. The unbinding process is referred to as *Kosterlitz-Thouless (KT) phase transition* and can be understood by considering the free energy associated with the introduction of a free vortex [37]. In 2D, this energy diverges logarithmically with the size of the system. However, the entropy is found to depend logarithmically on the system size, too, so that it is possible for the divergences to cancel. The consequence of the logarithmic dependence of both the energy and the entropy is that the system can lower its free energy by creating free topological charges above the critical temperature, which is given by $T_{\mathrm{KT}} = \frac{\pi}{2}\,\rho$. This condition holds a "universal jump" in the superfluid density, which is proportional to ρ, and is a characteristic of the KT phase transition.

Popov's original treatment of the 2D Bose gas does not exhibit this universal jump. However, it has been shown that a higher order treatment of interactions, leading to the introduction of the many-body T-matrix to describe collisions of thermal or condensate

atoms with the condensate, shows the universal jump in the superfluid density [69]. The inclusion of the many-body T-matrix and the study of collisions in two dimensions form a major part of our work.

1.2. Topic of this thesis and literature reference

This thesis is concerned with the finite temperature physics of a Bose gas which is confined to two dimensions. The reduction in dimensionality fundamentally influences the physics of the system and allows phenomena that do not exist or that are mostly suppressed in a three-dimensional condensate. The theory applied to a two-dimensional system is mostly analogous to that in three dimensions. However, differences prohibiting the existence of a finite-temperature BEC in a two-dimensional ideal gas arise in the density of states and other quantities. Approximations based on this, like the semi-classical approximation, have been found to give ambiguous and unsatisfactory results, predicting a condensate solution not for all temperatures below the critical temperature, and even a solution without a condensate [27]. For a long time it was not certain that BEC could occur in a trapped system at all [27, 110]. However, the trap suppresses phase fluctuations to a certain extent and makes BEC possible in two [32] and even one dimension at finite temperatures. The initial prospect of the work undertaken for this thesis was to clarify this issue by applying the quantum-mechanical Hartree-Fock-Bogoliubov (HFB) formalism, the numerical application to Bose-Einstein condensation developed by my supervisor, Dr. David Hutchinson, and co-workers for the three-dimensional case in [49, 50, 51, 52, 98], to the 2D Bose-Einstein condensate. Finite temperature calculations are computationally expensive even in static models, and we have implemented efficient methods to tackle the mean-field equations. The mutual dependence of the condensate and the non-condensate density on each other requires a self-consistent scheme. The solution of the HFB equations yields important quantities, among it the one particle density matrix of the condensed system, from which coherence properties can be derived [83]. The first order correlation function is closely related to the momentum distribution of the condensate [30] and, thus, accessible to measurement via Bragg spectroscopy. Measurements of the first and second order correlation function in a quasi-one-dimensional condensate have recently been carried out [43, 102] and we present corresponding results for the two-dimensional case.
Furthermore, the HFB equations yield the excitation spectrum of the condensate which

is relevant for comparison to future experiments.[2]

The effect on collision due to the reduction in dimensionality has been widely discussed in the literature [7, 66, 67, 73, 88, 89, 90, 91, 99, 109, 110]. On the one hand, many-body effects, which are important in the three-dimensional case only at high temperatures, have to be accounted for at all temperatures. On the other hand, scattering between particles becomes affected by the confinement when the characteristic length of the trap in the tightly confined dimension becomes comparable to the length scale on which collisions takes place.

1.3. Thesis outline

We start with a general description of the ideal Bose gas in the second chapter. Because many of the fundamental differences to the well-explored three-dimensional gas also apply for one-dimensional condensates, we formulate this chapter, like many other results, in a general D-dimensional form and annotate known differences to the one or three-dimensional case in the text.

The many-body problem of the dilute Bose gas is reviewed in Chapter 3, where we derive the mean-field equations from the grand-canonical many-body Hamiltonian, which are the basis of the Hartree-Fock Bogoliubov theory at finite temperatures. We also discuss details of the theory, such as ensemble averages in the quasiparticle basis, implications of the broken symmetry approach and collective excitations. We then describe in detail approximations to the full Hartree-Fock Bogoliubov equations, dealing with the gapless theories and the semi-classical approximation.

An issue in two dimensions is the treatment of interactions. Whereas in 3D a zero-momentum zero-energy approximation to the two-body transition matrix is used to parameterize scattering, in 2D many-body effects must be considered since the two-body limit goes to zero for condensate interactions. Therefore, the coupling strength must be carefully chosen, depending on how the reduced dimensionality influences collisions that take place on a very small length scale. This is subject of Chapter 4.

[2] Bose-Einstein condensation in two-dimensions has been achieved [39, 104], but excitation frequencies have not been measured yet.

Of special importance in lower dimensional systems in general are phase fluctuations, dominating the condensate at temperatures well below the phase transition temperature. This regime where global coherence is lost has recently gained interest through experimental exploration in one-dimensional systems [43, 102]. We describe the fundamental formalism needed to investigate and characterize phase fluctuations in Chapter 5, based on Penrose and Onsagers' concept of off-diagonal long-range order.

In Chapter 6 we explain in detail the methods we use to solve the mean-field equations by expanding into an appropriate basis set. Optimization methods and the numerical solution of the coupled finite temperature equations are described.

Finally, in Chapters 7 and 8 we carry out numerical calculations and present the results. In the first of these two chapters fundamental finite temperature results, obtained within the Popov approximation, such as the condensate population, excitations and coherence properties are presented. The second chapter is concerned with the results from using the gapless extensions to the Hartree-Fock Bogoliubov theory, presenting a renormalization scheme for the anomalous pair average which is necessary to avoid divergences contained in the full HFB theory. Then we investigate the regime dependent coupling parameter, based on two different approaches to determine the many-body T-matrix, and propose a method to chose the coupling strength in finite temperature calculations.

In the last chapter we conclude this thesis with a list of the achievements of the undertaken work and discuss future prospects.

2. The Ideal Bose Gas

We start the theoretical treatment of the weakly-interacting Bose gas with a brief summary of the physics of the non-interacting Bose gas. We discuss the general case of the D-dimensional Bose gas in the beginning, so that the key results are available for any dimension required. A reasonably detailed description of the two-dimensional Bose gas, which is subject of this work, follows in Section 2.3. We point out where divergences occur, being the cause of much trouble in the treatment of lower dimensional Bose-Einstein condensates. It is a well known fact that Bose-Einstein condensation cannot occur in two dimensions in the free ideal gas at finite temperatures. How this fact is changed by the presence of a trapping potential is an important focus in the last section.
Before we discuss the two-dimensional case, the results for the more familiar three-dimensional case are summarized for convenience in Section 2.2.

2.1. The Bose gas in D dimensions

2.1.1. Free case

We consider a free, non-interacting Bose gas where a single boson is described by the energy operator

$$\hat{h}(\mathbf{x}) = -\frac{\hbar^2}{2m}\Delta \ , \tag{2.1}$$

where $\mathbf{x}$ is the D-dimensional coordinate vector. We assume the particles are confined in a container of the D-dimensional volume V with periodic Born-von Karman boundary conditions. The momentum eigenstates are then simply given by plane waves $\langle \mathbf{x}|\mathbf{p}\rangle = V^{-1/2}\, e^{i\mathbf{p}\cdot\mathbf{x}/\hbar}$ with the single particle energies

$$\epsilon_{\mathbf{p}} = \frac{\mathbf{p}^2}{2m} \ , \tag{2.2}$$

where $\mathbf{p}$ denotes the momentum.

The occupation of a single particle energy level with energy $\epsilon_{\mathbf{p}}$ is determined by the Bose distribution function for the inverse temperature $\beta = (k_{\mathrm{B}}T)^{-1}$

$$f_{\mathrm{B}}(\epsilon_{\mathbf{p}}, T, N) = \frac{1}{z^{-1}\, e^{\beta\epsilon_{\mathbf{p}}} - 1} = \frac{1}{e^{\beta(\epsilon_{\mathbf{p}} - \mu)} - 1} \ , \tag{2.3}$$

so that the total particle number is given by the discrete sum over all single particle levels

$$N = \sum_{\mathbf{p}} f_{\mathrm{B}}(\epsilon_{\mathbf{p}}, T, N) \ .^{1} \tag{2.4}$$

In (2.3) we have introduced the fugacity $z = e^{\beta\mu}$ with the chemical potential μ. The chemical potential is determined through the total particle number in (2.4), so that the Bose-Einstein distribution function is actually dependent on N, rather than on μ. From (2.3) we see that the chemical potential must be smaller than the lowest single particle energy level.

For a large volume V we can take the lowest energy state to be $\epsilon_{\mathbf{0}} = 0$. Then, the distribution function has a singularity as $\mu \uparrow 0$. Anticipating that this leads to the macroscopic occupation of the ground state, we treat the zero energy term in the above sum separately.

For a large volume V, we can replace the sum in (2.4) by an integral

$$\sum_{\mathbf{p}} \quad \to \quad V \int_{-\infty}^{\infty} \frac{\mathrm{d}^D p}{(2\pi\hbar)^D} \ , \tag{2.5}$$

so that we write by virtue of (2.2), taking into account the above considerations,

$$N = N_0 + V \int_{-\infty}^{\infty} \frac{\mathrm{d}^D p}{(2\pi\hbar)^D} \ f_{\mathrm{B}}(\epsilon_{\mathbf{p}}, T, N) \ . \tag{2.6}$$

The first part corresponds to the atoms in the ground state $N_0 = z/(1-z)$, whereas the second part determines the number N_{ex} of particles in excited states. In order to transform the momentum integral into an energy integral, we consider the transformation from cartesian to spherical coordinates

$$\int_{-\infty}^{\infty} \mathrm{d}x_1 \cdots \mathrm{d}x_D = \int_0^{\infty} \mathrm{d}r \ S_D \, r^{D-1} \ , \tag{2.7}$$

where we have introduced the surface of the D-dimensional unit sphere

$$S_D = \frac{2\pi^{D/2}}{\Gamma\left(\frac{D}{2}\right)} \ . \tag{2.8}$$

[1] In the case of BEC, the atoms are usually trapped in a certain spin state, so that we here neglect a possible spin degeneracy factor.

Together with the dispersion relation (2.2), we use this to write

$$N_{\mathrm{ex}} = \frac{V}{\Gamma\left(\frac{D}{2}\right)}\left(\frac{m}{2\pi\hbar^2}\right)^{D/2}\int_0^\infty \mathrm{d}\epsilon\, \epsilon^{\frac{D}{2}-1} f_{\mathrm{B}}(\epsilon, T, N)\ . \tag{2.9}$$

From comparison with

$$N_{\mathrm{ex}} = \int_0^\infty \mathrm{d}\epsilon\, g_D(\epsilon)\, f_{\mathrm{B}}(\epsilon, T, N)\ , \tag{2.10}$$

we read for the density of states

$$g_D(\epsilon) = \frac{V}{\Gamma\left(\frac{D}{2}\right)}\left(\frac{m}{2\pi\hbar^2}\right)^{D/2}\epsilon^{\frac{D}{2}-1}\ . \tag{2.11}$$

This result can also be obtained from (C.3) with $V(r) = 0$.

It is convenient to express the thermodynamical quantities in terms of the thermal de Broglie wavelength

$$\lambda = \sqrt{\frac{2\pi\beta\hbar^2}{m}} \tag{2.12}$$

and the generaralized ζ-function[2]

$$\zeta_\nu(z) = \frac{1}{\Gamma(\nu)}\int_0^\infty \mathrm{d}x\ \frac{x^{\nu-1}}{z^{-1}e^x - 1}\ . \tag{2.13}$$

With this, the number of excited particles (2.9) can be rewritten, so that we get

$$N = N_0 + N_{\mathrm{ex}} = N_0 + \frac{V}{\lambda^D}\,\zeta_{D/2}(z)\ . \tag{2.14}$$

Critical Temperature. Varying the temperature, the chemical potential must adapt so that the total number of particles is conserved. On the other hand, the chemical potential is bound from above by zero. For this critical value of the chemical potential, the number of excited states in (2.14) reaches a maximum. If the total number of particles N exceeds the available excited energy levels, all excess particles must be accommodated in the ground state $\epsilon_{\mathbf{0}}$.

To calculate the limit $z \downarrow 1$, we use the series representation of the generalized ζ-function for small negative values of the chemical potential, see Appendix A, i. e.

$$\zeta_\nu(e^{\beta\mu}) = \Gamma(1-\nu)\,(-\beta\mu)^{\nu-1} + \sum_{k=0}^{\infty}\frac{(\beta\mu)^k}{k!}\,\zeta(\nu-k)\ . \tag{2.15}$$

Thus, in the limit $z \downarrow 1$, the generalized zeta function reduces to the Riemann zeta function

$$\lim_{z\downarrow 1}\zeta_{D/2}(z) = \zeta\left(\tfrac{D}{2}\right)\ .^{[3]} \tag{2.16}$$

[2] Some properties of the ζ-function, like the series expansion, are discussed in Appendix A.

[3] Note that, in the two-dimensional case, the limit $z \downarrow 1$ must be performed more carefully, since the ζ-function has a pole at $z = 1$, see Section 2.3.1.

For temperatures higher than the critical temperature, $N_{\rm ex} \leq N$ and the chemical potential has a negative value. As the system approaches the critical temperature, the chemical potential increases until we reach the limit $\mu \uparrow 0$, $z \downarrow 1$ as $T \to T_c$. For temperatures below T_c, μ remains zero so that N_0 increases while $N_{\rm ex}$ decreases. We now calculate the critical temperature at the onset of the phase transition, where the chemical potential vanishes. Then, using (2.14) and (2.16), the maximum number of particles in excited states is given by

$$N_{\rm ex}^{max} \equiv N = \frac{V}{\lambda^D}\,\zeta\big(\tfrac{D}{2}\big) \ . \tag{2.17}$$

With this, we arrive at the following expression for the critical temperature

$$k_{\rm B}T_c = \frac{2\pi\hbar^2}{m}\left(\frac{N}{V\,\zeta\big(\frac{D}{2}\big)}\right)^{2/D} \ . \tag{2.18}$$

The ground state fraction as a function of temperature now follows immediately from (2.14) and (2.18):

$$\frac{N_0}{N} = 1 - \left(\frac{T}{T_c}\right)^{D/2} \ . \tag{2.19}$$

2.1.2. Trapped case

In the presence of an isotropic trap, the density of states is modified and the thermal behaviour differs from that of the free gas. The density of states for the harmonic trapping potential is derived in Appendix C and is given by (C.8)

$$g_D(\epsilon) = \frac{\epsilon^{D-1}}{\Gamma(D)\,(\hbar\omega)^D} \ . \tag{2.20}$$

Using the methods of the previous section, we calculate the number of thermal atoms as

$$N_{\rm ex} = \int_0^\infty {\rm d}\epsilon\; g_D(\epsilon)\; f_{\rm B}(\epsilon, T, N) = \frac{\zeta_D(z)}{(\hbar\omega\beta)^D} \ , \tag{2.21}$$

where we have used (2.13). In analogy to the free gas, the maximum number of particles in the excited levels can be obtained from the limit $z \downarrow 1$, so that we now get

$$N_{\rm ex}^{max} \equiv N = \frac{\zeta(D)}{(\hbar\omega\beta)^D} \ .^{4} \tag{2.22}$$

[4] The problem mentioned in the previous footnote persists now in the one-dimensional case.

Hence, the critical temperature is given by

$$k_{\mathrm{B}}T_c = \hbar\omega \left(\frac{N}{\zeta(D)}\right)^{1/D} \tag{2.23}$$

and the temperature dependence of the condensate fraction is, in contrast to (2.19), expressed by

$$\frac{N_0}{N} = 1 - \left(\frac{T}{T_c}\right)^D \ . \tag{2.24}$$

2.2. The Bose gas in three dimensions

It is well-known that Bose-Einstein condensation occurs in the three-dimensional free Bose gas. The occurrence of this phase transition was first described by Einstein [25], based on work by Bose regarding the light quanta hypothesis and Planck's law [14]. Since it is important, but not the focus of this thesis, the three-dimensional gas is described only in brief.

Free case. We have derived all important quantities in the previous section, so that the results for the three-dimensional case are now obtained by setting $D = 3$ dimensions.

The density of states (2.11) gives

$$g_3(\epsilon) = \frac{2\pi V}{(2\pi\hbar)^3}\,(2m)^{3/2}\sqrt{\epsilon}\ . \tag{2.25}$$

With this, the total particle number can be calculated using (2.14)

$$N = N_0 + \frac{V}{\lambda^3}\,\zeta_{\frac{3}{2}}(z)\ . \tag{2.26}$$

We now look at the critical properties for $z \downarrow 1$. The condition for BEC to occur is that the number of excited particles reaches its maximum value, i. e. from (2.17)

$$n\lambda^3 \sim \zeta\left(\tfrac{3}{2}\right)\ , \tag{2.27}$$

where we have introduced the density $n = N/V$. This means that there exists a critical temperature at that the phase transition occurs. It is obtained from (2.18)

$$k_{\mathrm{B}}T_c = \frac{2\pi\hbar^2}{m}\left(\frac{N}{V\zeta(3/2)}\right)^{2/3}\ , \tag{2.28}$$

so that we get for the condensate fraction

$$\frac{N_0}{N} = 1 - \left(\frac{T}{T_c}\right)^{3/2}\ . \tag{2.29}$$

Trapped case. For the trapped gas, we get from (2.23) and (2.24) for the critical temperature

$$k_{\mathrm{B}}T_c = \hbar\omega\sqrt[3]{N/\zeta(3)} \approx 0.94\,\hbar\omega\sqrt[3]{N}\ . \tag{2.30}$$

The condensate fraction decreases with the temperature as

$$\frac{N_0}{N} = 1 - \left(\frac{T}{T_c}\right)^3\ . \tag{2.31}$$

2.3. The Bose gas in two dimensions

Unlike the three-dimensional case, the phenomenon of Bose-Einstein condensation cannot take place in lower dimensional, uniform gases at finite temperatures. While in the 2D case it is strictly possible only at zero temperature, the one-dimensional free Bose gas cannot Bose-condense at all. This is because the average number of particles for low momenta at finite temperatures is proportional to $1/p^2$, as shown by Bogoliubov [13], [94, §18]. The momentum integral of this is always divergent at low momenta in one and two dimensions. Thus, long-wavelength phase fluctuations make BEC impossible at finite temperatures [70, §24], see Chapter 5.
Nevertheless, the transition to BEC may occur in a trapped two-dimensional Bose gas, as we show in Section 2.3.2.

2.3.1. Free gas in 2D

In analogy to the three-dimensional case, we evaluate the results from Sections 2.1 and C.1 in the Appendix for $D = 2$. The density of states in two dimensions is independent of the energy and is simply given by

$$g_2 = \frac{mV}{2\pi\hbar^2}\ . \tag{2.32}$$

For the number of excited particles, we get

$$N_{\mathrm{ex}} = \frac{V}{\lambda^2}\,\zeta_1(z)\ . \tag{2.33}$$

This expression contains a significant difference to the three-dimensional case, since this ζ-function diverges at the pole $z = 1$. To look into this more closely, we again use

Robinson's formula. However, one has to consider the mathematical correct limit in (2.15) for $\nu \to 1$. This is done in Appendix A and the result is given by (A.10)

$$\lim_{\nu \to 1} \zeta_\nu(e^{\beta\mu}) = -\ln(-\beta\mu) + \sum_{k=1}^{\infty} \frac{(\beta\mu)^k}{k!}\, \zeta(1-k) \ . \tag{2.34}$$

We now substitute this into (2.33) and consider the limit $z \downarrow 1$, $\mu \uparrow 0$

$$\begin{aligned} N_{\text{ex}}^{max} &= \frac{V}{\lambda^2} \lim_{\mu \uparrow 0} \left(-\ln(-\beta\mu) + \sum_{k=1}^{\infty} \frac{(\beta\mu)^k}{k!}\, \zeta(1-k) \right) \\ &= -\frac{V}{\lambda^2} \lim_{\mu \uparrow 0} \ln(-\beta\mu) \ . \end{aligned} \tag{2.35}$$

From this we see that the integral over the density of states diverges logarithmically in two dimensions. Hence, there is no Bose-Einstein condensation at finite temperatures. This is true even when interactions are included and has been proved in the *Hohenberg theorem* [45]. Strictly, BEC is only possible in the theoretical limit, $T = 0\,\text{K}$, since in this case $N_{\text{ex}} \equiv 0$, as can be seen from (2.33).

2.3.2. Trapped gas in 2D

We now turn to the inhomogeneous case, where BEC can occur if the two-dimensional gas is trapped in a parabolic potential.

From (2.21) the number of thermal particles is determined by

$$N_{\text{ex}} = \frac{1}{(\hbar\omega\beta)^2}\, \zeta_2(z) \ . \tag{2.36}$$

We calculate the critical temperature from (2.23)

$$N_{\text{ex}} \equiv N = \frac{\zeta_2(1)}{(\hbar\omega\beta)^2} \ , \tag{2.37}$$

from which we get

$$k_{\text{B}} T_c = \sqrt{\frac{6N(\hbar\omega)^2}{\pi^2}} \ , \tag{2.38}$$

where we have used $\zeta_2(1) = \pi^2/6$.
The temperature dependence of the condensate fraction follows from (2.24)

$$\frac{N_0}{N} = 1 - \left(\frac{T}{T_c}\right)^2 \ . \tag{2.39}$$

The modified density of states in the harmonic trap overcomes the divergence problems of the free gas. In general, BEC can occur in two dimensions for any power law trapping potential $V \sim r^{\eta}$.[5] In the vicinity of $\eta = 2$ (parabolic trapping potential), the critical temperature has a broad maximum [5].

In the discussion of the ideal gas, interactions between the bosons have been neglected. To take two particle interactions into consideration, the much more complex formalism of quantum field theory will be applied to the Bose gas in the next chapter.

[5] In one dimension the confinement has to be stronger than parabolic for BEC to occur, i. e. $\eta < 2$ [5].

3. Mean-Field Theory of the Trapped, Interacting Bose Gas

When dealing with bosonic or fermionic quantum systems, the correct symmetry of the wave function has to be imposed. Within the standard formalism of quantum mechanics, this can be achieved by using symmetrization or antisymmetrization operators. A well-known result for a fermionic system is given by the Slater determinant, which leads to large expressions when there are more than just a few particles involved. When dealing with many-particle systems, like Bose-Einstein condensation, this method of assuring the correct symmetry becomes rather impractical.
By using the formalism of the second quantization, the symmetry of the system is naturally ensured to be correct by the mathematical nature of the quantum field operators.[1] Hence, this formalism is widely used when describing many-body quantum systems.

In the following, we start with the second quantized form of the Hamilton operator for a dilute, weakly-interacting Bose gas. The Bose-condensed system at finite temperatures is described by a generalized Gross-Pitaevskiĭ equation and the coupled Bogoliubov-de Gennes equations, which are derived in Section 3.2. These equations involve not only the condensate, but the thermal atoms as well. The theory described in this chapter is therefore an extension of the zero temperature Bogoliubov theory [12]. To derive this set of equations, a broken symmetry approach is used. The implication of this and the relationship to number conserving approaches is discussed afterwards in Section 3.5.

The discussion of the order of approximation that goes into the mean-field equations can be found in Section 3.4. The gapless HFB theories (Popov, G1, G2) are formulated in a unified notation. Furthermore, the semi-classical approximation, which is being used extensively for the work in this thesis, is derived in detail.

[1] For a bosonic system, they obey the usual Bose commutation relations (3.4), while for a fermionic system, the field operators are Grassmann variables and anticommute.

The final two sections are concerned with an alternative derivation of the Bogoliubov-de Gennes equations in Section 3.6 and the characterization of condensate excitations in Section 3.7.

3.1. The Gross-Pitaevskiĭ equation – An introduction to mean-field theory

Before we go into detail deriving the Hamiltonian and the field equations, we introduce the *Gross-Pitaevskiĭ equation*, which describes a great deal of the phenomena occurring in Bose-Einstein condensation very well.

When describing a many-particle system, like the dilute Bose gas in a trap, it is impossible in practice to take the motion of every single particle into account. A characteristic of the phenomenon of Bose-Einstein condensation is the occurrence of a macroscopically occupied state[2] that can be described by a classical wave function $\Psi_0(\mathbf{r})$. At temperatures well below the critical temperature, where the phase transition to Bose-Einstein condensation occurs, this is an excellent description of the condensed state. Even at higher temperatures one can treat the thermal atoms as fluctuations of this classical field to a very good approximation.
Important properties of the condensate, like its shape and its momentum distribution, can be described by a non-linear Schrödinger equation. The interactions between the atoms are accounted for by a term proportional to the condensate density $|\Psi_0(\mathbf{r})|^2$. This equation is the *Gross-Pitaevskiĭ equation (GPE)*, which is simply the Euler-Lagrange equation of the energy functional of the dilute trapped Bose gas. It reads

$$\left(-\frac{\hbar^2}{2m}\Delta + U_{\text{trap}}(\mathbf{r})\right)\Psi_0(\mathbf{r}) + g\,|\Psi_0(\mathbf{r})|^2\,\Psi_0(\mathbf{r}) = \mu\,\Psi_0(\mathbf{r}) \tag{3.1}$$

and determines the condensate wave function so that the energy of the system is at an extremum. The wave function is normalized to the number of condensed atoms, i. e. $\int \mathrm{d}\mathbf{r}\,|\Psi_0(\mathbf{r})|^2 = N_0$.
The Gross-Pitaevskiĭ equation can be solved in closed form when the number of atoms and the trap potential are known. The value μ is the eigenvalue of the condensate. In this work, the main interest lies in the finite temperature properties of the condensate. In this case, the thermal atoms cannot be neglected and have to be included in the

[2] In this context, it means that a large fraction of the particles occupy one single state.

Gross-Pitaevskiĭ equation. This leads to a generalized form of this equation that is derived in the following.

3.2. The grand-canonical many-body Hamiltonian

The second quantized form of the grand-canonical many-body Hamilton operator is given by

$$\begin{aligned}\hat{H} = &\int \mathrm{d}\mathbf{r}\, \hat{\psi}^\dagger(\mathbf{r},t)\, \left(\hat{h}(\mathbf{r},t) - \mu\right)\, \hat{\psi}(\mathbf{r},t) \\ &+ \frac{1}{2} \int \mathrm{d}\mathbf{r}\, \mathrm{d}\mathbf{r}'\, \hat{\psi}^\dagger(\mathbf{r},t)\hat{\psi}^\dagger(\mathbf{r}',t)\, V(\mathbf{r}-\mathbf{r}')\, \hat{\psi}(\mathbf{r}',t)\hat{\psi}(\mathbf{r},t)\ ,\end{aligned} \tag{3.2}$$

where $\hat{h}(\mathbf{r},t)$ is the single particle Hamiltonian

$$\hat{h}(\mathbf{r},t) = -\frac{\hbar^2}{2m}\,\Delta + U_{\mathrm{trap}}(\mathbf{r},t)\ . \tag{3.3}$$

Here, U_{trap} is the external potential of the atom trap. For this work, we adopt a harmonic, time independent potential, so that we drop the time dependence of the single particle Hamiltonian in the following, from now on denoted as $\hat{h}(\mathbf{r})$. The Bose field operators obey the equal time commutation relations

$$\begin{aligned}[\hat{\psi}(\mathbf{r},t), \hat{\psi}(\mathbf{r}',t)] = [\hat{\psi}^\dagger(\mathbf{r},t), \hat{\psi}^\dagger(\mathbf{r}',t)] = 0 \\ [\hat{\psi}(\mathbf{r},t), \hat{\psi}^\dagger(\mathbf{r}',t)] = \delta(\mathbf{r}-\mathbf{r}')\end{aligned} \tag{3.4}$$

and are normalized to the total particle number

$$\left\langle \int \mathrm{d}\mathbf{r}\, \hat{\psi}^\dagger(\mathbf{r},t)\hat{\psi}(\mathbf{r},t) \right\rangle = N\ . \tag{3.5}$$

Here $\langle \ldots \rangle$ describes the ensemble expectation value. The second line in the Hamiltonian (3.2) corresponds to two-particle interactions. Three body collisions and higher order interaction terms have been neglected in the dilute limit, $n_c a_{3\mathrm{D}}^3 \ll 1$, where $a_{3\mathrm{D}}$ is the s-wave scattering length in three dimensions and n_c is the condensate density. To find an expression for the interaction potential, usually hard sphere collisions are assumed so that the general potential $V(\mathbf{r}-\mathbf{r}')$ in D dimensions is replaced by the pseudo potential [46]

$$V(\mathbf{r}-\mathbf{r}') = g\,\delta^{(D)}(\mathbf{r}-\mathbf{r}')\ , \tag{3.6}$$

and the Hamilton operator (3.2) simplifies to

$$\begin{aligned}\hat{H} = &\int \mathrm{d}\mathbf{r}\, \hat{\psi}^\dagger(\mathbf{r},t)\, \left(\hat{h}(\mathbf{r}) - \mu\right)\, \hat{\psi}(\mathbf{r},t) \\ &+ \frac{g}{2} \int \mathrm{d}\mathbf{r}\, \hat{\psi}^\dagger(\mathbf{r},t)\hat{\psi}^\dagger(\mathbf{r},t)\, \hat{\psi}(\mathbf{r},t)\hat{\psi}(\mathbf{r},t)\ .\end{aligned} \tag{3.7}$$

For a dilute gas this is a good approximation, however one has to be careful with the coupling constant g. Usually it is derived from an approximation to the two-body T-matrix in the low-energy and low-momentum limit, as appropriate for scattering processes in an ultra-cold system. In three dimensions, the two-body T-matrix for a dilute gas is well described within the s-wave approximation, $g = 4\pi\hbar^2 a_{3\mathrm{D}}/m$. In two dimensions, however, the two-body T-matrix vanishes at zero energy. Therefore, many-body effects introduced by the surrounding medium must be taken into account when studying two-dimensional gases. For a trapped gas, this leads to a spatially dependent coupling parameter $g(\mathbf{r})$. For further discussion we refer to Chapter 4.

Bogoliubov approximation. Since we are interested in the case where a majority of the particles reside in the ground state, we may separate out the condensate part and write it as an ensemble average of the Bose field operator. The fraction of non-condensed atoms are treated as a fluctuation of this condensate field.

To proceed, we expand the Bose field operators (3.4) in a basis set of orthonormal single particle wave functions $\{\psi_i(\mathbf{r})\}$

$$\hat{\psi}(\mathbf{r},t) = \sum_{i=0}^{\infty} \hat{a}_i(t)\, \psi_i(\mathbf{r}) = \hat{a}_0(t)\, \psi_0(\mathbf{r}) + \sum_{i=1}^{\infty} \hat{a}_i(t)\, \psi_i(\mathbf{r})\ , \tag{3.8}$$

where the $\hat{a}_i(t)$, $\hat{a}_i^\dagger(t)$ are the single particle operators that annihilate or create one boson. They obey the equal time commutation relations

$$\begin{aligned}[\hat{a}_i(t), \hat{a}_j(t)] = [\hat{a}_i^\dagger(t), \hat{a}_j^\dagger(t)] = 0\ , \\ [\hat{a}_i(t), \hat{a}_j^\dagger(t)] = \delta_{ij}\ .\end{aligned} \tag{3.9}$$

The Bogoliubov approximation corresponds to replacing the operators $\hat{a}_0$ and $\hat{a}_0^\dagger$ by a simple number, i. e.

$$\hat{a}_0 = \hat{a}_0^\dagger = \sqrt{N_0}\ . \tag{3.10}$$

In the regime of Bose-Einstein condensation a large population occupies the ground state, so that N_0 is a large number and, hence, the difference between N_0 and $N_0 - 1$ is

small. The effect of the operators $\hat{a}_0$ and $\hat{a}_0^\dagger$ is therefore negligibly altered if $\sqrt{N_0 - 1}$ is replaced by $\sqrt{N_0}$ and the number state of the condensate remains unchanged.[3] The replacement of the operators by a number leads to a violation of particle conservation.[4] For that reason we work in the grand-canonical ensemble and ensure particle conservation by introducing the chemical potential as a Lagrange multiplier. This is done by replacing $\hat{H}$ by $\hat{H} - \mu\hat{N}$, where $\hat{N} = \hat{\psi}^\dagger(\mathbf{r}, t)\hat{\psi}(\mathbf{r}, t)$ is the number operator. From (3.8) we define the condensate and fluctuation[5] operators as

$$\Psi_0(\mathbf{r}) = \sqrt{N_0}\,\psi_0(\mathbf{r}) \ , \tag{3.11}$$

$$\delta\hat{\psi}(\mathbf{r}, t) = \sum_{i=1}^{\infty} \hat{a}_i(t)\psi_i(\mathbf{r}) \ , \tag{3.12}$$

and finally decompose the Bose field operator

$$\hat{\psi}(\mathbf{r}, t) \simeq \langle\hat{\psi}(\mathbf{r}, t)\rangle + \delta\hat{\psi}(\mathbf{r}, t) = \Psi_0(\mathbf{r}, t) + \delta\hat{\psi}(\mathbf{r}, t) \ , \tag{3.13}$$

where we have split off the time dependence[6] $\Psi_0(\mathbf{r}, t) = \Psi_0(\mathbf{r})e^{-i\mu t/\hbar}$. Here $\Psi_0(\mathbf{r})$ is a classical wave function that describes the macroscopic state of condensed atoms. From (3.11), it is normalized according to

$$\int \mathrm{d}\mathbf{r}\ |\Psi_0(\mathbf{r})|^2 \equiv \int \mathrm{d}\mathbf{r}\ n_c(\mathbf{r}) = N_0 \ , \tag{3.14}$$

where we have defined the condensate density $n_c(\mathbf{r}) = \Psi_0^*(\mathbf{r})\Psi_0(\mathbf{r})$. The fluctuation operator has zero ensemble average

$$\langle\delta\hat{\psi}(\mathbf{r}, t)\rangle = 0 \ , \tag{3.15}$$

as can be seen by taking the average of (3.13), since $\langle\hat{\psi}(\mathbf{r}, t)\rangle = \Psi_0(\mathbf{r})$. This approach was first taken by Bogoliubov [12] and the approximation has therefore acquired his name.[7]

[3] Naturally, replacing operators by numbers automatically leaves the state vector they are applied to unchanged.

[4] The subtle details of this fact are discussed in Section 3.5.

[5] Note that the sum for the fluctuation operator runs only over the excited states.

[6] This follows from the time dependent Gross-Pitaevskiĭ equation (3.62) with the eigenvalue μ of the condensate.

[7] Furthermore, Bogoliubov imposed the condition $N - N_0 \ll N$, which is fulfilled only close to zero temperature. Therefore *Bogoliubov approximation* normally stands for the zero-temperature approximation, see Section 3.4.2.

Constructing the Hamiltonian. In order to simplify the Hamiltonian, the decomposition (3.13) has to be substituted into (3.7). The details of the calculation can be found in Appendix B. This yields

$$\begin{aligned}\hat{H}_{\mathrm{HFB}} = &\int \mathrm{d}\mathbf{r}\, \Psi_0^*(\mathbf{r}) \left(\hat{h}(\mathbf{r}) - \mu + \frac{1}{2}\, g n_c(\mathbf{r})\right) \Psi_0(\mathbf{r}) \\ &+ \int \mathrm{d}\mathbf{r}\, \delta\hat{\psi}^\dagger(\mathbf{r})\, \hat{\mathcal{L}}\, \delta\hat{\psi}(\mathbf{r}) \\ &+ \frac{g}{2} \int \mathrm{d}\mathbf{r}\, \left(\Psi_0^2(\mathbf{r}) + \widetilde{m}(\mathbf{r})\right)\, \delta\hat{\psi}^\dagger(\mathbf{r}) \delta\hat{\psi}^\dagger(\mathbf{r}) \\ &+ \frac{g}{2} \int \mathrm{d}\mathbf{r}\, \left(\Psi_0^{*2}(\mathbf{r}) + \widetilde{m}^*(\mathbf{r})\right)\, \delta\hat{\psi}(\mathbf{r}) \delta\hat{\psi}(\mathbf{r}) \ ,\end{aligned} \tag{3.16}$$

where

$$\hat{\mathcal{L}} = \hat{h}(\mathbf{r}) - \mu + 2\, g n(\mathbf{r}) \tag{3.17}$$

and $n(\mathbf{r}) = n_c(\mathbf{r}) + \tilde{n}(\mathbf{r})$. The introduced quantities correspond to the thermal population and the anomalous average, respectively,

$$\tilde{n}(\mathbf{r}) = \langle \delta\hat{\psi}^\dagger(\mathbf{r}) \delta\hat{\psi}(\mathbf{r}) \rangle \tag{3.18}$$

$$\widetilde{m}(\mathbf{r}) = \langle \delta\hat{\psi}(\mathbf{r}) \delta\hat{\psi}(\mathbf{r}) \rangle \ . \tag{3.19}$$

The new Hamiltonian consists of a condensate part that governs the physics at very low temperatures and several terms that are quadratic in the fluctuation operators. Since the Hamiltonian is stationary if the condensate wave function satisfies the generalized Gross-Pitaevskiĭ equation, which corresponds to the Euler-Lagrange equation of the expectation value $\langle \hat{H}_{\mathrm{HFB}} \rangle$, the terms linear in the fluctuation operator vanish. The *generalized Gross-Pitaevskiĭ equation* is given by (B.8)

$$\left(\hat{h}(\mathbf{r}) - \mu\right)\, \Psi_0(\mathbf{r}) + g\left(n_c(\mathbf{r}) + 2\,\tilde{n}(\mathbf{r})\right) \Psi_0(\mathbf{r}) + g\widetilde{m}(\mathbf{r})\, \Psi_0^*(\mathbf{r}) = 0 \ . \tag{3.20}$$

3.2.1. Bogoliubov transformation

In the previous section we started with the grand-canonical Hamiltonian for the dilute gaseous system. We simplified the interactions by choosing a contact potential and split the condensate part off the field operator. This led to a Hamilton operator (3.16) that is quadratic in the fluctuation operators. In general, in order to find its eigenstates and eigenvalues, this Hamiltonian can be diagonalized by a unitary transformation, in

this context known as the *Bogoliubov transformation*. To do so, *quasiparticle operators* $\hat{\alpha}_i$ and $\hat{\alpha}_i^\dagger$ are introduced by the linear transformation

$$\begin{aligned} \delta\hat{\psi}(\mathbf{r},t) &= \sum_i \Big(\hat{\alpha}_i(t)\, u_i(\mathbf{r}) - \hat{\alpha}_i^\dagger(t)\, v_i^*(\mathbf{r}) \Big) \\ \delta\hat{\psi}^\dagger(\mathbf{r},t) &= \sum_i \Big(\hat{\alpha}_i^\dagger(t)\, u_i^*(\mathbf{r}) - \hat{\alpha}_i(t)\, v_i(\mathbf{r}) \Big) \ , \end{aligned} \tag{3.21}$$

with $\hat{\alpha}_i(t) = \hat{\alpha}_i e^{-iE_i t/\hbar}$. They obey the usual Bose commutators (3.4) and, therefore, show bosonic behaviour, similar to phonons that describe lattice vibrations in crystals. Here they correspond to elementary[8] excitations of the condensate with an energy E_i. The c-number functions $u(\mathbf{r})$ and $v(\mathbf{r})$ are referred to as *quasiparticle amplitudes*.
In order to satisfy the commutation relations, they must be normalized as

$$\int \mathrm{d}\mathbf{r}\ \big[u_i(\mathbf{r}) u_j^*(\mathbf{r}) - v_i(\mathbf{r}) v_j^*(\mathbf{r}) \big] = \delta_{ij} \ . \tag{3.22}$$

Since the quasiparticle transformation is straightforward and does not give a greater insight into the origin of the Hartree-Fock-Bogoliubov equations (HFB), we do not derive the following results in detail, but refer to [53, §13.2] for a treatment of the fermionic case, to [119, §5.13], or to [85] for a detailed calculation. The Bogoliubov transformation of the quadratic Hamiltonian (3.16) results in the diagonal[9] Hamiltonian

$$\begin{aligned} \hat{H}_{\mathrm{HFB}} = &\int \mathrm{d}\mathbf{r}\ \Psi_0(\mathbf{r}) \left(\hat{h}(\mathbf{r}) - \mu + \frac{1}{2} g n_c(\mathbf{r}) \right) \Psi_0(\mathbf{r}) \\ &+ \sum_i E_i\, \hat{\alpha}_i^\dagger \hat{\alpha}_i - \sum_i E_i \int \mathrm{d}\mathbf{r}\, |v_i(\mathbf{r})|^2 \ . \end{aligned} \tag{3.23}$$

The first term originates from the condensate part and is merely a c-number. The second term is the Hamiltonian for non-interacting quasiparticles. It is formally equivalent to the case of the harmonic oscillator and refers to the population of thermal atoms. The third term is a constant energy shift.[10]
The quasiparticle amplitudes and energies are determined by solving the *Bogoliubov-de Gennes* equations

$$\begin{aligned} \hat{\mathcal{L}}\, u_i(\mathbf{r}) - g\big(\Psi_0(\mathbf{r})^2 + \widetilde{m}(\mathbf{r}) \big)\, v_i(\mathbf{r}) &= E_i\, u_i(\mathbf{r}) \\ \hat{\mathcal{L}}\, v_i(\mathbf{r}) - g\big(\Psi_0^*(\mathbf{r})^2 + \widetilde{m}^*(\mathbf{r}) \big)\, u_i(\mathbf{r}) &= -E_i\, v_i(\mathbf{r}) \ . \end{aligned} \tag{3.24}$$

[8] See Section 3.7.2.

[9] Diagonal in the quasiparticle operators $\hat{\alpha}_i^\dagger \hat{\alpha}_i$.

[10] Note that we have omitted terms is the factorization of the field operators that would constitute another constant energy shift, see the discussion in Section B.1.

They arise from the requirement that $\hat{H}_{\mathrm{HFB}}$ is diagonal and form an infinite set of coupled linear differential equations. Together with the generalized Gross-Pitaevskiĭ equation we refer to them as the *Hartree-Fock-Bogoliubov equations*. They form the foundation of our description of a Bose condensed system at finite temperatures. For a detailed discussion, we refer to [8, 84].

3.3. Ensemble averages in the quasiparticle basis

The partition function in the grand-canonical ensemble is defined as

$$\mathcal{Z} = \sum_{\nu} e^{-\beta(E_\nu - \mu N_\nu)} \; . \tag{3.25}$$

Here, ν represents a microstate of the system. In the number representation of a many-body system of indistinguishable particles, ν is characterized by the particle numbers $\{n_i\} = \{n_1, n_2, \ldots, n_k, \ldots\}$. The grand-canonical partition function (3.25) can be written as a trace over the Boltzmann factor, i. e. $\mathcal{Z} = \mathrm{tr}\, e^{-\beta(\hat{H}-\mu\hat{N})}$. Since the grand-canonical Hamiltonian (3.23) already includes the chemical potential term $-\mu\hat{N}$, its explicit appearance in the exponential will be omitted in the following, keeping in mind that it is part of $\hat{H}$.
Expectation values or operator averages are defined as

$$\langle \hat{O} \rangle = \frac{1}{\mathcal{Z}} \mathrm{tr}\Big(\hat{O}\, e^{-\beta \hat{H}} \Big) \; . \tag{3.26}$$

The Hamiltonian for the excited state particles is given by the diagonal part of (3.23) which we refer to as $\hat{H}'_{\mathrm{HFB}}$.[11] Quasiparticle expectation values are therefore defined as

$$\langle \hat{O} \rangle' = \frac{1}{\mathcal{Z}'} \mathrm{tr}'\Big(\hat{O}\, e^{-\beta \hat{H}'_{\mathrm{HFB}}} \Big) \; , \tag{3.27}$$

where

$$\hat{H}'_{\mathrm{HFB}} = \sum_i E_i\, \hat{\alpha}_i^\dagger \hat{\alpha}_i - \sum_i E_i \int \mathrm{d}\mathbf{r}\, |v_i(\mathbf{r})|^2 \tag{3.28}$$

and $\mathcal{Z}'$ is the grand-canonical partition function with the trace taken over quasiparticle states, indicated by the prime.

[11] Note that this is only approximately correct because of the dependence of the condensate part in (3.23) on $\tilde{n}$ and $\tilde{m}$.

Thermal density and anomalous average. To get expressions for the non-condensate density and the anomalous average in terms of the quasiparticle amplitudes, we substitute the Bogoliubov transformation (3.21) into their definition (3.18) and (3.19). For the non-condensate density, this is

$$\begin{aligned}\langle \delta\hat{\psi}^\dagger(\mathbf{r})\,\delta\hat{\psi}(\mathbf{r})\rangle &= \Big\langle \sum_{i,j}\Big(u_i^*(\mathbf{r})\hat{\alpha}_i^\dagger - v_i(\mathbf{r})\hat{\alpha}_i\Big)\Big(u_j(\mathbf{r})\hat{\alpha}_j - v_j^*(\mathbf{r})\hat{\alpha}_j^\dagger\Big)\Big\rangle \\ &= \sum_{i,j}\Big\{u_i^*(\mathbf{r})u_j(\mathbf{r})\,\langle\hat{\alpha}_i^\dagger\hat{\alpha}_j\rangle + v_i(\mathbf{r})v_j^*(\mathbf{r})\,\langle\hat{\alpha}_i\hat{\alpha}_j^\dagger\rangle \\ &\qquad -v_i(\mathbf{r})u_j(\mathbf{r})\,\langle\hat{\alpha}_i\hat{\alpha}_j\rangle - u_i^*(\mathbf{r})v_j^*(\mathbf{r})\,\langle\hat{\alpha}_i^\dagger\hat{\alpha}_j^\dagger\rangle\Big\} \\ &= \sum_{i,j}\Big\{\big[u_i^*(\mathbf{r})u_j(\mathbf{r}) + v_i(\mathbf{r})v_j^*(\mathbf{r})\big]\,\langle\hat{\alpha}_i^\dagger\hat{\alpha}_j\rangle + v_i(\mathbf{r})v_j^*(\mathbf{r})\,\delta_{ij} \\ &\qquad -v_i(\mathbf{r})u_j(\mathbf{r})\,\langle\hat{\alpha}_i\hat{\alpha}_j\rangle - u_i^*(\mathbf{r})v_j^*(\mathbf{r})\,\langle\hat{\alpha}_i^\dagger\hat{\alpha}_j^\dagger\rangle\Big\}\ .\end{aligned} \tag{3.29}$$

Here we have used the commutators for the quasiparticle operators in the last step. To further simplify this expression, we make use of the fact that, within the quasiparticle approximation, the Hamiltonian is diagonal and, hence, all the non-diagonal averages and the averages over two creation or annihilation operators must be identically zero.[12] Therefore, from (3.29), we arrive at

$$\tilde{n}(\mathbf{r}) = \sum_i f_{\mathrm{B}}(E_i)\Big(|u_i(\mathbf{r})|^2 + |v_i(\mathbf{r})|^2\Big) + |v_i(\mathbf{r})|^2\ . \tag{3.30}$$

Following the same steps as in (3.29) we obtain for the anomalous average

$$\widetilde{m}(\mathbf{r}) = \sum_i \Big(2f_{\mathrm{B}}(E_i) + 1\Big)\,u_i(\mathbf{r})\,v_i^*(\mathbf{r})\ . \tag{3.31}$$

Furthermore, we have introduced the quasiparticle distribution function[13]

$$f_{\mathrm{B}}(E_i) = \langle\hat{\alpha}_i^\dagger\hat{\alpha}_i\rangle = \frac{1}{z^{-1}e^{\beta E_i} - 1}\ , \tag{3.32}$$

where the fugacity is given by $z = e^{\beta(\mu-\lambda)}$. Here μ is the chemical potential and λ the condensate eigenvalue, and the fugacity has this appearance since the energy of the quasiparticles is measured relative to the condensate[14].

[12] This is true to the order of approximation in which the Hamiltonian (3.28) is diagonal in these operators.

[13] The familiar form of the distribution function is not self-evident and should be understood as an approximate solution for $\langle\hat{\alpha}_i^\dagger\hat{\alpha}_i\rangle$, c. f. Section 3.3.1.

[14] This is because the creation of an excitation requires prior removal of particles from the condensate.

To understand the difference between the two, one must consider the mutual dependence of the involved quantities $\mu,\ N_0(\mu),\ N(N_0,\mu),\ E_i(N_0,\mu)$. At $T=0$ the chemical potential is defined as

$$\mu = \left.\frac{\partial \tilde{E}_0(N_0,\mu)}{\partial N}\right|_\mu + \left.\frac{\partial \tilde{E}(N_0,\mu)}{\partial N}\right|_\mu , \tag{3.33}$$

which implicitly defines N_0. The energies $\tilde{E}_0$ and $\tilde{E}$ refer to the condensate part (due to the condensate part in Eq. 3.23) and quasiparticle part (due to the diagonal part in Eq. 3.28) in the grand-canonical partition function, respectively. Only for a small thermal population, $N_{\mathrm{ex}} \ll N$ can we neglect the second term in (3.33) and identify the first term with the condensate eigenvalue λ. In this case, $\mu = \lambda$ and the fugacity $z = 1$, so that (3.32) becomes the Planck distribution, $f_{\mathrm{B}}(E_i) = (e^{\beta E_p} - 1)^{-1}$.
This distribution can lead to a population of quasiparticle states which exceeds the mean total particle number, so that the condensate density can become negative. Thus the simplification of neglecting the difference between the condensate eigenvalue and the chemical potential does not hold at higher temperatures, when $N_{\mathrm{ex}} \ll N$ is no longer fulfilled.
The difference between the condensate eigenvalue and the chemical potential is approximately given by

$$z^{-1} = 1 + \frac{1}{N_0} , \tag{3.34}$$

which we will use later on for the fugacity in the distribution function (3.32) to keep the condensate particle number positive. For further discussion, we refer to [48, 80].

3.3.1. Quasiparticle averages

To calculate ensemble averages in the quasiparticle basis (3.27), one must restrict the summation to those Fock states $\{n_i\}$, here denoted by ν', whose population does not exceed the total particle number. The associated quasiparticle energies $E_i(N_0,\mu)$ in (3.28) depend on the solution of the Bogoliubov-de Gennes equations, which, themselves, depend on the particle number of the condensate through the normalization of the condensate wave function. Furthermore they depend on μ, so that the total mean particle number is fixed to N. Together, the restriction of allowed states and the nonlinear nature of the BdG equations prohibit a factorization of the grand-canonical partition function

$$\mathcal{Z}' = \sum_{\nu'} e^{-\beta \hat{H}_{\mathrm{HFB}}} \tag{3.35}$$

and of (3.27) into sums over independent quasiparticle states. Therefore, it is not to be taken for granted that the quasiparticle average $\langle \hat{\alpha}_i^\dagger \hat{\alpha}_j \rangle$ in (3.29) can be evaluated and expressed as (3.32).
Rather, this is only possible due to the following considerations. Firstly, for clearly defined microstates of the system to exist, one must consider the thermal averages of those quantities that have been defined as pure states. In particular, this means that fluctuations of the condensate are neglected. Furthermore, if $N_{\mathrm{ex}} \ll N$ for those states significant in the partition function, the considerations from above dissipate and the quasiparticle states can be taken to be independent of one another. Then the grand-canonical partition function factorizes and quasiparticle averages can be calculated to a good approximation.

3.4. Approximations

In the following we will discuss the common approximations to the full Hartree-Fock-Bogoliubov (HFB) equations as derived. As they stand, they lead to ultraviolet and infrared divergences and predict an unphysical gap in the excitation spectrum. A commonly-used way to get rid of these problems is to simply neglect the anomalous average, which yields the so-called Popov approximation. The gapless theories G1 and G2 go beyond the Popov theory and include the anomalous pair average.

3.4.1. Problems of HFB

The HFB equations that were derived earlier take into account the static influence of the thermal cloud. The affects the condensate in two ways: Firstly, the condensate can interact with the thermal cloud, i. e. binary collisions between the condensate and the non-condensate are taken into account. Secondly, interactions within the condensate are altered due to the presence of the thermal cloud by modifying the effective trapping potential. These effects are introduced by the approximate inclusion of the higher order terms $\hat{H}_3$ and $\hat{H}_4$ in the Hamiltonian (B.7). The terms in the Hamiltonian up to second order in the fluctuation operators are exact while these two terms are treated approximately. This is because the operator averages (B.3) and (B.4) are defactorized in a way analogous to Wick's theorem and the emerging pair averages are then replaced by their expectation values in the quasiparticle basis. More specifically, since Wick's

theorem applies only to pairs of operator averages, it strictly cannot be applied to products of operators, as is done in (B.3) and (B.4). Furthermore, it has been shown that the mentioned approximate treatment of the triplet factorization (B.3) is invalid and the cause of many difficulties of the higher order theories [80], especially the failure of the full HFB theory to produce a gapless excitation spectrum.

The difficulties of the full HFB theory are summarized in the following:

1. The anomalous pair average $\widetilde{m}(\mathbf{r}) = \langle \delta\hat{\psi}(\mathbf{r})\delta\hat{\psi}(\mathbf{r})\rangle$ is ultraviolet divergent. Physically this comes from the approximative parameterization of collisions through a hard sphere interaction potential, which treats collisions of different momenta with the same probability. In reality, however, collisions with high energies are much more unlikely in the Bose condensed system and this unequal treatment leads to the divergence in the anomalous average. Instead, a consistent introduction of the two-body T-matrix resolves the problem, because it introduces a renormalization of $\widetilde{m}$ [80], c. f. Section 4.4.1.

2. The HFB theory is not gapless. The excitation spectrum contains a finite energy gap $\propto g^2 n_c |\widetilde{m}|$ [41, 48, 100], which is a relic of divergences in the homogeneous case at low momenta. Genuine divergences, though, are only a feature of the homogeneous case, since the trap naturally introduces a low-energy cutoff. Goldstone's theorem [38], however, requires the theory to be gapless.[15] It predicts a mode with energy vanishing linearly with the wave number for a system with a spontaneously broken symmetry, c. f. Section 3.5, and, hence, in the long wavelength limit, a zero energy mode must exist. This mode corresponds to a rotation of the condensate phase.

   Technically, the reason for the occurrence of the energy gap can be found to be the approximate factorization of the operator averages[16] and the resulting inconsistent treatment of interactions [80]. In the full HFB theory, the anomalous average introduces many-body effects for scattering processes within the condensate not consistently in both the GPE and the BdG equations. To yield a gapless spectrum, many-body effects have to be included consistently for *each class*[17] of

[15] One can do the same argument invoking the more general Hugenholtz-Pines theorem [47].

[16] Furthermore, the HFB equations can be shown to fulfill the usual conservation laws, such as the equation of continuity. In general, such a conserving approximation does not necessarily lead to a physical spectrum for the single-particle Green's function and one is not assured of a gapless spectrum. For further discussion see [41].

[17] i. e. interactions of the condensate atoms with other condensate atoms or with thermal atoms

scattering processes, which is forced in the gapless theories G1 and G2, described in the following paragraph, or for *none* of them, which leads to the Popov approximation[18]. The flaw in the HFB equations is that this is done inconsistently and only for one class of scattering processes.

3.4.2. Bogoliubov approximation for T = 0 K

The simplest approximation is to neglect the non-condensate density and the anomalous average completely in (3.20). In this case the generalized Gross-Pitaevskiĭ equation reduces to the form given in (3.1), which can be solved straightforwardly[19]. This approximation has been done by Bogoliubov who imposed the condition of small depletion of the condensate, $N - N_0 \ll N$. This requires the temperature to be small compared to the transition temperature and is a stronger restriction than (3.10), which only requires a finite condensate density in the thermodynamic limit [28].
The Bogoliubov approximation corresponds to neglecting the terms $\hat{H}_3$, $\hat{H}_3$ and $\hat{H}_4$ in (B.5, B.6), or, equally, to setting $\tilde{n}$ and $\widetilde{m}$ equal to zero.

3.4.3. Gapless finite temperature approximations

In comparison to the Bogoliubov approximation, the described finite temperature methods are computationally more challenging, because the condensate and non-condensate densities have to be determined iteratively by the successive solution of the generalized Gross-Pitaevskiĭ equation and the Bogoliubov-de Gennes equations.

For the sake of comparison between the different theories, we write the Gross-Pitaevskiĭ and BdG equations in a unified form

$$\left(\hat{h}(\mathbf{r}) - \mu + g_{\mathrm{con}}(\mathbf{r})\, n_c(\mathbf{r}) + 2\, g_{\mathrm{exc}}(\mathbf{r})\, \tilde{n}(\mathbf{r})\right) \Psi_0(\mathbf{r}) = 0 \tag{3.36}$$

$$\begin{pmatrix} \hat{\mathcal{L}} - E_i & \mathcal{M} \\ \mathcal{M} & \hat{\mathcal{L}} + E_i \end{pmatrix} \begin{pmatrix} u(\mathbf{r}) \\ v(\mathbf{r}) \end{pmatrix} = \mathbf{0}\ , \tag{3.37}$$

[18] To tie up to the last footnote, the Popov theory does not fulfill the equation of continuity [41].
[19] Since the thermal depletion of the condensate is neglected, the Bogoliubov-de Gennes equations do not need to be solved.

where

$$\hat{\mathcal{L}} = \hat{h}(\mathbf{r}) - \mu + 2\left(g_{\mathrm{con}}(\mathbf{r})\, n_c(\mathbf{r}) + g_{\mathrm{exc}}(\mathbf{r})\, \tilde{n}(\mathbf{r})\right) \tag{3.38}$$

$$\mathcal{M} = g_{\mathrm{con}}(\mathbf{r})\, n_c(\mathbf{r}) \ . \tag{3.39}$$

Here we have introduced two different coupling parameters for interactions of the condensate with itself, $g_{\mathrm{con}}(\mathbf{r})$, and with the excited atoms, $g_{\mathrm{exc}}(\mathbf{r})$.

3.4.3.1. Popov approximation

The simplest method to treat the collisions between atoms consistently in order to produce a gapless spectrum is done by dropping the anomalous average[20] $\widetilde{m}$ in the generalized GPE (3.20) and the BdG equations (3.24), which leads to[21]

$$\left(\hat{h}(\mathbf{r}) - \mu\right) \Psi_0(\mathbf{r}) + g\left(n_c(\mathbf{r}) + 2\,\tilde{n}(\mathbf{r})\right) \Psi_0(\mathbf{r}) = 0 \ , \tag{3.40}$$

$$\begin{aligned} \hat{\mathcal{L}}\, u_i(\mathbf{r}) - g n_c(\mathbf{r})\, v_i(\mathbf{r}) &= E_i\, u_i(\mathbf{r}) \ , \\ \hat{\mathcal{L}}\, v_i(\mathbf{r}) - g n_c(\mathbf{r})\, u_i(\mathbf{r}) &= -E_i\, v_i(\mathbf{r}) \ , \end{aligned} \tag{3.41}$$

where $\hat{\mathcal{L}}$ is given by (3.17). This is the Popov approximation, which corresponds to setting $g_{\mathrm{con}}(\mathbf{r}) = g_{\mathrm{exc}}(\mathbf{r}) = g$ in (3.36), (3.37) and, thus, an off-diagonal potential given by $\mathcal{M} = g n_c(\mathbf{r})$. In the previously mentioned Bogoliubov approximation $g_{\mathrm{con}}(\mathbf{r}) = g$ and $g_{\mathrm{exc}}(\mathbf{r}) = 0$. The Popov approximation is a finite temperature approximation, since it contains condensate interactions with both condensate and thermal atoms. The collisions are described by the two-body T-matrix and many-body effects on the scattering processes are neglected. In the three-dimensional case, the numerical Popov results reproduce the excitation frequencies from the JILA experiment [58] up to about 0.6 T_c, as shown in [48]. For higher temperatures, the validity of the Popov approximation cannot be guaranteed and it has been shown to fail in the anisotropic case [49].

Note that for low temperatures the non-condensate density goes to zero and the GPE reduces to that of the Bogoliubov approximation.[22]

[20] As mentioned before, all the problems of the HFB theory arise from introducing the anomalous average.

[21] For the symmetric case, the phase of the condensate wave function can be omitted, as it is done here in the definition of the condensate density.

[22] However, there is a very small depletion of the condensate even at zero temperature due to the non-thermal term in (3.30) and (3.31), referred to as *quantum depletion*.

3.4.3.2. Gapless HFB

Since the gap in the excitation spectrum in the HFB theory has been recognized to come from the inconsistent introduction of many-body effects through the anomalous average $\widetilde{m}$, it seems natural to introduce many-body effects in a consistent way. This has been done in two different ways, referred to as G1 and G2 [48, 49, 80, 97, 98, 114]. Another approach has been undertaken in [62, 63, 64], where the two sorts of collisions are treated with a many-body T-matrix, evaluated at different energies.[23]

G1 theory. To go consistently beyond the Popov approximation, many-body effects have to be included for scattering between the condensate and both condensate and thermal atoms. Firstly, if we look at the generalized Gross-Pitaevskiĭ equation (3.20) from the HFB theory and compare it to (3.36), we read

$$g_{\mathrm{con}}(\mathbf{r}) = g\left(1 + \frac{\widetilde{m}(\mathbf{r})}{\Psi_0(\mathbf{r})^2}\right) \equiv T_{\mathrm{MB}}(\mathbf{r}) \ . \tag{3.42}$$

This expression is the many-body T-matrix, introduced by the appearance of the anomalous average, c. f. Section 4.3.3.
If we use this coupling parameter in the BdG equations (3.37) and compare with those from the HFB theory (3.24), we see that the equations of the full HFB formalism are not consistent with (3.36) and (3.37). A consistent introduction of many-body effects is done in the G1 theory by replacing the coupling parameter g_{con} in (3.36) and (3.37) with (3.42) while the coupling parameter for non-condensate interactions remains $g_{\mathrm{exc}}(\mathbf{r}) = g$. This leads to the terms

$$\hat{\mathcal{L}}_{\mathrm{G1}} = \hat{h}(\mathbf{r}) - \mu + 2\,g\,(n_c(\mathbf{r}) + \tilde{n}(\mathbf{r})) \ , \tag{3.43}$$

$$\mathcal{M}_{\mathrm{G}} = g\Psi_0(\mathbf{r})^2 + g\widetilde{m}(\mathbf{r}) \ . \tag{3.44}$$

Here the index 'G' denotes the off-diagonal potential in the gapless extensions, since it is the same in both the G1 and the G2 theory. Morgan has shown that this formalism is justified by treating the triplet and quartet operator averages (B.3) and (B.4) up to second order perturbation theory [80]. It turns out that the result of perturbation theory for the quartet averages coincides with the approximation (B.4). The trouble within the full HFB theory arises from an incorrect treatment of the triplet terms.

[23] However, our attempt to implement their theory with the methods described in the named publications has turned out to be unsuccessful, and we believe that there are issues with the theory that are not fully discussed in this publication.

G2 theory. A natural extension is to include many-body effects via the many-body T-matrix in the condensate – non-condensate interactions as well, i. e. setting $g_{\mathrm{con}}(\mathbf{r}) = g_{\mathrm{exc}}(\mathbf{r}) = T_{\mathrm{MB}}(\mathbf{r})$. This means explicitly for the diagonal and off-diagonal terms, using (3.42),

$$\hat{\mathcal{L}}_{\mathrm{G2}} = \hat{h}(\mathbf{r}) - \mu + 2\,g\left(n_c(\mathbf{r}) + \tilde{n}(\mathbf{r}) + \widetilde{m}(\mathbf{r}) + \frac{\widetilde{m}(\mathbf{r})\tilde{n}(\mathbf{r})}{\Psi_0(\mathbf{r})^2}\right)\,, \tag{3.45}$$

$$\mathcal{M}_{\mathrm{G}} = g n_c(\mathbf{r}) + g\widetilde{m}(\mathbf{r})\,. \tag{3.46}$$

There is no rigorous proof of the validity of this replacement so far.[24] Certainly the same effective interaction should be assumed for all low energy collisions, but the many-body T-matrix has been calculated in the limit of low collision momenta. Hence it is only appropriate if the collisions with the non-condensate occur with low energy. For collision energies much larger than the mean-field energy, the G1 theory should be used.

Numerical results based on the G2 theory have been calculated [49] and compared to experimental data [58]. The G2 theory can describe the energy shift of the quadrupole mode ($m = 2$) of a 3D condensate in an anisotropic trap correctly, where the Popov theory had failed. Both theories fail to describe the anomalous behaviour of the breathing mode ($m = 0$), that has been shown to arise from experimental perturbation of the thermal cloud [82]. The extended theory presented in this publication is a full second order treatment and includes the dynamics of the thermal cloud that leads to thermal driving of the condensate.

3.4.4. Semi-classical approximation

At temperatures that are large compared to the energy level spacing of the trap, one can use the semi-classical or WKB approximation. Usually this approximation holds if the typical de Broglie wavelengths are small compared to the length scales over which the trapping potential and the particle densities vary significantly. Then the gas can be treated as locally uniform. While giving good results for the interacting gas under these conditions in three dimensions, in two dimensions the semi-classical

[24] These extensions to HFB cannot be rigorously proven, in general. However, one can make assumptions about consistency and validity of the approximations. While G1 has been shown to be justified from first and second order perturbation theory, nothing like that has been done for G2. Presumably it is justified by higher order perturbation theory.

approximation fails. This failure has led to confusion and to the question whether Bose-Einstein condensation is possible at all in an interacting gas [5, 27]. Since the HFB formalism clarifies this issue, it is important to understand the failure of the semi-classical approximation. Before we look at the interacting gas, the result for the ideal gas shall be given.

Ideal gas. We use the energy dispersion of a classical free particle, $\epsilon_{\mathbf{p}} = \mathbf{p}^2/2m + V(\mathbf{r})$ and a simplified distribution function $f(\mathbf{r})$, so that $f(\mathbf{r})\,\mathrm{d}^D p\,\mathrm{d}^D r/(2\pi\hbar)^D$ denotes the mean particle number in the D-dimensional phase space element $\mathrm{d}^D p\,\mathrm{d}^D r$. The distribution function is given by

$$f(\mathbf{r}) = \frac{1}{z^{-1}(\mathbf{r})\,e^{\beta\frac{\mathbf{p}^2}{2m}} - 1} \;, \tag{3.47}$$

where $z(\mathbf{r}) = e^{\beta[\mu - V(\mathbf{r})]}$. For an ideal two-dimensional gas, the momentum integral over (3.47) yields the simple expression, c. f. Section 2.3.2,

$$\tilde{n}(\mathbf{r}) = \frac{\zeta_2(z(\mathbf{r}))}{\lambda^2} \;, \tag{3.48}$$

where λ is the thermal wavelength (2.12).

Interacting gas. We start from the Bogoliubov-de Gennes equations (3.41) of the Popov approximation and replace the quasiparticle amplitudes by

$$u_j(\mathbf{r}) \approx u(\mathbf{r})\,e^{i\varphi(\mathbf{r})} \;, \quad v_j(\mathbf{r}) \approx v(\mathbf{r})\,e^{i\varphi(\mathbf{r})} \;. \tag{3.49}$$

The common phase defines a quasiparticle momentum, $\mathbf{p} = \hbar\,\mathrm{grad}\,\varphi$. We assume that u, v and $\mathbf{p}$ vary slowly in space so that spatial derivatives can be neglected. This approximation is referred to as the *local density approximation (LDA)*.
Inserting (3.49) into (3.41) turns out to yield exactly the same results as replacing the quantum mechanical momentum operator with its classical equivalent: $-\hbar^2\Delta/2m \to \mathbf{p}^2/2m$. Redefining the operator $\hat{\mathcal{L}}$ as

$$\mathcal{L}_{\mathrm{sc}} = \frac{\mathbf{p}^2}{2m} + U_{\mathrm{trap}}(\mathbf{r}) - \mu + 2g\,n(\mathbf{r}) \;, \tag{3.50}$$

we can write the BdG equations in the form

$$\begin{pmatrix} \mathcal{L}_{\mathrm{sc}} - E_{\mathbf{p}}(\mathbf{r}) & g\,n_c(\mathbf{r}) \\ g\,n_c(\mathbf{r}) & \mathcal{L}_{\mathrm{sc}} + E_{\mathbf{p}}(\mathbf{r}) \end{pmatrix} \begin{pmatrix} u(\mathbf{r}) \\ v(\mathbf{r}) \end{pmatrix} = \mathbf{0} \;. \tag{3.51}$$

The secular equation yields the dispersion relation for the Popov approximation

$$E_{\mathbf{p}}^{\mathrm{Pop}}(\mathbf{r}) = \sqrt{\mathcal{L}_{\mathrm{sc}}^2 - \left(gn_c(\mathbf{r})\right)^2} \; . \tag{3.52}$$

The energies depend on the quasiparticle momentum $\mathbf{p}$. For notational simplicity, we write E for $E_{\mathbf{p}}^{\mathrm{Pop}}(\mathbf{r})$ and omit spatial dependencies in the following calculation. The functions u and v are given by [87, §8.1], [84, §9.2]

$$u^2 = \frac{\mathcal{L}_{\mathrm{sc}} + E}{2E} \; , \quad v^2 = \frac{\mathcal{L}_{\mathrm{sc}} - E}{2E} \; . \tag{3.53}$$

Now the density of excited particles can be calculated from the momentum integral

$$\tilde{n} = \frac{1}{(2\pi\hbar)^2} \int_{-\infty}^{\infty} \mathrm{d}^2 p \left\{ \left(|u|^2 + |v|^2\right) f_{\mathrm{B}}(E) + |v|^2 \right\} . \tag{3.54}$$

A straightforward calculation yields

$$\begin{aligned} \tilde{n} = \frac{m}{2\pi\hbar^2} \int_0^{\infty} \mathrm{d}E \; \Bigg\{ & f_{\mathrm{B}}(E) + \frac{1}{2} - \frac{E}{2\sqrt{E^2 + (gn_c)^2}} \\ & \times \Theta\left(E - \sqrt{\left(U_{\mathrm{trap}} - \mu + 2gn\right)^2 - \left(gn_c\right)^2} \right) \Bigg\} \; , \end{aligned} \tag{3.55}$$

where the Heaviside function stems from the square root in (3.52). We introduce the following variables: $t = \beta(U_{\mathrm{trap}} - \mu + 2gn)$, $s = \beta\, gn_c$, and further the thermal wavelength λ. The solution of (3.55) is given by

$$\tilde{n} = \frac{1}{\lambda^2} \left\{ -\ln\left[1 - e^{-\sqrt{t^2 - s^2}} \right] + t - \sqrt{t^2 - s^2} \right\} \; . \tag{3.56}$$

This is the expression for the thermal density within the semi-classical approximation. Together with the Gross-Pitaevskiĭ equation and the normalization condition, $N_0 = N - \int \mathrm{d}\mathbf{r}\, \tilde{n}$, it forms a closed set of equations. However, no self-consistent solutions can be found. To see this, in the thermodynamic limit, assume a Thomas-Fermi wave function[25] for the condensate

$$n_c = g^{-1} \left(\mu - U_{\mathrm{trap}} - 2g\tilde{n}\right) \times \Theta\left(\mu - U_{\mathrm{trap}} - 2g\tilde{n}\right) \; . \tag{3.57}$$

With this, the non-condensate density is obviously not well defined, since $t = s$, so that the integral (3.55) diverges at the lower limit. Since in the TF limit the energy spectrum (3.52) is approximately phonon-like, $E \approx \mathbf{p}^2 \sqrt{\mathbf{p}^2/2m + 2gn_c}/2m \approx \mathbf{p}^2 \sqrt{2gn_c}/2m$, the authors of [27] drew the false conclusion that the condensate is destabilized by long wavelength phonons in the 2D thermodynamic limit. We show that taking into account the discrete nature of the trap dissolves these difficulties and the problem is instead simply a failure of the semi-classical approximation.

[25] The TF approximation neglects the kinetic energy term and is valid for large particle numbers, which means a large mean-field interaction (c. f. [87]).

Hartree-Fock approximation. A possible way to remove the divergence problems of the semi-classical HFB equations is to neglect the $v(\mathbf{r})$ terms. This leads to the simplified Hartree-Fock (HF) energy spectrum

$$E_{\mathbf{p}}^{\mathrm{HF}}(\mathbf{r}) = \mathcal{L}_{\mathrm{sc}} \overset{(3.57)}{=} \frac{\mathbf{p}^2}{2m} + g n_c \ . \tag{3.58}$$

This spectrum predicts single particle like excitations and introduces an energy cutoff of size gn_c. This cutoff allows for a self-consistent solution at all temperatures, including a possible, additional uncondensed solution, i. e. a solution that does not invoke the existence of a condensate. In [27] the solution invoking the existence of a condensate has been found to have a lower free energy. Therefore, the HF approximation to the semi-classical equations predicts the existence of a condensate. However, the calculation of the condensed solution fails beyond a certain temperature, which is found to be about $0.8\,T_c$ for 10^4 atoms in this publication. Only for the uncondensed case have they found solutions at all temperatures.

Anomalous average. Later on we will need a semi-classical expression for the anomalous average. This is easily found by following the steps that lead to (3.55). Starting from

$$\widetilde{m} = \frac{1}{(2\pi\hbar)^2} \int \mathrm{d}^2 p \ \ u\, v^* \left(2\, f_{\mathrm{B}}(E) + 1\right) \ , \tag{3.59}$$

we perform the same steps and arrive at

$$\begin{aligned} \widetilde{m} = -\frac{m}{2\pi\hbar^2} \int_0^\infty \mathrm{d}E \, \left(2\, f_{\mathrm{B}}(E) + 1\right) \frac{g n_c}{\sqrt{E^2 + (g n_c)^2}} \\ \times \Theta\left(E - \sqrt{\left(U_{\mathrm{trap}} - \mu + 2gn\right)^2 - (g n_c)^2}\right) \ . \end{aligned} \tag{3.60}$$

The integral is logarithmically divergent for the non-thermal part on the upper boundary. Despite this, the semi-classical approximation will be used to calculate the anomalous average above the energy cutoff that is due to the limited number of basis states of our calculation. To do so, the integral (3.60) has to be renormalized in order to give finite results. The renormalization is described in detail in Section 6.5.

Need for a quantum mechanical calculation. Obviously the results from the semi-classical approximation of the HFB theory are not satisfying at all. The full semi-classical HFB equations indicate that BEC is not possible in 2D, because the condensate is destabilized by long wavelength phonons. The HF approximation predicts a

condensed solution and suppresses these phonons by introducing an energy cutoff, but still this solution cannot be found at all temperatures.
These problems with the semi-classical approximation were one motivation for the calculations undertaken for this thesis. The low-energy excitations of the condensate have to be treated fully quantum mechanically to take into account the discrete nature of the trap.

3.5. Broken symmetry and number conservation

In this section, we will briefly discuss the implications of the Bogoliubov approximation that was introduced in Section 3.2.
Assume the state of the condensate Ψ_0 to be a coherent state, so that

$$\hat{a}_0|\Psi_0\rangle = \sqrt{N_0}|\Psi_0\rangle \ . \tag{3.61}$$

Only then would replacing the operators $\hat{a}_0$ and $\hat{a}_0^\dagger$ by the c-number $\sqrt{N_0}$ be correct. A coherent state is constructed on a variable particle number, since it is an eigenstate of the creation and annihilation operators. However, this is not in accordance with the description of a state where the mean particle number is conserved and, therefore, cannot be combined with the description of BEC, since particle conservation is a crucial requirement for the occurrence of BEC, see Chapter 2.

The replacement of the ladder operators by numbers breaks the U(1) gauge symmetry of the Hamiltonian, since one chooses a *definite* ground state that naturally has a definite phase. An equivalent in the Ginzburg-Landau theory of magnetism is the choice of a specific direction for the magnetization. The choice of a definite phase implies the existence of an excitation mode of the condensate that corresponds to a rotation of this phase. Since the Hamiltonian does not depend on the phase, this mode must have zero energy.[26] It is the reason why a theory can only describe the excitation spectrum of the condensate correctly if it reproduces this mode, i. e. if it is gapless.

[26] This zero energy mode can be interpreted in terms of a massless particle, the Goldstone boson. It appears when a continuous symmetry is spontaneously broken. Assume a parabolic effective potential which is symmetric around the z-axis and an order parameter in two dimensions, corresponding to the phase of a condensate, residing in the origin of this effective potential. We define a vector $\mathbf{r}$, orthogonal to $\mathbf{z}$, from the z-axis to the surface of the effective potential. It can be shown within the Ginzburg-Landau theory, that the Goldstone mode corresponds to fluctuations of the order parameter that are *normal* to the vector $\mathbf{r}$ and to $\mathbf{z}$, and, thus, to a rotation of the phase of the order parameter.

It is worth mentioning that, complementary to the broken symmetry approach, number conserving approaches exist [17, 29, 35, 80]. In this case, no chemical potential is used, but another parameter ensures that particles added to the condensate must be taken away from the thermal atoms. This parameter defines the energy needed to add a particle *to the condensate* and corresponds to the chemical potential[27] in the broken symmetry approach. In fact, it is equal up to a difference $\sim 1/N_0$ to the chemical potential [79].

3.6. Linear response of the condensate – An alternative derivation of the Bogoliubov-de Gennes equations

Another way to derive the Bogoliubov-de Gennes equations is based on the linear response of the time dependent Gross-Pitaevskiĭ equation to a weak harmonic perturbation. Within the Popov approximation, we start with the time dependent GPE

$$i\hbar \frac{\partial \Psi(\mathbf{r},t)}{\partial t} = \left(\hat{h}_0(\mathbf{r}) + g\left[|\Psi(\mathbf{r},t)|^2 + 2g\tilde{n}(\mathbf{r})\right]\right)\Psi(\mathbf{r},t)\ . \tag{3.62}$$

The time dependence of the condensate state is given by $\Psi(\mathbf{r},t) = \Psi_0(\mathbf{r})\, e^{-i\mu t/\hbar}$. Inserting this in (3.62) yields the stationary GPE with the condensate eigenvalue μ.
As an ansatz for $\Psi(\mathbf{r},t)$, we superimpose a weak harmonic perturbation to the condensate wave function

$$\Psi(\mathbf{r},t) = e^{-i\mu t/\hbar}\left(\Psi_0(\mathbf{r}) + u_j(\mathbf{r})\, e^{-i\omega_j t} + v_j^*(\mathbf{r})\, e^{i\omega_j t}\right) \tag{3.63}$$

and then look for linear solutions in u and v. These coincide with the equations (3.41) that we have derived earlier from the grand-canonical Hamiltonian. The frequencies $\omega_j = E_j/\hbar$ are the collective excitation frequencies of the perturbatively driven condensate. They correspond to the quasiparticle energies in the Bogoliubov-de Gennes equations that were derived in 3.2.1. Generally, one has to distinguish between the collective nature of the excitations from the linear response approach and the elementary nature from the quasiparticle approach. However, for BEC the distinction vanishes and we refer to Section 3.7.2 for further discussion.
The linear response method leads somewhat more directly to the Bogoliubov equations without involving field theoretical methods. The validity of this method therefore underlines the classical nature of the condensate wave function within mean-field theory.

[27] Which, in the grand-canonical ensemble, defines the energy needed to add a particle *to the system.*

3.7. Excitations of the condensate

A condensate in a trap can be driven to carry out harmonic oscillations. One way to do so is to modulate the trapping potential with a certain frequency. For some frequencies the condensate will show resonance behaviour and carry out oscillations. These excitations have a collective nature, since they involve the motion of the whole condensate, see Section 3.7.2.
The first three excitation modes with the lowest energies are the *Kohn mode*, which corresponds to a center-of-mass motion of the condensate in the trap, the *breathing mode*, where the radius of the condensate shrinks and expands equally, and the *quadrupole mode* with an asymmetric breathing oscillation. Superimposed on this is also a rotational motion, since the angular momentum differs from zero. The generalized Kohn theorem [24] predicts the Kohn mode to be exactly at the trapping frequency if the confining potential is parabolic. This is well satisfied at low temperatures. Closer to the critical temperature there are noticeable deviations, because the actual potential is modified by the thermal atoms and not longer well approximated by a parabolic shape. The breathing mode has, as one would expect, a higher frequency, since the condensate is deformed by the motion. In two dimensions, it holds a peculiarity that will be presented in the following section.

By the time of writing this thesis, no excitation frequencies of a two-dimensional BEC have been measured. The group in Innsbruck has recently achieved Bose-Einstein condensation in 2D and has announced intentions to measure the excitation spectrum shortly [104].

3.7.1. Hidden symmetry of the 2D Hamiltonian

It has been shown that a trapped two-dimensional system, which is described by the Gross-Pitaevskiĭ equation, has oscillatory modes with a fundamental[28] frequency of 2ω, where ω is the trap frequency [60, 92]. Indeed, it can be shown that, in general, for a system of interacting particles in a harmonic trap that has a certain scaling behaviour, there exist fundamental modes with the frequency 2ω [93]. It is not a consequence of the mean-field theory, but a symmetry property of the quantum mechanical Hamiltonian.

[28] Independent of any parameters, like interaction strength, temperature or particle number and, therefore, an intrinsic property of the system.

Since it is a very elegant method and we observe such a mode in our calculation, we follow the outline of the publication from Pitaevskii and Rosch to explain the occurrence of these frequencies.

A uniform interacting system with a Hamilton operator

$$\hat{H}_0 = \sum_i -\frac{\hbar^2}{2m}\Delta + \sum_{i<j} V(\mathbf{r}_i - \mathbf{r}_j) \tag{3.64}$$

is scale invariant under a transformation $\mathbf{r} \to \lambda\,\mathbf{r}$, $\Psi_0(\mathbf{r}) \to \lambda\,\Psi_0(\mathbf{r})$ for a potential $V(\mathbf{r}-\mathbf{r}')$ that scales like

$$V(\lambda\,\mathbf{r}) = \lambda^{-2}\,V(\mathbf{r})\ . \tag{3.65}$$

This is easily proved by inserting the transformation into the Hamilton operator (3.64). In particular this is fulfilled for the two-dimensional contact interaction potential (3.6), given by $V(\mathbf{r}-\mathbf{r}') \sim \delta^{(2)}(\mathbf{r}-\mathbf{r}')$.
Adding the harmonic oscillator potential of the trap obviously breaks this symmetry. Nevertheless it is possible to construct a spectrum generating algebra that has a constant level spacing of $2\hbar\omega$ and is based on a symmetry of the full Hamiltonian[29]. This can be seen from the commutator of the full Hamiltonian with an operator that generates the described scale transformation. The results can then be summarized in an algebra which is formally equivalent to that of the two-dimensional Lorentz group,[30] i. e.

$$\begin{aligned}\left[\hat{L}_1, \hat{L}_2\right] = -i\hat{L}_3, \qquad \left[\hat{L}_2, \hat{L}_3\right] = i\hat{L}_1\\ \left[\hat{L}_3, \hat{L}_1\right] = -i\hat{L}_2\ .\end{aligned} \tag{3.66}$$

The operators $\hat{L}_i$ can be written as $\hat{L}^{\pm} \propto \hat{L}_1 \pm i\,\hat{L}_2$, so that one gets for the spectrum of an eigenstate $\hat{H}|\Psi_0\rangle = E_0|\Psi_0\rangle$

$$\hat{H}\hat{L}^{+}|\Psi_0\rangle = (E_0 + 2\hbar\omega)\,\hat{L}^{+}|\Psi_0\rangle\ . \tag{3.67}$$

The infinite number of these excitation modes with energy $2\hbar\omega$ can be each identified with a pulsation of the condensate by evaluating the operator for the mean-square displacement of the particles, i. e. the change of the size of the condensate, $\hat{I}(t) = \sum_i \mathbf{r}_i(t)^2$.

[29] That is $\hat{H} = \hat{H}_0 + \sum_i m\omega^2\mathbf{r}_i^2/2$.

[30] This algebra has a SU(1, 1) or SO(2, 1) symmetry. All the operators, including the Casimir operator of the group $\hat{C} = \hat{H}^2 - (2\omega)^2(\hat{L}_1^2 + \hat{L}_2^2)$ have analogies in the theory of relativity.

The equation of motion for $\hat{I}$ can equivalently be derived by completely classical considerations. To fully appreciate the physics of this hidden symmetry, this shall be done in a few lines. Assume an interaction potential that scales like $V(\lambda\,\mathbf{r}_i) = \lambda^n\,V(\mathbf{r}_i)$ and further a harmonic trapping potential $V_{\mathrm{tr}}(\mathbf{r}_i) = \sum_i \frac{1}{2}\,m\omega^2\mathbf{r}_i^2$. Analogous to the Virial theorem, we calculate

$$\begin{aligned}\frac{m}{2}\,\ddot{I} = \partial_t \sum_i \mathbf{p}_i\,\mathbf{r}_i = \sum_i \mathbf{p}_i\,\dot{\mathbf{r}}_i - \sum_i \mathbf{r}_i\,\mathrm{grad}_i\big(V(\mathbf{r}_i) + V_{\mathrm{tr}}(\mathbf{r}_i)\big)\\ = (2\,T - n\,V) - 2\,V_{\mathrm{tr}}\ ,\end{aligned} \tag{3.68}$$

where $\mathbf{p}_i = m\dot{\mathbf{r}}_i$ and $E = T + V$ the total, kinetic and potential energy, respectively. We see that for the same scaling behaviour named above in (3.65), $n = -2$, we get $\ddot{I} = 4E/m - 4I\omega^2$ with an oscillatory solution $I = A\,\cos(2\omega t + \gamma) + E/(m\omega^2)$. In this classical analogy we find pulsations of the condensate that also have a fundamental frequency of 2ω, which is due to the scaling behaviour of the two-dimensional δ-interaction.

Validity in three dimensions. In the three-dimensional case, the variables T and V are themselves dynamical quantities and will, in general, shift the frequency of 2ω. In certain limiting cases, as for cigar-shaped elongated condensates, this shift becomes small [55]. A transverse breathing mode with frequency 2ω has been observed in such a 3D elongated condensate [19].

3.7.2. Collective and elementary excitations

In a non-interacting gas excitations are particle like, since they are simply eigenmodes of the trap, or plane waves in the uniform case.
In an interacting system, single particle excitations are modified by the interaction with the surrounding atoms. In order to describe these excitations still as particle-like, the concept of quasiparticles is introduced. These represent the 'dressed' single particle excitations of atoms travelling past other atoms and interacting on the way. The physical properties of the quasiparticles are determined by the nature of the interactions. Particle like excitations exist in both the interacting and non-interacting gas and are referred to as *elementary excitations* of the system.

Another kind of excitations in many-body systems are *collective excitations*. They involve the simultaneous, wave-like motion of the whole system. Normally, these are

density fluctuations. For collective modes to exist, interactions between the atoms are crucial.

However, since a Bose-Einstein condensate is a superposition of single particle states, elementary excitations automatically involve the motion of the whole condensate. Hence, for a Bose condensed system, the two kinds of excitations coincide.
Formally, the elementary excitations are the quasiparticles that were introduced by the Bogoliubov transformation to diagonalize the full Hamiltonian in Section 3.2.1. The linear response approach in Section 3.6 yields the collective modes, since the linear response of the time dependent Gross-Pitaevskiĭ equation is the collective response of the whole condensate. As pointed out before, both approaches yield the Bogoliubov-de Gennes equations that are used to calculate the excitations of the condensate. A more detailed discussion can be found in [42].

4. Interactions

In this chapter we discuss the aspects of scattering in a two-dimensional Bose-Einstein condensate that are relevant for the Hartree-Fock-Bogoliubov theory used in this work. After some short comments on the three-dimensional case, we discuss in Section 4.2 how the coupling parameter is modified due to the reduction of dimensionality in the Gross-Pitaevskiĭ equation. The following sections go into more detail and we outline the derivation of the many-body T-matrix and its connection to the off-shell two-body T-matrix in the homogeneous limit. The anomalous average is of great importance for this discussion, and we show in detail in Section 4.4 how the ultraviolet divergences of the HFB theory are avoided by renormalizing the anomalous average.

We would like to point out that the theory of the treatment of scattering in dilute gases cannot be fully described within the frame of this thesis. For the sake of brevity some derivations and assumptions are merely sketched, and the reader is referred to [7, 48, 72, 73, 79, 80, 81, 98, 109, 111] for further details.

4.1. Coupling parameter

As an introduction, we briefly discuss the well-established results in three dimensions and then compare these with the two-dimensional case. The role of the coupling parameter g in the self-consistent HFB equations is discussed in the context of the two-dimensional Gross-Pitaevskiĭ equation in Section 4.2, especially in 4.2.2.
In three dimensions, the coupling parameter g is determined by the zero-energy and zero-momentum limit of the two-body transition matrix (T-matrix, Eqn. 4.13). Within this approximation, the coupling parameter depends on the s-wave scattering length[1]

[1] The scattering length a_{3D} is a quantity known from experimental results. In the genuine two-dimensional case we encounter a two-dimensional scattering length which is not known from experiment. However, it can be approximated through the 3D scattering length as long as we are in the quasi-2D regime, c. f. Section 4.2.2.

a_{3D} via

$$g = \frac{4\pi\hbar^2}{m} a_{3D} \ . \tag{4.1}$$

This, in combination with a contact interaction potential, as was introduced in Chapter 3, is a widely used approximation. However, many-body effects on the scattering process are neglected completely. The limit of this approximation for the coupling parameter becomes apparent in the excitation spectrum of a condensate in an anisotropic trap at finite temperatures [49].

In two dimensions, the described approach cannot be taken since the two-body T-matrix vanishes at all temperatures in the zero-energy limit. Thus, many-body effects must be taken into account via the many-body T-matrix even in the first order approximation. This can be done analytically at zero Kelvin by evaluating the two-body T-matrix at a shifted energy [73], c. f. Section 4.3.2.1. At finite temperatures this approximation, as derived in [73], is no longer a good description for the coupling parameter, and another approach to obtain the many-body T-matrix, which originates from the gapless HFB theories and involves the anomalous average, must be considered.

4.2. Reduction of dimensionality in the Gross-Pitaevskiĭ equation

We consider the condensate to be trapped in a three-dimensional, parabolic potential $U_{\text{trap}}(\mathbf{r}) = m\omega_\perp^2 r^2/2 + m\omega_z^2 z^2/2$, where $\omega_\perp$ and ω_z are the trapping frequencies in radial and axial direction, respectively. By increasing the trapping frequency in the axial direction, the confinement along this axis is increased. We are interested in the two-dimensional regime, where the condensate becomes flat in the sense that its mean-field energy is small compared to the energy spacing of the trap in the axial direction. Then, the dynamics of the system in this direction is restricted to zero-point oscillations, and the axial part of the wave function can be factorized, so that the system can be approximately described by a two-dimensional Gross-Pitaevskiĭ equation.

However, one must distinguish between different regimes for the scattering processes:

1. *Quasi-2D with 3D scattering:* The oscillator length l_z in the tightly confined direction is much larger than the 3D scattering length a_{3D} of the system. Collisions take place on the small length scale a_{3D}, and can, therefore, be considered to be three-dimensional, characterized by a coupling parameter g'_{3D}. However, the

extension of the wave function in the radial direction modifies the 3D coupling parameter as described in the Sections 4.2.1 and 4.2.2, c. f. (4.6).

2. *Quasi 2D:* If the scattering length becomes comparable to l_z , $l_z \gtrsim a_{3D}$, scattering can no longer be considered to be three-dimensional. The scattering problem in an axially confined geometry must be considered in detail, as done in [89]. This leads to an energy and trapping frequency dependent coupling parameter g_{q2D}. However, the result in [89] can also be expressed through the many-body T-matrix by the choice of an appropriate two-dimensional scattering length, as shown in [73], c. f. Section 4.2.2.

3. *Genuine 2D:* For $l_z \lesssim a_{3D}$, scattering must be considered purely two-dimensional. The many-body T-matrix in two dimensions must be evaluated with a genuine two-dimensional scattering length [73]. At the time of writing this thesis this regime is not yet experimentally accessible.

4.2.1. The two-dimensional GPE

We outline the steps that lead to the two-dimensional GPE. Even though it is structurally identical to the well-known three-dimensional case, it is instructive to see how interactions are affected by factorizing the tightly confined component. We follow the work of [54, 106].
In the regime in which we refer to the condensate as being two-dimensional, the dynamics along the tightly confined axis is restricted to zero-point oscillations, and we may separate that part from the three-dimensional condensate wave function

$$\Psi_0(\mathbf{r}) \equiv \Psi_0(r, \varphi, z) = \Psi_\perp(r, \varphi)\ \Psi_z(z, \rho_\perp)\ . \tag{4.2}$$

The axial part itself depends on the density of the condensate in the radial direction, $\rho_\perp(r, \varphi) = \int \mathrm{d}z\, |\Psi_0(\mathbf{r})|^2$.[2] We take the axial wave function to be normalized and real[3], so that $\rho_\perp(r, \varphi) = \Psi_\perp(r, \varphi)^2$. Now the radial part can be projected out of the GPE

[2] Depending on the density of the radial component, the axial wave function is more Gaussian or more Thomas-Fermi like [106].

[3] Due to the strong confinement along the axial direction, one can assume the condensate to be always in equilibrium, since the dynamics along the axis is much faster than in the radial plane. Hence, one can choose Ψ_z to be real, because a non-zero phase gradient implies condensate motion in this direction [106].

(3.40) for the wave function (4.2) by multiplying with $\Psi_z(z, \rho_\perp)$ and integrating over z. Doing so, we end up with an equation identical to (3.40) for $\Psi_\perp(r, \varphi)$, except that the three-dimensional coupling parameter has been replaced by

$$g'_{3\mathrm{D}} = g_{3\mathrm{D}} \int \mathrm{d}z \, \Psi_z(z, \rho_\perp)^4 \, . \tag{4.3}$$

Here, Ψ_z is simply given by the ground state of the harmonic oscillator, i. e. a Gaussian [73]

$$\Psi_z(z) = \sqrt[4]{\frac{m\omega_z}{\pi\hbar}} \, e^{-m\omega_z^2 z^2/2\hbar} \, . \tag{4.4}$$

This results in a modified GPE in two dimensions[4], where the 3D coupling parameter has been modified according to (4.3) by the integration, i. e.

$$\left(-\frac{\hbar^2}{2m} \Delta + \frac{m}{2} \omega_\perp^2 r^2 - \mu \right) \Psi_0(\mathbf{r}) + g'_{3\mathrm{D}} \left(n_c(\mathbf{r}) + 2\,\tilde{n}(\mathbf{r}) \right) \Psi_0(\mathbf{r}) = 0 \, , \tag{4.5}$$

where $\Psi_0(\mathbf{r}) \equiv \Psi_\perp(r, \varphi)$ now denotes the two-dimensional part of the condensate wave function.

The factorization of the tightly confined component can be done for each of the three cases described on page 46, since the crucial point for the separation ansatz (4.2) lies in the elimination of the condensate dynamics in this dimension and is not affected by the nature of collisions. The difference lies then in the treatment of the modified coupling parameter which appears in the lower dimensional GPE.

4.2.2. Coupling parameter in the two-dimensional GPE

We now discuss in detail which form the coupling parameter takes in each of the three cases listed in the beginning of this chapter.

First case *(quasi-2D with 3D scattering)*. To consider the first case, in which scattering processes still take place in three dimensions, one can assume the axial part of the wave function to be given by (4.4). With this, we can evaluate (4.3) and obtain the coupling parameter in the quasi-2D regime with three-dimensional scattering

$$g'_{3\mathrm{D}} = \sqrt{\frac{m\omega_z}{2\pi\hbar}} \, g_{3\mathrm{D}} \, . \tag{4.6}$$

Here, the coupling parameter in three dimensions is the two-body T-matrix in the low-energy low-momentum limit, given by (4.1).

[4] Exactly the same considerations lead to a one-dimensional equation, if one separates out two tightly confined dimensions.

Third case *(genuine 2D)*. In the genuine 2D limit, the many-body T-matrix approach described in detail in Section 4.3.2 leads to a coupling parameter of the form [73]

$$T_{\mathrm{MB}}(E=0) \equiv g_{\mathrm{2D}} = -\frac{4\pi\hbar^2}{m}\frac{1}{\ln(\mu m a_{\mathrm{2D}}^2/4\hbar^2)} \,. \tag{4.7}$$

The two-dimensional scattering length is a genuinely two-dimensional quantity and is not directly related to the scattering length in 3D. From a theoretical point of view the genuine-2D case is interesting since it constitutes the *true* two-dimensional regime, although it is not accessible to current experiments.

This result for the many-body T-matrix is strictly true only at zero temperature. At finite temperatures the T-matrix can be found numerically from the gapless HFB equation (4.36). For details refer to Section 4.3.2.

Second case *(quasi-2D)*. For the second case, interactions must be treated more carefully than in the first case. A detailed study of the modification of scattering processes within the quasi-2D regime is undertaken in [89]. We quote their result for the coupling parameter, keeping the notation used in [73], i. e.

$$g_{\mathrm{q2D}} = \sqrt{\frac{8\pi\omega_z\hbar^3}{m}}\left[\frac{1}{a_{\mathrm{3D}}} + \sqrt{\frac{m\omega_z}{2\pi\hbar}}\,\ln\left(\frac{B\hbar\omega_z}{2\mu\pi}\right)\right]^{-1} \,. \tag{4.8}$$

where $B \approx 0.915$. This coupling parameter interpolates between the quasi-2D regime with three-dimensional scattering ($l_z/a_{\mathrm{3D}} \gg 1$) and the regime where scattering is affected by the reduction in dimensionality ($l_z/a_{\mathrm{3D}} \gtrsim 1$). In the large l_z limit, the $1/a_{\mathrm{3D}}$ term dominates (4.8) and we retrieve (4.6). As l_z decreases, the second term dominates and we retrieve the equation for the many-body T-matrix (4.7), where the 2D scattering length a_{2D} has been approximated by

$$a_{\mathrm{2D}} = \sqrt{\frac{16\,\pi}{B}}\,l_z \exp\left(-\sqrt{\pi}\,\frac{l_z}{a_{\mathrm{3D}}}\right) \,. \tag{4.9}$$

Thus, the quasi-2D limit can be modelled via the many-body T-matrix approach by using a quasi-2D scattering length.

Trapped gas

Equations (4.7) and (4.8) are valid for the homogeneous gas. In a trap the coupling parameter depends on the condensate density, which can substitute the chemical potential via a local-density approach, see Section 4.3.2.3.

Note that through the dependence on the trapping frequency the 2D gas represents a system where the interparticle interaction strength can be tuned by modulating the confining potential in the z-direction in a manner analogous to the use of the Feshbach resonance in 3D [108]. It has even been suggested that the sign of the interaction strength (and hence whether the interactions are attractive or repulsive) can be changed by tuning the confining potential in the third direction [88].

4.3. Scattering theory

We give a brief motivation for the introduction of the transition matrix. For a detailed discussion we refer to [72, 73, 81, 111]. We consider the collision between two identical, free particles. In centre of mass coordinates, this process is described by the Schrödinger equation

$$\left[-\frac{\hbar^2}{2m}\,\Delta + V(\mathbf{r})\right]\psi(\mathbf{r}) = E_{\mathbf{k}}\,\psi(\mathbf{r})\ , \tag{4.10}$$

where m is the reduced mass, $\mathbf{r} = \mathbf{r}_1 - \mathbf{r}_2$ and $\mathbf{k} = (\mathbf{k}_1 - \mathbf{k}_2)/2$. At large distances from the scattering event, we consider an incoming particle in the form of a plane wave with momentum $\mathbf{k}$ that is scattered elastically and emerges as a spherical wave of momentum $\mathbf{k}'$, i. e.

$$\psi(\mathbf{r},\mathbf{k}) \xrightarrow{r\to\infty} e^{i\mathbf{k}\cdot\mathbf{r}} - \frac{2m}{4\pi\hbar^2}\,f(\mathbf{k}',\mathbf{k})\,\frac{e^{ik'r}}{r}\ , \tag{4.11}$$

where $k' = |\mathbf{k}'|$. The probability amplitude of the scattering event is determined by the factor in front of the outgoing wave. We identify the function $f(\mathbf{k}',\mathbf{k})$ with the two-body T-matrix which is discussed in the following section. In the case that $|\mathbf{k}| = |\mathbf{k}'|$, we refer to $f(\mathbf{k}',\mathbf{k})$ as the *half-on-shell* two-body T-matrix, and as the *off-shell* T-matrix if there are no restrictions whatsoever on $\mathbf{k}$ and $\mathbf{k}'$.

4.3.1. The two-body T-matrix

The two-body T-matrix describes collisions between two particles in vacuum. Effects of any surrounding medium are neglected. In terms of a general bare interaction potential $V(\mathbf{r})$, the off-shell two-body T-matrix is defined through the Lippmann-Schwinger

equation [73, 111]

$$\langle \mathbf{k}'|T_{2\mathrm{B}}(\bar{E})|\mathbf{k}\rangle = \langle \mathbf{k}'|V(\mathbf{r})|\mathbf{k}\rangle + \sum_{\mathbf{q}} \langle \mathbf{k}'|V(\mathbf{r})|\mathbf{q}\rangle \frac{1}{\bar{E} - (\epsilon^{\mathrm{sp}}_{\mathbf{K}/2+\mathbf{q}} + \epsilon^{\mathrm{sp}}_{\mathbf{K}/2-\mathbf{q}})} \langle \mathbf{q}|T_{2\mathrm{B}}(\bar{E})|\mathbf{k}\rangle \ . \tag{4.12}$$

The physical processes that contribute to the two-body T-matrix in this recursive equation are direct scattering from the momentum state $\mathbf{k}$ into the state $\mathbf{k}'$, and all processes that involve scattering through intermediate states of momentum $\mathbf{q}$. The intermediate states are *single particle states* with the single particle energies $\epsilon^{\mathrm{sp}}_{\mathbf{q}} = \hbar^2\mathbf{q}^2/2m$. We have omitted the contribution of the centre-of-mass momentum $\mathbf{K}$ and will do so in the remainder of this chapter, since it cancels in the denominator of (4.12). The single-particle states are plane wave states, since the two-body T-matrix accounts for vacuum contributions when there is no condensate present. The energy $\bar{E}$ is measured relative to that of a stationary particle.

In the low-momentum limit the T-matrix can be shown to depend only on the energy of the collision. This is the reason why the spatial dependence of the T-matrix can be modelled by a contact potential, i. e. $T_{2\mathrm{B}}(\mathbf{r}, \mathbf{r}', \bar{E}) = g(\bar{E})\,\delta(\mathbf{r})\delta(\mathbf{r} - \mathbf{r}')$ [81].

A solution to (4.12) can be found analytically in the zero-momentum limit at low energies under the assumption that the particles interact via a hard sphere potential with the hard-sphere radius a, i. e. in three, two and one dimensions

$$\langle \mathbf{0}|T^{3D}_{2\mathrm{B}}(\bar{E})|\mathbf{0}\rangle = \begin{cases} \dfrac{4\pi\hbar^2 a}{m}\left[1 - i\sqrt{m\bar{E}/\hbar^2}\,a - m\bar{E}a^2/3\hbar^2\right] & \text{for } E > 0 \\ \dfrac{4\pi\hbar^2 a}{m}\left[1 + \sqrt{m|\bar{E}|/\hbar^2}\,a - m\bar{E}a^2/3\hbar^2\right] & \text{for } E < 0\ , \end{cases} \tag{4.13}$$

$$\langle \mathbf{0}|T^{2D}_{2\mathrm{B}}(\bar{E})|\mathbf{0}\rangle = \frac{4\pi\hbar^2/m}{\pi i - 2\gamma - \ln(m\bar{E}a^2/4\hbar^2)} + O\left(\frac{Ea^2}{\ln(Ea^2)}\right)\ , \tag{4.14}$$

$$\langle 0|T^{1D}_{2\mathrm{B}}(\bar{E})|0\rangle = \begin{cases} -\dfrac{2\hbar^2}{ma}\left[i\sqrt{m\bar{E}/\hbar^2}\,a + m\bar{E}a^2/\hbar^2\right] & \text{for } E > 0 \\ -\dfrac{2\hbar^2}{ma}\left[\sqrt{m|\bar{E}|/\hbar^2}\,a - m\bar{E}a^2/\hbar^2\right] & \text{for } E < 0\ , \end{cases} \tag{4.15}$$

the last of which we give for completeness. In the three-dimensional case, we see that the familiar expression (4.1) is the leading order term in (4.13). In the two-dimensional case, the constant $\gamma \approx 0.577$ is the Euler constant.

Normally, scattering within the condensate is considered to take place at zero energy. From (4.14) we see that the transition matrix in two dimensions vanishes at zero

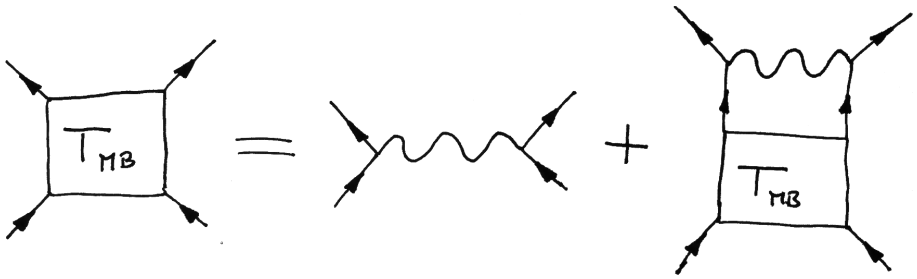

Figure 4.1.: Diagrammatic representation of the many-body T-matrix. The wavy line represents the interaction with the potential V. The solid lines correspond to the dressed one-particle propagator.

energy. Therefore, in 2D, the many-body T-matrix, which accounts for the background medium, must be used even to first order.

4.3.2. Scattering in a medium – The many-body T-matrix

The presence of the condensate alters scattering processes in two ways: Firstly, the scattering probability into and out of a certain momentum state, $\pm\hbar\mathbf{q}$ respectively, is enhanced by the population $n_{\pm\mathbf{q}}$ of this mode by a factor $1 + n_{\mathbf{q}} + n_{-\mathbf{q}}$.[5] Secondly, the excitation modes are modified by the underlying medium as described in Section 3.7.2. Therefore, the populations and energies of the single particle states in (4.12) are replaced by those of the quasiparticle states. This leads to a Lippmann-Schwinger equation that defines the many-body T-matrix analogous to (4.12), i. e.

$$\begin{aligned}\langle \mathbf{k}'|T_{\mathrm{MB}}(E)|\mathbf{k}\rangle = \langle \mathbf{k}'|V(\mathbf{r})|\mathbf{k}\rangle \\ + \sum_{\mathbf{q}} \langle \mathbf{k}'|V(\mathbf{r})|\mathbf{q}\rangle \frac{1 + n_{\mathbf{q}} + n_{-\mathbf{q}}}{E - (\epsilon^{\mathrm{qp}}_{\mathbf{q}} + \epsilon^{\mathrm{qp}}_{\mathbf{q}})} \langle \mathbf{q}|T_{\mathrm{MB}}(E)|\mathbf{k}\rangle \ .\end{aligned} \tag{4.16}$$

Here, the $\epsilon^{\mathrm{qp}}_{\mathbf{q}}$ denote quasiparticle energies.[6] Unlike the case for the two-body T-matrix, these energies actually depend on the center of mass momentum, but again we consider only the case $\mathbf{K} = \mathbf{0}$. The energy E is measured relative to the condensate and is, therefore, shifted to the energy $\bar{E}$ used in the previous section discussing $T_{2\mathrm{B}}$. The scattering event described through the T-matrix can be represented in diagrammatic form, shown in Figure 4.1.

[5] Scattering into a momentum state $\hbar\mathbf{q}$ is enhanced by a factor $n_{\mathbf{q}} + 1$, while scattering out of this state is just given a factor $n_{\mathbf{q}}$, so that we get $(n_{\mathbf{q}} + 1)(n_{-\mathbf{q}} + 1) - n_{\mathbf{q}} n_{-\mathbf{q}} = 1 + n_{\mathbf{q}} + n_{-\mathbf{q}}$.

[6] Usually in this thesis, we denote the quasiparticle energies with E, if E is not used differently.

4.3.2.1. Expressing $\mathbf{T_{MB}}$ in terms of $\mathbf{T_{2B}}$

The Lippmann-Schwinger equation (4.16) cannot be solved in such a straightforward manner as is possible for (4.12). Since it is possible to find an analytical expression for the two-body T-matrix, it is desirable to express the many-body T-matrix in terms of the two-body T-matrix. A simple way to do so, as used in the literature [73], is to compare (4.12) and (4.16) at zero temperature, where the population terms vanish. From this, the difference can only lie in the denominators. At zero temperature, we can use the Bogoliubov approximation, c. f. Section 3.4.2, in which the dispersion relation for the quasiparticles is given by

$$\epsilon_{\mathbf{q}}^{\mathrm{qp}} = \sqrt{\left(\epsilon_{\mathbf{q}}^{\mathrm{sp}}\right)^2 + 2\,\epsilon_{\mathbf{q}}^{\mathrm{sp}}\mu}\ . \tag{4.17}$$

For $\mu \lesssim \epsilon_{\mathbf{q}}^{\mathrm{sp}}$, we can expand this expression and get

$$\epsilon_{\mathbf{q}}^{\mathrm{qp}} \simeq \epsilon_{\mathbf{q}}^{\mathrm{sp}} + \mu\ . \tag{4.18}$$

Replacing this in the denominator of (4.16) shows that the many-body T-matrix is equivalent to the two-body T-matrix evaluated at the negative energy $\bar{E} = -2\mu$. Note that the negative sign of the energy removes the imaginary part in (4.14), since $\ln(-1) = i\pi$.

This simple justification for replacing the many-body T-matrix by the off-shell two-body T-matrix, evaluated at a negative energy, is only approximately correct.

A maybe more convincing analysis can be performed by minimizing the correction term $T_{\mathrm{corr}}(E, \bar{E})$ when writing down the relation

$$\langle \mathbf{k}'|T_{\mathrm{MB}}(E)|\mathbf{k}\rangle = \langle \mathbf{k}'|T_{\mathrm{2B}}(\bar{E})|\mathbf{k}\rangle + \langle \mathbf{k}'|T_{\mathrm{corr}}(E,\bar{E})|\mathbf{k}\rangle\ . \tag{4.19}$$

Rearranging (4.12) and substituting into (4.16), the correction term can be straightforwardly shown to be [73]

$$\begin{aligned}\langle \mathbf{k}'|T_{\mathrm{corr}}(E,\bar{E})|\mathbf{k}\rangle = &\sum_{\mathbf{q}\neq\mathbf{0}} \frac{\langle \mathbf{k}'|T_{\mathrm{2B}}(\bar{E})|\mathbf{q}\rangle(1+n_{\mathbf{q}}+n_{-\mathbf{q}})\langle \mathbf{q}|T_{\mathrm{MB}}(E)|\mathbf{k}\rangle}{E-(\epsilon_{\mathbf{q}}^{\mathrm{qp}}+\epsilon_{-\mathbf{q}}^{\mathrm{qp}})} \\ &- \sum_{\mathbf{q}} \frac{\langle \mathbf{k}'|T_{\mathrm{2B}}(\bar{E})|\mathbf{q}\rangle\langle \mathbf{q}|T_{\mathrm{MB}}(E)|\mathbf{k}\rangle}{\bar{E}-(\epsilon_{\mathbf{q}}^{\mathrm{sp}}+\epsilon_{-\mathbf{q}}^{\mathrm{sp}})}\ .\end{aligned} \tag{4.20}$$

Again, we set the centre-of-mass momentum to zero. Assuming that for some value $\bar{E} = \bar{E}^*$ the term $T_{\mathrm{corr}}(E, \bar{E}^*)$ vanishes and

$$\langle \mathbf{k}'|T_{\mathrm{MB}}(E)|\mathbf{k}\rangle = \langle \mathbf{k}'|T_{\mathrm{2B}}(\bar{E}^*)|\mathbf{k}\rangle\ , \tag{4.21}$$

we can determine $\bar{E}^*$ by setting $\langle \mathbf{k}'|T_{\mathrm{corr}}(E,\bar{E}^*)|\mathbf{k}\rangle = 0$. Using (4.21) in (4.20), we get in the limit $E = 0,\ \mathbf{k},\mathbf{k}' = \mathbf{0}$

$$\begin{aligned} 0 = &\sum_{\mathbf{q}\neq 0} \frac{\langle \mathbf{0}|T_{2\mathrm{B}}(\bar{E})|\mathbf{q}\rangle(1+n_{\mathbf{q}}+n_{-\mathbf{q}})\langle \mathbf{q}|T_{2\mathrm{B}}(\bar{E}^*)|\mathbf{0}\rangle}{-(\epsilon^{\mathrm{qp}}_{\mathbf{q}}+\epsilon^{\mathrm{qp}}_{-\mathbf{q}})} \\ &- \sum_{\mathbf{q}} \frac{\langle \mathbf{0}|T_{2\mathrm{B}}(\bar{E})|\mathbf{q}\rangle\langle \mathbf{q}|T_{2\mathrm{B}}(\bar{E}^*)|\mathbf{0}\rangle}{\bar{E}^* - (\epsilon^{\mathrm{sp}}_{\mathbf{q}}+\epsilon^{\mathrm{sp}}_{-\mathbf{q}})} \ . \end{aligned} \tag{4.22}$$

Since we expect the correction term to vanish, we can simply divide by the T-matrices. Firstly we look at the zero-temperature case, where the population terms in the first nominator are zero. A continuum approximation of (4.22) yields the general D-dimensional integral equation

$$0 = \int_0^\infty \mathrm{d}k \ \left\{ \frac{k^{D-1}}{-2\epsilon^{\mathrm{qp}}_{\mathbf{k}}} - \frac{k^{D-1}}{\bar{E}^* - 2\epsilon^{\mathrm{sp}}_{\mathbf{k}}} \right\} \ , \tag{4.23}$$

where the quasiparticle energies are given by the dispersion relation (4.18). In two dimensions this equation can be solved analytically to give $\bar{E}^* = -\mu$, thus

$$T^{2D}_{\mathrm{MB}}(0) = T^{2D}_{2\mathrm{B}}(-\mu) \ . \tag{4.24}$$

This somewhat better justified ansatz leads to the same result as the method explained in the beginning of this section, although the exact energy at that we have to evaluate $T_{2\mathrm{B}}$ is only half the value.

The described treatment is exact to the level of approximations we use. Thus, Eqns. (4.20) and (4.24) are exact if there exists a solution to (4.23). In the one-dimensional case, the integral (4.23) diverges and the validity of the result is somewhat delicate to justify. However, the many-body T-matrix is found to be $\propto |\Psi_0|^2$ in the Tonks-Gireadeau regime, so that the nonlinearity in the GPE is $\propto |\Psi_0|^4$ [73]. This agrees with the exact known results [36] for the 1D gas in this regime.

4.3.2.2. Expressing $\mathbf{T_{MB}}$ in terms of $\mathbf{T_{2B}}$ at finite temperatures

In order to go beyond the zero temperature limit, we consider the continuum limit of (4.22) with the population terms in two dimensions. To facilitate a numerical solution, we divide the whole equation by $\hbar^2/2m$ and substitute $2m\mu/\hbar^2 = k_\mu$, $2m\bar{E}^*/\hbar^2 = \widetilde{E}^*$, $2mk_{\mathrm{B}}T/\hbar^2 = \widetilde{T}$, which leads to the following equation

$$0 = \int_{k_{\mathrm{cut}}}^\infty \mathrm{d}k \ \left\{ \frac{(2f_{\mathrm{B}}+1)\,k}{-2\sqrt{k^4+2k^2k_\mu^2}} - \frac{k}{\widetilde{E}^* - 2k^2} \right\} \ , \tag{4.25}$$

where $f_{\mathrm{B}} = \left(\exp\left[\left(-\sqrt{k^4 + 2k^2k_\mu^2} - k_\mu^2\right)/\widetilde{T}\right] - 1\right)^{-1}$. The solution to this equation is to be found in the three-dimensional parameter space $\{T, \mu, k_{\mathrm{cut}}\}$, where we hope the dependence on the explicit choice of the chemical potential and the cutoff are weak so that a dependence upon T can be extracted at least for very low temperatures. However, we found the dependence on the cutoff was not negligible.

The difficulties in solving this equation lie in the divergence of the integral (4.25) at the lower boundary. This arises from the background that there is no condensate at finite temperatures in the homogeneous case, where the expressions for the T-matrices are derived. By introducing a cutoff in k-space, we implicitly assume that we still have a large population of *different* energy levels up to this cutoff which we treat as equivalent to a condensate. If we choose the cutoff high enough, the solution of the integral should be independent of it, since the states with high momenta are expected to be only sparsely populated. Following this, the cutoff must correspond to an energy of the order of the chemical potential, which can be found from the self-consistent solution of the HFB equations beforehand. For our parameters, a typical value for the maximal condensate density is $10^{13}\,\mathrm{m}^{-2}$, which gives $\mu = gn_c \approx 10^{-32}\,\mathrm{J}$. This corresponds to a k-value of $k_\mu \approx 10^6$ and the cutoff should be chosen of this magnitude.

Another possibility to avoid divergence problems is to use the approximation (4.18) for the quasiparticle spectrum, which naturally introduces an energy cutoff which is consistent with the previously discussed cutoff. This approach has been investigated recently in the homogeneous limit [99]. Nevertheless, the density of the condensate cannot be neglected at higher temperatures and we found large discrepancies between the results obtained within the Thomas-Fermi approximation in this publication and our results, obtained by using gapless HFB, where the density is naturally included in the many-body T-matrix.

4.3.2.3. Non-uniform case

The expressions for the two-body T-matrix derived above are strictly valid in the homogeneous gas, since the trapping potential has not been taken into account in the derivation of (4.14). Provided the trapping potential varies slowly on the length scale on which interactions take place, one can use the homogeneous relation $\mu = gn_c(\mathbf{r})$ within a local density approximation. This results in a spatially dependent coupling

parameter in 2D [73]

$$g_{2\mathrm{D}}(\mathbf{r}) = \langle \mathbf{0}|T_{2\mathrm{B}}^{2D}(-\mu)|\mathbf{0}\rangle = -\frac{4\pi\hbar^2}{m}\frac{1}{\ln\left(n_c(\mathbf{r})\, g_{2\mathrm{D}}(\mathbf{r})\, m a_{2\mathrm{D}}^2/4\hbar^2\right)} \,. \tag{4.26}$$

To first order, this is approximated from iteration by

$$g_{2\mathrm{D}}(\mathbf{r}) \approx -\frac{4\pi\hbar^2}{m}\frac{1}{\ln\left(n_c(\mathbf{r})\, \pi a_{2\mathrm{D}}^2\right)} \,, \tag{4.27}$$

which we use as a starting point in solving (4.26) self-consistently. The scattering length $a_{2\mathrm{D}}$ depends on the regime we are in. In the case of a purely two-dimensional condensate ($l_z \lesssim a_{3\mathrm{D}}$) the correct value must actually be measured in a genuinely 2D experiment. In the quasi-2D regime, $a_{2\mathrm{D}}$ can be expressed through the three-dimensional scattering length and the oscillator length in the tightly confined dimension to recover the results derived in [89], i. e.

$$a_{2\mathrm{D}} = 4\sqrt{\frac{\pi}{B}}\, l_z\, e^{-\sqrt{\pi}\, l_z/a_{3D}} \,, \tag{4.28}$$

where the constant is $B \approx 0.915$ [73]. Regarding the different regimes, see also Section 4.2.

4.3.3. The many-body T-matrix in gapless HFB

We now show how the many-body T-matrix arises from the anomalous average in the G1 and G2 theories. The proof is based on an analogous definition of the many-body T-matrix and the off-diagonal potential $\mathcal{M}_{\mathrm{G}}$ in gapless HFB, c. f. (3.43) and (3.45), in the homogeneous limit, where the Bogoliubov-de Gennes equations can be solved analytically. A slightly different approach can be found in [50, 98].

We start with the homogeneous expressions (3.53) for the quasiparticle amplitudes and insert these into the expression (3.31) for the anomalous average, i. e.

$$\begin{aligned} \widetilde{m} &= \sum_i \frac{\sqrt{\mathcal{L}_{\mathrm{sc}}^2(E_i) - E_i^2}}{2E_i}\Big(2f_{\mathrm{B}}(E_i) + 1\Big) \\ &= -\sum_i \frac{g n_c}{2E_i}\Big(2f_{\mathrm{B}}(E_i) + 1\Big) \,, \end{aligned} \tag{4.29}$$

where we have used (3.52). We can identify the condensate density with the off-diagonal potential $\mathcal{M}$, given by $g n_c(\mathbf{r})$ in the Popov case, c. f. Section 3.4.3.1, so that we can write the anomalous average as

$$\widetilde{m}(\mathbf{r}) = -\mathcal{M}\sum_i \frac{1}{2E_i}\Big(2f_{\mathrm{B}}(E_i) + 1\Big) \,. \tag{4.30}$$

This follows from the BdG equations in the homogeneous case and is in general independent on the approximation (Popov, G1, G2). This means that (4.30) can be shown to define the anomalous average in terms of the off-diagonal potential in the BdG equations, independent of the explicit form $\mathcal{M}$. Here, we have chosen $\mathcal{M} = gn_c$ from the Popov approximation, but the calculation for any different off-diagonal potential leads to the same relation. In the gapless extension, the off-diagonal potential contains an additional term

$$\mathcal{M}_{\mathrm{G}} = g\Psi_0(\mathbf{r})^2 + g\widetilde{m}(\mathbf{r}) \ . \tag{4.31}$$

Substituting $\widetilde{m}$ in (4.31) by inserting (4.30) leads to a Lippmann-Schwinger equation for the off-diagonal potential, i. e.

$$\frac{\mathcal{M}_{\mathrm{G}}}{\Psi_0(\mathbf{r})^2} = g + g\,\frac{\mathcal{M}_{\mathrm{G}}}{\Psi_0(\mathbf{r})^2}\sum_i \frac{1}{-2E_i}\Big(2f_{\mathrm{B}}(E_i)+1\Big) \ . \tag{4.32}$$

This equation is equivalent to the definition of the many-body T-matrix introduced in the beginning of Section 4.3.2. To see this, we consider the zero-energy low-momentum limit of (4.16) at zero temperature. In order to evaluate the matrix elements, we use a contact interaction potential, which means

$$\langle \mathbf{0}|V(\mathbf{r}-\mathbf{r}')|\mathbf{0}\rangle = g\,\delta(\mathbf{r}-\mathbf{r}') \ , \quad \langle \mathbf{0}|T_{\mathrm{MB}}(0)|\mathbf{0}\rangle = T_{\mathrm{MB}}(\mathbf{r})\delta(\mathbf{r}) \ . \tag{4.33}$$

With this, we get from (4.16)

$$T_{\mathrm{MB}}(\mathbf{r}) = g + g\,T_{\mathrm{MB}}(\mathbf{r})\sum_i \frac{1}{-2E_i}\Big(2f_{\mathrm{B}}(E_i)+1\Big) \ . \tag{4.34}$$

Direct comparison of (4.32) and (4.34) yields

$$T_{\mathrm{MB}}(\mathbf{r}) \equiv \frac{\mathcal{M}_{\mathrm{G}}}{\Psi_0(\mathbf{r})^2} \ . \tag{4.35}$$

Hence, in gapless HFB the many-body T-matrix is introduced through the occurrence of the anomalous average in the explicit form

$$T_{\mathrm{MB}}(\mathbf{r}) = g\left(1+\frac{\widetilde{m}(\mathbf{r})}{\Psi_0(\mathbf{r})^2}\right) \ . \tag{4.36}$$

4.4. Renormalization of the anomalous average

The anomalous average in the HFB theory is ultraviolet divergent, c. f. Section 3.4.1. As can be seen from both the discrete sum in (3.31) and the semi-classical expression

(3.60), this divergence comes from the non-thermal part, i. e. the '1' in $(2f_{\mathrm{B}}(E_i)+1)$. The usual method to resolve this problem is to drop the '1' [48]. However, for the two-dimensional case which is subject of this work, we have found it necessary to study the renormalization of this divergence more carefully and to use a more sophisticated renormalization method. This is because through the ansatz in Section 4.3.3 and the alternative method described in Section 4.3.2.1, we can directly compare the results arising from two different backgrounds for the many-body T-matrix. Its definition by the off-shell two-body T-matrix depends only on the condensate density. The gapless HFB theory defines the many-body T-matrix via the anomalous average and, hence, the many-body T-matrix is also dependent on the renormalization of $\widetilde{m}$. Since both approaches must agree at zero temperature, we can infer information about the validity of the renormalization.

4.4.1. Origin of the renormalization

To motivate the renormalization procedure, we briefly discuss its origin from the relation between the anomalous average and the T-matrix. Details can be found in [79]. In Section 4.3.3 we have outlined how the many-body T-matrix is defined through the anomalous average in the homogeneous limit. This follows from the Lippmann-Schwinger type of equation for the off-diagonal matrix element $\mathcal{M}_{\mathrm{G}}$, which is defined in terms of the bare interaction potential $V(\mathbf{r}-\mathbf{r}')$. In the pseudo potential approximation, the matrix elements of the bare potential are replaced by the contact interaction δ-potential. However, if instead the two-body T-matrix is used, this leads to the appearance of an extra term which, together with $\widetilde{m}$, we identify as a renormalized anomalous average $\widetilde{m}^R$. Thus, replacing the bare interaction potential by the two-body T-matrix is consistent to all orders in the Lippmann-Schwinger equation if it is accompanied by this renormalization.

4.4.2. Renormalization procedure

In this section we introduce two different methods for the renormalization procedure. We use the semi-classical renormalization scheme for our calculations.

4.4.2.1. Method one – Semi-classical calculation

To simplify the formulation within this section, we omit the notation of spatial dependencies and introduce the following notation for the different parts of the anomalous average

$$\begin{aligned}\widetilde{m}^R &= \sum_i \left(2f_{\mathrm{B}}(E_i)+1\right) u_i v_i \times \Theta(\epsilon_{\max}-E_i) \\ &\quad + \int_{\epsilon_{\max}}^{\infty} \mathrm{d}E\ \{\widetilde{m}'_{\mathrm{sc}}(E)-\widetilde{m}'_{\mathrm{r}}(E)\} - \int_0^{\epsilon_{\mathrm{cut}}} \mathrm{d}E\ \widetilde{m}'_{\mathrm{r}}(E) \\ &\equiv \widetilde{m}_{\mathrm{qm}} + \widetilde{m}_1 - \widetilde{m}_2\ .\end{aligned} \tag{4.37}$$

Here, the first part $\widetilde{m}_{\mathrm{qm}}$ is calculated quantum mechanically by explicitly evaluating the sum according to (3.31). The second part, $\widetilde{m}_1$, contains the contribution from the energy levels above the energy cutoff $\epsilon_{\max}$, which arises from the finite number of basis states, c. f. Section 6.4.4. The third part, $\widetilde{m}_2$, is the renormalization of $\widetilde{m}_{\mathrm{qm}}$. Both $\widetilde{m}_1$ and $\widetilde{m}_2$ are calculated within the semi-classical approximation. This is justified since the derivation of the many-body T-matrix is exact only in the homogeneous limit and the renormalization of $\widetilde{m}$ should be performed within the same approximation in which scattering is treated. The prime indicates that $\widetilde{m}'_{\mathrm{sc}}$ and $\widetilde{m}'_{\mathrm{r}}$ are only the integrands in (4.37).

We start from the semi-classical expression (3.60) for the anomalous average, of which the integrand is given by

$$\begin{aligned}\widetilde{m}'_{\mathrm{sc}}(E) = &-\frac{m}{2\pi\hbar^2}\left(2\,f_{\mathrm{B}}(E)+1\right)\frac{gn_c}{\sqrt{E^2+(gn_c)^2}} \\ &\times\Theta\left(E-\sqrt{(U_{\mathrm{trap}}-\mu+2gn)^2-(gn_c)^2}\right)\ .\end{aligned} \tag{4.38}$$

To calculate the excessive contribution towards the anomalous average, we consider the case $n_c \to 0$. In this sense we keep only terms linear in the condensate density. This arises from the assumption that we renormalize the vacuum contributions to $\widetilde{m}$ at zero temperature that have already been accounted for in the measured scattering length in the two-body T-matrix. In the limit that there is no condensate present, the quasiparticle energies are replaced by the single particle energies. Since the quasiparticle energies are measured relative to the condensate, we replace

$$E \quad \to \quad E+\mu\ . \tag{4.39}$$

Doing so in (4.38) and regarding only the temperature independent part leads to

$$\widetilde{m}_{\mathrm{r}}(E) = -\frac{m}{2\pi\hbar^2}\,\frac{gn_c}{E+\mu}\ . \tag{4.40}$$

Above the Energy Cutoff. With this, we can calculate the semi-classical part of $\widetilde{m}^R$ above the energy cutoff

$$\widetilde{m}_1 = \int_{E_{\mathrm{min}}}^{\infty} \mathrm{d}E\,\left(\widetilde{m}_{\mathrm{sc}}(E) - \widetilde{m}_{\mathrm{r}}(E)\right)\ . \tag{4.41}$$

The lower limit of the integral is determined by the maximum of the Heaviside function in (3.60) and the cutoff energy, i. e.

$$E_{\mathrm{min}} = \max\left\{\epsilon_{\mathrm{max}}, \sqrt{(U_{\mathrm{trap}} - \mu + 2gn)^2 - (gn_c)^2}\right\}\ . \tag{4.42}$$

Note that the shift of the energy in the denominator of (4.40) prevents the integral from being singular at the upper limit.

Since the semi-classical part (4.38) of the anomalous average is divergent at the upper boundary, the renormalization (4.40) must be subtracted under the same integral, so that we get for (4.41)

$$\widetilde{m}_1 = -\frac{m}{2\pi\hbar^2}\int_{E_{\mathrm{min}}}^{\infty}\mathrm{d}E\ gn_c\left(\frac{2\,f_{\mathrm{B}}(E)+1}{\sqrt{E^2-(gn_c)^2}} - \frac{1}{E+\mu}\right). \tag{4.43}$$

Below the Energy Cutoff. Since the sum in $\widetilde{m}_{\mathrm{qm}}$ has a natural cutoff it does not diverge in the calculation. However, it contains contributions from the zero-temperature limit that must be renormalized by subtracting the integral of $\widetilde{m}_{\mathrm{r}}$ below the energy cutoff. In analogy to (4.43), this is given by

$$\widetilde{m}_2 = -\frac{m}{2\pi\hbar^2}\int_0^{E_{\mathrm{min}}}\mathrm{d}E\ \frac{gn_c}{E+\mu}\ . \tag{4.44}$$

4.4.2.2. Method two – Perturbative calculation

Another method to renormalize the anomalous average is based on a perturbative treatment of the quasiparticle amplitudes. This calculation is based on the quantum mechanical calculation, as opposed to the method described in the previous section, which is based on the semi-classical approximation. Naturally, this method is subjected

to an energy cutoff and is unable to renormalize any semi-classical contribution to $\widetilde{m}$ above this cutoff. If a semi-classical approximation is used, the previously described renormalization method must be used in addition. Still, Method one seems to be better justified, since the contributions that need to be renormalized originate from regions where the Bose condensed system is treated within a semi-classical or local density approach. The renormalization technique should be based on the same approximation. However, theoretically this approach is justified and leads to comparable results.

The following description omits details of the calculation, but makes clear what steps are undertaken in order to obtain the renormalized anomalous average. We denote the part of $\widetilde{m}$ that contains the renormalization with $\widetilde{m}_{\mathrm{pert}}$. This part is to be subtracted from the quantum mechanical part $\widetilde{m}_{\mathrm{qm}}$ in (4.37), i. e. $\widetilde{m}^R = \widetilde{m}_{\mathrm{qm}} - \widetilde{m}_{\mathrm{pert}}$.

To calculate the perturbative limit, we consider the case that the condensate fraction goes to zero, $n_c \to 0$. We expand the quasiparticle amplitudes in the basis of the harmonic oscillator, $\{\chi_\alpha\}$,

$$u_i^p = \sum_\alpha a_\alpha^i \chi_\alpha \ , \qquad v_i^p = \sum_\alpha b_\alpha^i \chi_\alpha \ . \tag{4.45}$$

The perturbative limit of $\widetilde{m}$ is then given by

$$\widetilde{m}_{\mathrm{pert}} = \sum_i u_i^p v_i^p \ . \tag{4.46}$$

To obtain the expansion coefficients α_i, β_i, we insert (4.45) into the BdG equations (3.41) and consider the condensate density to be only a small perturbation to the non-interacting case, since the non-linearity goes to zero as $n_c \to 0$. In the non-interacting case, the eigensolutions of the GPE are given by the eigenstates of the trap.[7] The expansion coefficients and the energies in (4.45) are then given by

$$a_\alpha^i = \delta_{i\alpha} + \delta a_\alpha^i \ , \tag{4.47}$$

$$b_\alpha^i = \delta b_\alpha^i \ , \tag{4.48}$$

$$E_i = \epsilon_i + \delta E_i \ . \tag{4.49}$$

Using this in the BdG equations and neglecting all terms of second or higher order in n_c, the coefficients can be shown to be

$$\delta a_\alpha^i = g \frac{\int \mathrm{d}^2 r \ \chi_\alpha^* n_c \chi_i}{\epsilon_\alpha - (-1)^{\delta_{\alpha i}} \epsilon_i} \ , \tag{4.50}$$

$$\delta b_\alpha^i = g \frac{\int \mathrm{d}^2 r \ \chi_\alpha^* n_c \chi_i}{\epsilon_\alpha + \epsilon_i} \ . \tag{4.51}$$

[7] This means, the Hartree-Fock basis (c. f. Section 6.3.2) becomes the basis of the harmonic oscillator.

With this, the sum (4.46) can be evaluated.

5. Phase Fluctuations

A defining characteristic of a Bose-Einstein condensate is its property of coherence. Two overlapping Bose-Einstein condensates show interference fringes [3], and coherence is also the fundamental requirement for output coupling of an atom laser beam. A BEC is a coherent matter wave source, as the resonator of a laser beam is a source of coherent electro-magnetic waves. This aspect of BEC is the most crucial requirement for potential applications.

While phase coherence is normally taken for granted in three-dimensional condensates, in lower dimensions it is more easily disturbed by the increased occurrence of phase fluctuations. In three dimensions, these are mostly suppressed so that fluctuations of the condensate are mainly density fluctuations (see Section 5.3). Only close to the critical temperature is there a phase fluctuating regime, referred to as the *Ginzburg region*. In two dimensions however, phase fluctuations are responsible for the destruction of the global phase of the condensate at finite temperatures well below the critical temperature, where the transition to the superfluid phase occurs. This leads to the definition of a *quasicondensate*. The transition from a true condensate to a quasicondensate is of central interest in current studies of two- (and one-) dimensional Bose condensed systems.

In this chapter, the formalism required for the description of phase fluctuations is summarized. We start with the characterization of a phase-fluctuating condensate in Section 5.1. Then the fundamental principle of off-diagonal long-range order is demonstrated from a many-particle point of view in Section 5.2.1 and set into context with the mean-field description of the correlation function in Sections 5.2.2 and 5.2.3. The original definition of Bose-Einstein condensation by Penrose and Onsager in terms of the decay behaviour of the correlation function is given in Sections 5.2.4 and 5.2.5. Section 5.3 takes a mean-field approach based on the work by Petrov and Shylapnikov to gain a quantitative result for the onset of the phase-fluctuating regime. The last Section then reviews two experiments that are directly concerned with the measurement of the correlation function and, therefore, have influenced the work on this thesis.

5.1. Characterization of phase-fluctuating condensates

The new term of a *quasicondensate* is introduced to address the phenomenon of a condensate with a *coherence length* l_ϕ that is smaller than its extension, $l_\phi < R$ [88, 90]. In a true BEC, the coherence length is of the same size as the condensate. This means that a global phase extends throughout the whole BEC. In highly distorted condensates, i. e. quasi-1D elongated cigar shaped [91] or 2D pancake shaped, however, the phase is not globally coherent, but fluctuating at temperatures higher than a certain temperature T_ϕ, which is smaller than the critical temperature $T_\phi < T_c$. In the regime between T_ϕ and T_c, we refer to the condensate as a quasicondensate. This is coherent only in blocks of a characteristic size l_ϕ. In systems that are likely to show phase fluctuations, a true BEC is achievable only at temperatures below T_ϕ.

The phase fluctuating regime of a two-dimensional quasicondensate is often referred to as the Kosterlitz-Thouless (KT) phase.[1] The temperature T_ϕ is the critical temperature at which the system is expected to undergo another phase transition into the KT phase (c. f. Section 1.1).[2] However, the exact properties of this fluctuating phase still need to become investigated.

The distinction between a quasicondensate and a true condensate is not obvious at first sight. The density distribution remains unchanged by the emergence of phase fluctuations. Differences can be seen in the momentum profile, which has a temperature dependent half width, c. f. Section 5.2.2, or the failure to produce an interference pattern when overlapping two quasicondensates. Furthermore, the study of coherence properties based on interferometric measurements has been shown to be very successful in elongated, quasi one-dimensional condensates, c. f. Section 5.4.2.

[1] The KT phase is a phase-fluctuating state dominated by bound vortex/antivortex pairs, constituting topological charges or defects of the system. The phase-fluctuating condensate does, however, not necessarily have to be in this state. The nature of the phase-fluctuating regime will be studied in our group in the future.

[2] This is not the temperature at which the KT phase transition occurs. With T_ϕ, we define the lower temperature boundary of the KT phase, whereas the transition at the upper boundary is referred to as the KT phase transition. This transition refers to the case when the phase fluctuations in the form of bound vortex/antivortex pairs unbind and become free topological charges.

5.2. Off-diagonal long-range order

A quantitative and qualitative description of phase fluctuations in the system is possible by means of the *correlation* or *coherence function* of the condensate. The underlying principle is the occurrence of long-range order in density matrices of the many-body system. The following section is based on a formulation in terms of the many-body wave function of the system. The more practical form for our purposes in terms of the Bose field operators is introduced in the Sections 5.2.2 and 5.2.3.

5.2.1. Diagonal and off-diagonal long-range order – Definition of the diagonal and off-diagonal density matrix

In order to investigate correlations in a physical system, one must determine the density matrix and study its properties. A crystalline system, where the spacing between atoms is based on a regular pattern, shows long-range order in the diagonal density matrix (DLRO). In superfluid systems, like BEC, the correlations within the condensate are not that obvious anymore. However, the mere existence of a defined condensate phase[3] is connected to a certain kind of order in the long-range behaviour of the off-diagonal single-particle density matrix $\tilde{\rho}_1(\mathbf{r}, \mathbf{r}')$, namely off-diagonal long-range order (ODLRO).

We begin by introducing the density matrices in terms of the many-body wave function. In this form, the physical content is more obvious, even though it is equivalent to the operator form introduced in the two following sections.
Consider the normalized wave function $\Psi_0(\mathbf{r}_1, \ldots, \mathbf{r}_N)$ of a many-body system. We define the diagonal and off-diagonal density matrix as

$$\rho_N(\mathbf{r}_1, \ldots, \mathbf{r}_N) = |\Psi_0(\mathbf{r}_1, \ldots, \mathbf{r}_N)|^2 \tag{5.1}$$

$$\text{and} \quad \tilde{\rho}_N(\mathbf{r}_1, \ldots, \mathbf{r}_N, \mathbf{r}'_1, \ldots, \mathbf{r}'_N) = \Psi_0^*(\mathbf{r}_1, \ldots, \mathbf{r}_N)\Psi_0(\mathbf{r}'_1, \ldots, \mathbf{r}'_N) \ , \tag{5.2}$$

respectively. From this, we obtain the diagonal and off-diagonal one-particle density matrix by integrating over all but one set of coordinates in the following way,

$$\rho_1(\mathbf{r}_1) = \int \mathrm{d}\mathbf{r}_2 \cdots \mathrm{d}\mathbf{r}_N \ |\Psi_0(\mathbf{r}_1, \ldots, \mathbf{r}_N)|^2 \tag{5.3}$$

$$\tilde{\rho}_1(\mathbf{r}_1, \mathbf{r}'_1) = \int \mathrm{d}\mathbf{r}_2 \cdots \mathrm{d}\mathbf{r}_N \ \Psi_0^*(\mathbf{r}_1, \mathbf{r}_2, \ldots, \mathbf{r}_N)\Psi_0(\mathbf{r}'_1, \mathbf{r}_2, \ldots, \mathbf{r}_N) \ , \tag{5.4}$$

[3] Here 'phase' refers to the fraction of atoms in a single quantum state and not to the mathematical phase of the wave function.

where in the off-diagonal case the sets that are integrated over are set equal.[4]
We define a function

$$G^{(1)}(\mathbf{r}_1 - \mathbf{r}_1') \propto \tilde{\rho}_1(\mathbf{r}_1, \mathbf{r}_1') \tag{5.5}$$

that depends only on the distance between two particles in the one-particle off-diagonal density matrix. We identify $G^{(1)}(\mathbf{r}_1 - \mathbf{r}_1')$ with the first order correlation function.

5.2.2. Correlation function and momentum distribution

Consider the Bose field operator $\hat{\psi}(\mathbf{r})$ and its Fourier transform

$$\hat{\phi}(\mathbf{k}) \equiv \int \mathrm{d}^2 r \; e^{-i\mathbf{k}\cdot\mathbf{r}} \, \hat{\psi}(\mathbf{r}). \tag{5.6}$$

To find the number of particles with momentum $\mathbf{k}$, we look at the average

$$n(\mathbf{k}) = \langle \hat{\phi}^\dagger(\mathbf{k}) \hat{\phi}(\mathbf{k}) \rangle = \int \mathrm{d}^2 r \, \mathrm{d}^2 r' \; e^{i\mathbf{k}\cdot(\mathbf{r}-\mathbf{r}')} \, \langle \hat{\psi}^\dagger(\mathbf{r}) \hat{\psi}(\mathbf{r}') \rangle \; . \tag{5.7}$$

The function $n(\mathbf{k})$ is the momentum distribution of the many-body system. It is the Fourier transform of the quantity $\langle \hat{\psi}^\dagger(\mathbf{r}) \hat{\psi}(\mathbf{r}') \rangle$ and we now show that the r. h. s. is equivalent to the previously defined function (5.5).

The r. h. s. of (5.7) depends only on the difference $\mathbf{s} = \mathbf{r} - \mathbf{r}'$. To see this, consider the transformation to center of mass coordinates $\mathbf{r} = \mathbf{R} + \mathbf{s}/2$, $\mathbf{r}' = \mathbf{R} - \mathbf{s}/2$. Inserting this into (5.7) gives

$$n(\mathbf{k}) = \int \mathrm{d}^2 R \, \mathrm{d}^2 s \; e^{i\mathbf{k}\cdot\mathbf{s}} \, \langle \hat{\psi}^\dagger(\mathbf{R} + \mathbf{s}/2) \hat{\psi}(\mathbf{R} - \mathbf{s}/2) \rangle \; . \tag{5.8}$$

From this, we define

$$G^{(1)}(\mathbf{s}) = \int \mathrm{d}^2 R \; \langle \hat{\psi}^\dagger(\mathbf{R} + \mathbf{s}/2) \hat{\psi}(\mathbf{R} - \mathbf{s}/2) \rangle \; , \tag{5.9}$$

which is the correlation function where the center coordinate has been integrated out. Comparing this equation with (5.4), we see that the physical meaning of both equations is equivalent: In (5.4), the many-body wave function is taken with two particles at $\mathbf{r}$ and $\mathbf{r}'$ and then all other particle coordinates are averaged over. The form (5.9) represents the same physical contents: Regard two bosons at the positions $\mathbf{r}$ and $\mathbf{r}'$, i. e. separated by the distance $\mathbf{s}$, and take the ensemble average over all other coordinates.

[4] This averaging over $N - m$ coordinate sets to gain ρ_{N-m} is equivalent to taking the trace $\rho_{N-m} = \mathrm{tr}_{m,\ldots,N} \{\rho_N\}$, where the trace is taken with respect to all but $N - m$ particles.

The inverse Fourier transform of (5.8) yields an expression for $G^{(1)}(\mathbf{s})$ in terms of the momentum distribution

$$G^{(1)}(\mathbf{s}) = \frac{1}{2\pi\hbar}\int \mathrm{d}^2k\; e^{-i\mathbf{k}\cdot\mathbf{s}}\, n(\mathbf{k}) \tag{5.10}$$

and makes the correlation function directly accessible to experimental measurements. For elongated, quasi-one-dimensional Bose-Einstein condensates, the correlation function has been determined by measuring the momentum distribution, see Section 5.4.1. For an application of the described theoretical relationship between momentum distribution and coherence function, we refer to [30] and to further references within Section 5.4.1.

5.2.3. Definition of the correlation function

We now introduce the normalized first and second order correlation functions

$$g^{(1)}(\mathbf{r},\mathbf{r}') = \frac{\langle\hat{\psi}^\dagger(\mathbf{r})\hat{\psi}(\mathbf{r}')\rangle}{\sqrt{\langle\hat{\psi}^\dagger(\mathbf{r})\hat{\psi}(\mathbf{r})\rangle\langle\hat{\psi}^\dagger(\mathbf{r}')\hat{\psi}(\mathbf{r}')\rangle}} \tag{5.11}$$

and

$$g^{(2)}(\mathbf{r}_1,\mathbf{r}_2,\mathbf{r}_2',\mathbf{r}_1') = \frac{\langle\hat{\psi}^\dagger(\mathbf{r}_1)\hat{\psi}^\dagger(\mathbf{r}_2)\hat{\psi}(\mathbf{r}_2')\hat{\psi}(\mathbf{r}_1')\rangle}{\sqrt{\langle\hat{\psi}^\dagger(\mathbf{r}_1)\hat{\psi}(\mathbf{r}_1)\rangle\cdots\langle\hat{\psi}^\dagger(\mathbf{r}_1')\hat{\psi}(\mathbf{r}_1')\rangle}}\,. \tag{5.12}$$

Higher order coherence function are defined in analogy. In this definition, n^{th} order coherence relates to the factorization properties of a time-ordered product of n field operators. In terms of a quantum mechanical, operator defined field, coherence implies a behaviour of this field that is as close as possible to a classical field. In the case of ideal coherence, i. e. $\langle\hat{\psi}^\dagger(\mathbf{r}_1)\hat{\psi}^\dagger(\mathbf{r}_2)\cdots\hat{\psi}(\mathbf{r}_2')\hat{\psi}(\mathbf{r}_1')\rangle = \psi^*(\mathbf{r}_1)\psi^*(\mathbf{r}_2)\cdots\psi(\mathbf{r}_2')\psi(\mathbf{r}_1')$ [83]. First order coherence is a weaker requirement than second order coherence. For the case of perfect coherence, the correlation functions have the value $g^{(n)} = 1$. However, this is not achievable in an atomic system [83].
Of special interest to this work is the first order coherence function, which is directly connected to local phase fluctuations, yielding the contrast achievable in an interference experiment [83]. The second order function is connected to the two-body collision rate in the condensate [16] and is of importance for the measurement technique briefly discussed in Section 5.4.2.

5.2.4. Criteria for Bose-Einstein condensation

One possible and widely accepted definition for BEC is the existence of long-range order in the reduced off-diagonal density matrix (5.4). It has been introduced by Penrose and Onsager [86] and later named by Yang [118] in order to unify the different definitions for the occurrence of superfluidity in liquid Helium and Bose-Einstein condensation in ideal gases. In the original notation, it reads $n_M/N = e^{O(1)}$, where n_M is the largest eigenvalue of (5.4) and $A = e^{O(1)}$ means the existence of some positive finite value of A for N larger than a certain value N^*.[5]
In terms of the previously introduced quantities, this can be expressed using (5.5) as [76]

$$G^{(1)}(\infty) = N_0 \quad \Leftrightarrow \quad \text{BEC} \; . \tag{5.13}$$

Numerically we consider the function[6] $\tilde{\rho}_1(\mathbf{0}, \mathbf{r}) \propto g^{(1)}(\mathbf{0}, \mathbf{r})$ to investigate the coherence properties of the condensate. Since we consider a condensate of finite size, the criteria (5.13) can only hold within the spatial extension R of the condensate, so that, for a true BEC, $g^{(1)}(\mathbf{0}, \mathbf{r}) = 1$ for $|\mathbf{r}| < R$.

The existence of off-diagonal long-range order is a property that only systems without *configurational long-range order* can posses (fluids or gases, but not solids). Configurational long-range order is expressed in terms of the diagonal two-body density matrix $\rho_2(\mathbf{r}_1, \mathbf{r}_2)$, that is obtained in analogy to (5.3) [76]. It is the underlying order of the structure in a crystal. Since the wave function has only values other than zero if the coordinates $\mathbf{r}_1$, $\mathbf{r}_2$ are close to two lattice sites, the condition (5.13) for large distances between $\mathbf{r}_1$ and $\mathbf{r}_2$ cannot be fulfilled. Therefore, BEC cannot occur in a solid [86].

5.2.5. Decay behaviour of the off-diagonal density matrix

More information is held within the decay behaviour of the first order correlation, see [63] for application to the 1D, 2D and 3D Bose gas:

[5] The definition of BEC through the reduced density matrix is valid for interacting systems, since there, the density matrix is a well defined quantity. Originally, the definition for BEC in an ideal gas required the existence of a macroscopic occupation in the lowest single particle level. In an interacting system this is not a valid definition anymore, because then there are no single particle levels [86].

[6] We define the correlation function $g^{(1)}$ always to be normalized, see (5.11), whereas the normalization of the density matrix depends on the normalization of the condensate wave function Ψ_0.

1. *exponential decay:* no long-range correlation among the particles at all and the system is not in a Bose-condensed or superfluid state.

2. *algebraic decay:* characteristic for a phase-fluctuating Kosterlitz-Thouless phase or a quasicondensate [18].

3. *not decaying to zero:* superfluid with coherent phase or true BEC, the value $G^{(1)}(\infty)$ can be identified with the population of the lowest momentum state.

5.3. Phase and density fluctuations

Insight into the phase fluctuating regime can be found from another decomposition of the Bose field operator. This approach has widely been used to study phase fluctuations of lower dimensional condensates [16, 30, 70, 88, 90, 91, 94], especially within the Thomas-Fermi (TF) approximation for which analytic solutions can be obtained.

An alternative to the cartesian decomposition (3.13) of the Bose field operator is the complex representation

$$\hat{\psi}(\mathbf{r}) \simeq \langle\hat{\psi}(\mathbf{r})\rangle + \delta\hat{\psi}(\mathbf{r}) = \sqrt{\hat{n}(\mathbf{r})}\, e^{i\hat{\phi}(\mathbf{r})} \,. \tag{5.14}$$

Here, we have a density and phase fluctuating part of the field operator. We have presumed the existence of a condensate, write the density fluctuations as $\hat{n}(\mathbf{r}) = n_c(\mathbf{r}) + \delta\hat{n}(\mathbf{r})$ and linearize in the fluctuation operators, so that we obtain

$$\hat{\psi}(\mathbf{r}) \simeq \sqrt{n_c(\mathbf{r})} + \frac{\delta\hat{n}(\mathbf{r})}{2\sqrt{n_c(\mathbf{r})}} + i\sqrt{n_c(\mathbf{r})}\,\hat{\phi}(\mathbf{r}) \,. \tag{5.15}$$

From comparison with (5.14) we identify the first term with $\langle\hat{\psi}(\mathbf{r})\rangle \equiv \Psi_0(\mathbf{r})$ and the remainder with $\delta\hat{\psi}(\mathbf{r})$. Using the above, we find for the non-condensate density from (3.18)

$$\tilde{n}(\mathbf{r}) = \left\langle \frac{\delta\hat{n}(\mathbf{r})^2}{4n_c(\mathbf{r})} + \frac{i}{2}\left[\delta\hat{n}(\mathbf{r}), \hat{\phi}(\mathbf{r})\right] + n_c(\mathbf{r})\hat{\phi}(\mathbf{r})^2 \right\rangle \,. \tag{5.16}$$

In order to obtain an expression for the density and phase fluctuation operator in terms of the field operators, we use (5.15) and its hermitian conjugate to get

$$\delta\hat{n}(\mathbf{r}) = \left(\delta\hat{\psi}(\mathbf{r}) + \delta\hat{\psi}^\dagger(\mathbf{r})\right)\Psi_0(\mathbf{r}) \tag{5.17}$$

$$\hat{\phi}(\mathbf{r}) = \frac{\delta\hat{\psi}(\mathbf{r}) - \delta\hat{\psi}^\dagger(\mathbf{r})}{2i\,\Psi_0(\mathbf{r})} \,. \tag{5.18}$$

We revert to the Bogoliubov transformation in Section 3.2.1 and write these equations in terms of the auxiliary functions $\psi_i^{(\pm)}(\mathbf{r}) = u_i(\mathbf{r}) \pm v_i(\mathbf{r})$, where the u_i and v_i are real,

$$\delta\hat{n}(\mathbf{r}) = \sum_i \Psi_0(\mathbf{r}) \, (\hat{\alpha}_i + \hat{\alpha}_i^\dagger) \, \psi_i^{(-)}(\mathbf{r}) \tag{5.19}$$

$$\hat{\phi}(\mathbf{r}) = \sum_i \frac{(\hat{\alpha}_i - \hat{\alpha}_i^\dagger) \, \psi_i^{(+)}(\mathbf{r})}{2i \, \Psi_0(\mathbf{r})} \, , \tag{5.20}$$

where we have used (3.21).

Since the divergence problems in 2D occur at low momenta, c. f. Section 3.4.4, we look at the low-energy limit of (5.19) and (5.20). Since, for large wavelengths, the quasiparticle amplitudes diverge equally ($v_i(\mathbf{r}) \to u_i(\mathbf{r}) \propto \mathbf{k}^{-1/2}$) [87, §7.2], we see that phase fluctuations are enhanced whereas density fluctuations are suppressed ($\psi_i^{(-)}(\mathbf{r}) \to 0$ as $\mathbf{k} \to \mathbf{0}$), c. f. [88].
This justifies the simpler notation for (5.14) where the density fluctuations around the condensate density are neglected

$$\hat{\psi}(\mathbf{r}) \approx \sqrt{n_c(\mathbf{r})} \, e^{i\hat{\phi}(\mathbf{r})} \, . \tag{5.21}$$

Doing so in (5.16), we see that the leading order term of the phase fluctuations is given by

$$\langle \hat{\phi}(\mathbf{r})^2 \rangle \approx \frac{\tilde{n}(\mathbf{r})}{n_c(\mathbf{r})} \, . \tag{5.22}$$

Thus, phase fluctuations are negligible as long as $n_c(\mathbf{r}) \gg \tilde{n}(\mathbf{r})$. The condition proposed in [88] for the crossover from a true condensate to a quasicondensate is

$$\langle \hat{\phi}(\mathbf{r})^2 \rangle \gtrapprox 1 \quad \Leftrightarrow \quad \text{quasicondensate} \tag{5.23}$$

for temperatures smaller than T_c. An analytic expression for the squared average of the phase fluctuation operator within the TF-limit is given in the aforesaid publication by Petrov *et al.*, it reads

$$\langle \hat{\phi}(\mathbf{r})^2 \rangle \approx \frac{T}{T_c} \sqrt{\frac{mg}{4\pi\hbar^2}} \, \ln N \, . \tag{5.24}$$

For completeness in this context, we also refer to [44] for a study of the dependence of the magnitude of the phase fluctuations on the collective excitations.

5.4. Measurement

So far, no group has published measurements of coherence properties of a two-dimensional Bose-Einstein condensate. Nevertheless, experiments have been done in

elongated three-dimensional condensates that reside in the quasi-1D regime. These measurements are either based on momentum spectroscopy or interferometry. The relation of the first method to the correlation function has been described in Section 5.2.2, whereas the second method is a direct study of the interference pattern of the condensate.

5.4.1. Momentum spectroscopy

Based on the theory developed in [88, 91], the spatial correlation function and the momentum profile for an elongated 3D condensate is calculated in [30] within the TF-limit. The inhomogeneous shape of the condensate is taken into account via a local density approach. The momentum distribution of the quasicondensate is found to have the characteristic shape of a Lorentzian, rather than a Gaussian which is characteristic for a true condensate [102]. Therefore, a measured momentum profile that fits to a Lorentzian is considered to be the signature of a phase-fluctuating quasicondensate.

Recently, the group in Orsay has measured the momentum profile of a quasi-1D condensate via Bragg scattering [15, 102], the results of this experiment were presented at the ICOLS 2003 conference in Palm Cove, Australia, by Alain Aspect [4]. In fact, a Lorentzian type momentum spectrum was found within a temperature range between ca. 100 and 350 nK.

The Bragg method, however, is limited by the resolution. The more coherent the condensate is, the narrower gets the Fourier transform (5.10) and, with this, the Bragg resonance. The longest coherence length that could be resolved is this experiment was $l_\phi \sim 40\,\mu m$ [15]. To investigate the crossover regime from phase-fluctuating to phase-coherent condensate, another method must be employed (c. f. the next section).

Bragg momentum spectroscopy

To make it possible to qualitatively compare the results from the quasi-1D experiment with the correlation function calculated for this thesis, we briefly comment on some aspects of the Bragg experiment.

Bragg scattering is a velocity selective method of spectroscopy. Due to their speed, the energy of the particles in the condensate is Doppler-shifted, so that atoms with

different speeds obey different resonance conditions. To do Bragg scattering with a BEC, normally a propagating light field, created by two laser beams, is moved through the resting condensate. The part of the condensate that is resonant with the light field is scattered into a different momentum state ($\pm n\hbar k$ for a n-photon process). The population of the scattered fraction of the condensate is measured after time-of-flight.

The propagation speed of the Bragg field is determined by the detuning of the crossed beams. Therefore, the spectral response of the condensate is measured as a function of the detuning. To establish the relationship with the momentum distribution within the condensate, we use the relation between the detuning δ and the momentum within the condensate plane $p_\perp$

$$\delta = \frac{n\, k_L p_\perp}{2\pi\, m} \ , \tag{5.25}$$

where $k_L = 2\pi/\lambda$, λ the wavelength of the light field (780.02 nm for Rubidium [102], 589 nm for Sodium [117]), and m the mass of the atoms. This is obtained by considering energy and momentum conservation for the Bragg condition. A meanfield shift has been neglected.

For general reference and especially for a detailed discussion of the relationship between the actual measured *spectral response function* and the momentum distribution in a Bragg experiment, we list the publications [10, 11].

5.4.2. Interferometric measurement

Another method to measure correlations in an elongated 3D condensate has been employed by Hellweg *et al.* [43]. We mentioned in the introduction, that two quasicondensates brought to overlap do not show a regular interference pattern, since the phase coherence is destroyed by the presence of phase fluctuations. However, coherence information can be obtained by correlating two output ports of an interferometer and measuring the *intensity correlations*.
Intensity correlations are not connected to the first order, but to the second order coherence function (5.12). This is because the intensity $\Psi_0^*\Psi_0$ is measured many times at two detectors that are correlated with each other, so that the result refers to an averaged product of four field operators.
The coherence length of the quasicondensate can be obtained directly from the decay behaviour of the second order correlation function.

The interferometric method is suited to measure long coherence lengths and enables one to study the crossover regime from quasicondensate to BEC. For a detailed description of the theory of this experiment, refer to [16]. Results using this method can be expected from Alain Aspect's group in Orsay shortly [15, see §4.2].

Part II.

Numerics

6. Computational Methods

In Chapter 3 we have derived the Hartree-Fock-Bogoliubov (HFB) equations that describe the Bose-Einstein condensate at finite temperatures. At temperatures close to zero Kelvin nearly all atoms have accumulated in the ground state where they form the condensate. At larger temperatures, though, the thermal cloud constitutes an important part of the gaseous system as well. The goal in solving the HFB equations is to describe the static properties of the Bose-Einstein condensate, whilst including the effects of the thermal cloud on the condensed atoms.
In order to do so, we have to solve the Gross-Pitaevskiĭ equation (3.36) in combination with the Bogoliubov-de Gennes equations (3.37). This can only be done self-consistently, so that the calculation has to follow an iterative scheme:

1. Calculate the condensate wave function (and density) from the GPE (where in the first run, the thermal density $\tilde{n}$ is set to zero).
2. Solve the BdG equations with the calculated condensate density, which yields the energies of the excited states of the condensate.
3. Populate the excited states according to the quasiparticle distribution function (3.32) to calculate $\tilde{n}$ and the anomalous average $\widetilde{m}$.
4. The densities $\tilde{n}$ and $\widetilde{m}$ are mixed into the previous solution of the GPE and the whole process is repeated until convergence.

This chapter contains different aspects of the computational methods involved in solving the HFB equations. We begin with the introduction of dimensionless units in the two-dimensional Gross-Pitaevskiĭ equation (4.5) in Section 6.1. In the context of solving the Gross-Pitaevskiĭ equation, the utilized optimization methods are explained in Section 6.2. Afterwards, the calculation of the thermal densities $\tilde{n}$ and $\widetilde{m}$ by solving the Bogoliubov-de Gennes equations is outlined in Section 6.3. Finally, in Sections 6.4 and 6.5, some general important technical aspects for the numerical calculation are discussed.

6.1. Computational units

We start from the generalized GPE (4.5) for a symmetrically trapped, two-dimensional condensate,

$$\left(-\frac{\hbar^2}{2m}\,\Delta + \frac{m}{2}\,\omega_\perp^2 r^2 - \mu\right)\,\Psi_0(\mathbf{r}) + g\left(n_c(\mathbf{r}) + 2\tilde{n}(\mathbf{r})\right)\Psi_0(\mathbf{r}) = 0\ . \tag{6.1}$$

In Section 3.4.3.2, we introduced different coupling parameters for collisions between condensate atoms and other condensate atoms, or the thermal cloud. Since the actual form of the coupling parameter is not important for the following discussion, we postpone the introduction of unequal coupling parameters. They will be brought in at a later point when the implementation of the gapless theories G1 and G2 is discussed (c. f. Section 6.5).

The spatial variable $\mathbf{r}$ can be written in cylindrical coordinates, and, since we assume cylindrical symmetry, all quantities depend only on r.

The Laplacian in cylindrical coordinates in two dimensions is given by

$$\Delta = \frac{\partial^2}{\partial r^2} + \frac{1}{r}\,\frac{\partial}{\partial r} + \frac{1}{r^2}\,\frac{\partial^2}{\partial \varphi^2}\ . \tag{6.2}$$

In order to do calculations within the accuracy range of a computer, all quantities have to be scaled to computational units. To go to dimensionless units, we write r in units of the harmonic oscillator length

$$a_0 = \sqrt{\frac{\hbar}{m\omega_\perp}} \tag{6.3}$$

and all energies in units of the 1D harmonic oscillator energy quantum

$$E_0 = \frac{\hbar\omega_\perp}{2}\ . \tag{6.4}$$

The scaled quantities are denoted by the tilde,

$$\tilde{r} = \frac{r}{a_0}\ , \quad \tilde{\mu} = \frac{\mu}{E_0}\ , \tag{6.5}$$

which we will drop in the sections following this one. The two-dimensional condensate wave function itself has the dimension $[length]^{-1}$. Therefore,

$$\tilde{\Psi}_0(\tilde{r}) = \frac{a_0}{\sqrt{N_0}}\,\Psi_0(r)\ , \tag{6.6}$$

which additionally incorporates the normalization of the wave function to unity, i. e.

$$\int \mathrm{d}^2\tilde{r}\,|\tilde{\Psi}_0(\tilde{r})|^2 = 1\ . \tag{6.7}$$

In order to calculate the dimensionless form of the GPE, we need the first and second derivative with respect to r, which are simply given by $\partial_r \Psi_0(r) = a_0^{-1}\,\partial_{\tilde{r}}\tilde{\Psi}_0(\tilde{r})$ and $\partial_{rr}\Psi_0(r) = a_0^{-2}\,\partial_{\tilde{r}\tilde{r}}\tilde{\Psi}_0(\tilde{r})$, respectively. Using this with (6.2) in (6.1), we get

$$\left\{-\frac{\partial^2}{\partial\tilde{r}^2} + \tilde{r}^2 - \tilde{\mu} + \frac{2\,g}{\hbar\omega_\perp a_0^2}\left(\tilde{n}_c(\tilde{r}) + 2\,\tilde{\tilde{n}}(\tilde{r})\right)\right\}\,\tilde{\Psi}_0(\tilde{r}) = 0\ , \tag{6.8}$$

where

$$\tilde{n}_c(\tilde{r}) = N_0|\tilde{\Psi}_0(\tilde{r})|^2\ , \quad \tilde{\tilde{n}}(\tilde{r}) = a_0^2\,\tilde{n}(r)\ . \tag{6.9}$$

Furthermore, we redefine the coupling parameter g and the single particle Hamiltonian

$$\tilde{g} = \frac{2\,g}{\hbar\omega_\perp a_0^2}\ , \quad \tilde{\tilde{h}} = -\frac{\partial^2}{\partial\tilde{r}^2} + \tilde{r}^2\ , \tag{6.10}$$

so that the dimensionless GPE (6.8) has the usual appearance

$$\left(\tilde{\tilde{h}} - \tilde{\mu} + \tilde{g}\,[\tilde{n}_c(\tilde{r}) + 2\,\tilde{\tilde{n}}(\tilde{r})]\right)\,\tilde{\Psi}_0(r) = 0\ . \tag{6.11}$$

Equivalently, the BdG equations in dimensionless units are written as in (3.37) with equal coupling parameters g, scaled quasiparticle energies $\tilde{E}_i = 2E_i/\hbar\omega_\perp$ and:

$$\hat{\mathcal{L}} = -\frac{\partial^2}{\partial\tilde{r}^2} + \tilde{r}^2 - \tilde{\mu} + 2\,\tilde{g}\left(\tilde{n}_c(\tilde{r}) + \tilde{\tilde{n}}(\tilde{r})\right) \tag{6.12}$$

$$\mathcal{M} = \tilde{g}\,\tilde{n}_c(\tilde{r})\ . \tag{6.13}$$

6.2. Optimization methods – Solving the Gross-Pitaevskiĭ equation

The Gross-Pitaevskiĭ equation is applicable to a wide variety of problems and provides a very good description of even complicated physical processes in a Bose-Einstein condensate. The time independent form yields not only the ground state of the condensate, but also excited states, such as for example a vortex solution. Given a certain initial state, the time-dependent GPE can be used to study dynamical effects, such as scattering in a Bragg light field or matter wave mixing.

For this study, only the ground state solution of the stationary GPE is of interest. Nevertheless, since it is a non-linear differential equation of second order, its solution is all but trivial. In the following sections appropriate methods for finding a stationary solution of the time-independent GPE will be described. The implementation in the actual code uses the `fsolve` routine that is part of MATLAB's *Optimization Toolbox* and will be described in greater detail in Section 6.2.3. References for this section are [9, 96, 112].

6.2.1. Formulation of the problem

We consider an equation of the type

$$\mathbf{f}(\mathbf{x}) = \mathbf{0} \ , \tag{6.14}$$

where the vector-valued function $\mathbf{f}(\mathbf{x}) = [f_1(\mathbf{x}), \ldots, f_m(\mathbf{x})]^T$ depends on a set of variables $\mathbf{x} = [x_1, \ldots, x_n]^T$. The function $\mathbf{f}$ is non-algebraic so that a direct solution is not possible. We introduce the following notations for

$$\text{the gradient vector:} \quad \mathbf{g}_i(\mathbf{x}) = \begin{pmatrix} \frac{\partial f_i}{\partial x_1} \\ \frac{\partial f_i}{\partial x_2} \\ \vdots \end{pmatrix} \tag{6.15}$$

$$\text{the Jacobi matrix:} \quad J(\mathbf{x}) = \begin{pmatrix} \frac{\partial f_1}{\partial x_1} & \frac{\partial f_1}{\partial x_2} & \cdots \\ \frac{\partial f_2}{\partial x_1} & \frac{\partial f_2}{\partial x_2} & \cdots \\ \vdots & \vdots & \ddots \end{pmatrix} \tag{6.16}$$

$$\text{and the Hesse matrix:} \quad H_i(\mathbf{x}) = \begin{pmatrix} \frac{\partial^2 f_i}{\partial x_1 \partial x_1} & \frac{\partial^2 f_i}{\partial x_1 \partial x_2} & \cdots \\ \frac{\partial^2 f_i}{\partial x_2 \partial x_1} & \frac{\partial^2 f_i}{\partial x_2 \partial x_2} & \cdots \\ \vdots & \vdots & \ddots \end{pmatrix} \ . \tag{6.17}$$

6.2.2. Zero-finding: Newton-Raphson algorithm

Provided a good initial guess to start with, the Newton-Raphson method is an efficient and simple method of zero-finding. We name $\mathbf{x}$ a wanted root of the function $\mathbf{f}$ and $\mathbf{x}^*$ a point in its neighbourhood[1]. We start from the multi-dimensional, linear Taylor expansion for the displacement $\boldsymbol{\delta}$

$$\mathbf{f}(\mathbf{x}^* + \boldsymbol{\delta}) = \mathbf{f}(\mathbf{x}^*) + J(\mathbf{x}^*)\, \boldsymbol{\delta} + O(\delta^2) \ . \tag{6.18}$$

Setting the l. h. s. to zero yields a set of equations that determine the *Newton step* $\boldsymbol{\delta}$

$$J(\mathbf{x}^*)\, \boldsymbol{\delta} = -\mathbf{f}(\mathbf{x}^*) \quad \Leftrightarrow \quad \boldsymbol{\delta} = -J^{-1}(\mathbf{x}^*)\, \mathbf{f}(\mathbf{x}^*) \ , \tag{6.19}$$

so that adding the step to the initial vector

$$\mathbf{x}^* + \boldsymbol{\delta} = \mathbf{x}_{\text{new}} \tag{6.20}$$

[1] Here, 'neighbourhood' corresponds to the convergence radius of the Taylor expansion.

brings us closer to the root $\mathbf{x}$. Together, (6.19) and (6.20) form a *Newton iteration*.

On the other hand, we can use this method to obtain an analytical expression for the Jacobian J of $\mathbf{f}$, which we do in Section D.2 of the Appendix. However, if an analytical expression for the Jacobian cannot be found, it can still be calculated numerically by using finite differences. This is a rather time consuming process. When a solution of a non-linear equation is iteratively calculated, an analytical expression that can be passed on to the `fsolve` routine is indispensable.

6.2.3. Optimization routines

Finding the zeros of a multi-dimensional function requires a good knowledge of the results one anticipates. There are no 'good' general algorithms that could be applied. A common strategy is to map the zero-finding problem of a function $\mathbf{f}$ to the minimization (or *optimization*) of another function $\mathbf{F}$. Even though optimization means nothing but zero-finding of the gradient vector, the gradient components must satisfy certain integrability conditions and are, therefore, not arbitrarily independent[2] of each other. This property makes optimization a much stronger technique than root-finding.

To formulate the optimization problem, we consider a *scalar* function $F(\mathbf{x})$ and expand the function for a vector $\mathbf{x}^*$. In the neighbourhood of the minimum, we expect the Taylor expansion up to the second order to be in good agreement with the actual function,

$$F(\mathbf{x}^* + \boldsymbol{\delta}) = F(\mathbf{x}^*) + \mathbf{g}(\mathbf{x}^*)\,\boldsymbol{\delta} + \frac{1}{2}\,\boldsymbol{\delta}^T H(\mathbf{x}^*)\,\boldsymbol{\delta} + O(\delta^3)\ . \tag{6.21}$$

We find the minimum by setting the gradient of this function to zero, i. e.

$$H(\mathbf{x}^*)\,\boldsymbol{\delta} = -\mathbf{g}(\mathbf{x}^*)\ . \tag{6.22}$$

This is the general formulation for the Newton step.

The `fsolve` routine makes use of three different optimization algorithms for medium-scale[3] problems: The Least-Squares (Gauß-Newton) algorithm, the Levenberg-Mar-

[2] The gradient gives always the direction towards a minimum from a given current point, whereas there is not information about the search direction for the root finding problem of independent, arbitrary functions [96, c. f. Section 9.6].

[3] One distinguishes between different orders of magnitude of the parameter space. Optimization routines for many variables (about $> 10^4$) must work differently from the ones described for practical reasons like memory usage and speed.

quardt algorithm, or the trust-region dogleg method. The limitation to these optimization methods is given by two factors: The memory needed to store the Jacobian and the factorization time to solve (6.22). The required memory goes as $(2n)^2$ bytes, where n is the number of (single word) variables. For 1 GB RAM, this means a limitation to about $20,000$ variables. For the needs of this thesis, the optimization is done for a set of basis expansion coefficients that represent a one-dimensional GPE. Hence, memory and time consumption of the `fsolve` routine do not constitute a problem.

6.2.3.1. Least-Squares optimization

Getting closer to the zero of $\mathbf{f}$, the sum of its squares must decrease. Hence, rather than finding the root of $\mathbf{f}$, one can as well look for the minimum[4] of the collapsed function

$$F(\mathbf{x}) = \frac{1}{2}\,\mathbf{f}^*(\mathbf{x})^T\mathbf{f}(\mathbf{x}) = \frac{1}{2}\,|\mathbf{f}(\mathbf{x})|^2 \ . \tag{6.23}$$

In the special case (6.23), the gradient vector and the Hesse matrix can be expressed in terms of the Jacobian and the residuals $f_i(\mathbf{x})$

$$\mathbf{g}(\mathbf{x}) = J(\mathbf{x})^T F(\mathbf{x}) \tag{6.24}$$

$$H(\mathbf{x}) = J(\mathbf{x})^T J(\mathbf{x}) + Q(\mathbf{x}) \ , \tag{6.25}$$

where the matrix Q is given by

$$Q(\mathbf{x}) = \sum_{i=1}^{m} f_i(\mathbf{x}) H_i(\mathbf{x}) \ . \tag{6.26}$$

It has the property that it goes to zero as the current vector $\mathbf{x}^*$ improves towards the solution $\mathbf{x}$ of $\mathbf{f}(\mathbf{x}) = \mathbf{0}$. Hence, it can be neglected in the expression for H.
With this, the Newton step (6.22) for the least-squares problem becomes

$$J(\mathbf{x}^*)^T\, F(\mathbf{x}) + J(\mathbf{x}^*)^T J(\mathbf{x}^*)\, \boldsymbol{\delta} = \mathbf{0} \quad \text{or} \quad J(\mathbf{x}^*)\, \boldsymbol{\delta} = -F(\mathbf{x}^*) \ . \tag{6.27}$$

6.2.3.2. Dogleg trust-region method

The idea of trust-region algorithms is to substitute the arbitrary function $F(\mathbf{x})$ by a simpler function $q(\mathbf{s})$. Normally, this is just the quadratic Taylor expansion, which is

[4] Eqn. (6.23) is positive definite.

assumed to be a good approximation within a certain *trust-region* S around $\mathbf{x}$. The Newton step is then computed by solving the subproblem

$$\min_{\mathbf{s}}\{q(\mathbf{s}) \mid \mathbf{s} \in S\} \ . \tag{6.28}$$

MATLAB restricts the subproblem to a two-dimensional subspace S, since the minimization problem in a two-dimensional space is trivial. The *Optimization Toolbox* chooses $S = \mathrm{span}\{\mathbf{s}_1, \mathbf{s}_2\}$ in a way that combines local and global convergence criteria. The direction $\mathbf{s}_1 \equiv \mathbf{g}$ is that of the gradient vector and $\mathbf{s}_2$ is either given by a Newton step to increase local convergence speed, if it can be calculated, or it is a direction of negative curvature. Explicitly, $\mathbf{s}_2$ is a solution of $H(\mathbf{s})\,\mathbf{s}_2 = -\mathbf{g}(\mathbf{s})$ or $\mathbf{s}_2^T H(\mathbf{s})\,\mathbf{s}_2 < 0$, respectively. This stops the algorithm from failing when a Gauß-Newton step cannot be calculated or a local minimum has been found. The step size is scaled according to the extension of the trust-region and calculated in a further step.

Since the minimum of the function $F(\mathbf{x})$ (6.23) is not necessarily a root of $\mathbf{f}(\mathbf{x})$, a better choice for the function to be minimized can be found from (6.27). Since $\boldsymbol{\delta}$ is a root of (6.27), it is also a minimum of

$$m(\boldsymbol{\delta}^*) = \frac{1}{2}\,|J(\mathbf{x}^*)\,\boldsymbol{\delta}^* + F(\mathbf{x}^*)|^2 \ . \tag{6.29}$$

6.2.4. Solving the GPE

Consider the dimensionless GPE (6.11), which is an equation of the type (6.14).[5] A straightforward way to formulate an optimization problem for the GPE would be to discretize it on an equally spaced grid and to replace the Laplacian by a finite difference operator D. This is a non-local operator in coordinate space, since it depends on several adjacent grid points. In this case, the equation $\mathbf{f}(\mathbf{x}) = \mathbf{0}$ of the optimization problem contains the GPE, evaluated on each grid point, and furthermore some boundary and normalization conditions.

For the purpose of our work, another method is better suited and computationally less expensive. By expanding the solution Ψ_0 of the GPE into a suitable basis set, the explicit evaluation of the Laplacian can be avoided. Furthermore, rather than optimizing on each grid point, one optimizes the expansion coefficients. Since these are independent of the number of grid points, the dimension of the optimization problem

[5] Indeed, it is a vector-valued function, see the following example or c. f. (6.35) on page 85.

now depends on the number of basis states that are needed, rather than on the grid size. Thus, we formulate the optimization problem[6]

$$\left.\frac{\delta \mathbf{f}[\phi]}{\delta\phi(\boldsymbol{\phi})}\right|_{\phi=\Psi_0} = 0 \ , \tag{6.30}$$

where the functional $\mathbf{f}$ stands for the GPE (6.14), and the solution vector $\boldsymbol{\phi}$ contains the expansion coefficients ϕ_i.

6.2.4.1. Numerical method

In order to solve the GPE numerically, one must choose an initial guess $\phi(r)$ to start with. The GPE is then evaluated for this wave function and a Newton step $\delta(r)$ is calculated. In the next iteration, the evaluation starts with the improved solution $\phi(r) + \delta(r)$, which will be closer to the final solution $\Psi_0(r)$ if the initial guess was any good. Hence, we formulate the zero-finding problem in analogy to (6.18), with $\mathbf{f}$ the GPE, $\mathbf{x}$ the guess $\phi(r)$ and $\boldsymbol{\delta}$ the Newton step $\delta(r)$, and evaluate

$$\mathbf{f}[\phi(r) + \delta(r),\, \mu_\phi + \delta\mu] = 0 \ . \tag{6.31}$$

The square brackets denote the functional dependence of $\mathbf{f}$. Note that the guess ϕ in the GPE has an eigenvalue μ_ϕ that differs from that of the ground state solution Ψ_0, and we write $\mu \simeq \mu_\phi + \delta\mu$ in the sense that the value of the r. h. s. of this equation is closer to the true chemical potential of the ground state.

Evaluating (6.31) from the GPE (6.11) gives

$$\begin{aligned} &\left[\hat{h} - \mu_\phi + g\left(\phi^2(r) + 2\,\tilde{n}(r)\right)\right]\,\phi(r) \\ &\quad + \left[\hat{h} - \mu_\phi + g\left(3\phi^2(r) + 2\,\tilde{n}(r)\right)\right]\,\delta(r) - \delta\mu\,\phi(r) = 0 \ , \end{aligned} \tag{6.32}$$

where terms quadratic in the small variables $\delta(r)$ and $\delta\mu$ have been neglected. We identify the first line of (6.32) with the GPE for the guess $\phi(r)$, whereas the second line contains the information about the Jacobian (c. f. 6.18). Although not obvious, the term $\delta\mu_\phi\,\phi(r)$ is proportional to $\delta(r)$ due to the dependence on $\delta\mu_\phi$, as shown in the Appendix, so that from comparing the coefficients it is possible to obtain an analytical expression for the Jacobi matrix.

[6] The zero-finding problem will be reformulated by the `fsolve` routine, so that optimization algorithms of the *Optimization Toolbox* can be applied.

Basis expansion. We now expand the guess $\phi(r)$ in the basis $\{\chi_i\}$ of the harmonic oscillator, derived in detail in Appendix C,

$$\phi(r) = \sum_i \phi_i \, \chi_i(r) \ . \tag{6.33}$$

The index i here is a short notation for the two quantum numbers $\{n, m\}$. In Appendix D we find for the GPE in terms of the expansion coefficients the following equation for each of the coefficients ϕ_i

$$(\epsilon_i - \mu_\phi)\, \phi_i + g \int \mathrm{d}^2 r \, \Big[\chi_i(r)\, \phi(r)^3 + 2\, \chi_i(r)\, \tilde{n}(r)\, \phi(r) \Big] = 0 \ . \tag{6.34}$$

In vector notation, this can be written with the definitions (D.9), see Appendix D for the calculation, as

$$(\boldsymbol{\epsilon} - \mu_\phi)\boldsymbol{\phi} + g\, \mathbf{u} + 2g\, \mathbf{v} = \mathbf{0} \ . \tag{6.35}$$

This is an equation of the type (6.14).

Jacobian. Also in the Appendix, the affiliated Jacobi matrix is derived. It is needed to be passed on to the `fsolve` routine with the GPE (6.34) (or 6.35) and is given by the following expression

$$J = (\boldsymbol{\epsilon} - \mu_\phi)\, I + 3g\, U + 2g\, V - \Big(2\, \boldsymbol{\phi} \cdot \boldsymbol{\epsilon} + 4\, \boldsymbol{\phi}^T V + 4\, \mathbf{u}^T \Big)\, I \ . \tag{6.36}$$

Here I is the identity matrix and the other quantities are, again, defined in (D.9).

6.2.4.2. The `fsolve` routine

In (6.35) and (6.36) the zero-finding problem for the Gross-Pitaevskiĭ equation is defined in analogy to the fundamental method described in Section 6.2.2. Internally, the `fsolve` routine collapses the vector-valued zero-finding problem into a number-valued optimization problem, as discussed in Section 6.2.3. The actual form of the function then to be minimized depends on the chosen algorithm. We found the dogleg trust-region method, briefly introduced on page 82, to be the fastest method to solve the GPE. In fact, the dogleg algorithm is about three times faster than the Gauß-Newton method and up to four times faster than the Levenburg-Marquardt algorithm.[7]

[7] These numbers stem from calculations with different numbers of basis functions and different numbers of grid points.

6.2.4.3. Initial guess

Sensible results can only be expected when the initial guess is already reasonably close to the function we wish to find. For the case of the condensate wave function, a very good guess to start with is given by the *Thomas-Fermi* approximation. If the number of particles is large, the mean-field energy is much larger than the kinetic energy, and the term containing the Laplace operator can then be neglected. Since the non-condensate density is zero in the beginning of the iteration, the Thomas-Fermi wave function follows from (6.11) to be

$$\Psi_{\mathrm{TF}}(r) = \sqrt{\frac{\mu - U_{\mathrm{trap}}(r)}{g}} \times \Theta\left(\frac{\mu - U_{\mathrm{trap}}(r)}{g}\right) . \tag{6.37}$$

In two dimensions, from the normalization condition (3.14), we get for the chemical potential

$$\mu = \sqrt{\frac{2gN_0}{\pi}} . \tag{6.38}$$

This works well as an initial guess for values of $gN_0 > 5$. If the kinetic energy term can definitely not be neglected, as is the case for studies of the non-interacting gas ($g = 0$), the Thomas-Fermi approximation fails. The solution for the GPE in the non-interacting case is simply given by the ground state $\chi_{0,0}(r)$ of the harmonic oscillator (C.21) which then constitutes a good initial guess. The chemical potential is determined by (C.19), i. e. $\mu \equiv \epsilon_{0,0} = 2$ in our units of $\hbar\omega_\perp/2$.

6.3. Numerical solution of the Hartree-Fock-Bogoliubov equations

In this section, we describe the method we use to obtain a numerical solution to the HFB equations. The whole calculation consists of two basic parts that are treated separately. Firstly, the GPE has to be solved to obtain the condensate density. Section 6.2.4 is concerned with this topic. In a second step, the BdG equations are solved to get the excited modes of the condensate. The thermal density is then calculated by populating these modes. Like the solver for the GPE, this following method also relies on an expansion in a suitable basis set.

The description of the numerical methods in this paragraph follows the outline in [48]. The relevant steps undertaken to obtain a solution of the BdG equations can be summarized to be the following:

1. We solve the nonlinear GPE in the basis of the harmonic oscillator. This gives the condensate density and the condensate eigenvalue, see Section 6.2.4.

2. Then, the solutions to the GPE with higher eigenvalues are calculated. Since the condensate density is known at this stage, it is simply a linear problem. The condensate state is removed from these solutions and the remaining functions form the *Hartree-Fock (HF) basis*.

3. Finally, the decoupled BdG equations are solved in the HF basis.

6.3.1. Decoupling the BdG equations

The BdG equations can be decoupled by a linear transformation. In the Popov approximation, we introduce the following notation for the Hamiltonian that appears in the GPE (3.20)

$$\hat{h}_{\mathrm{GP}} \equiv \hat{h} + g\left(n_c(\mathbf{r}) + 2\,\tilde{n}(\mathbf{r})\right) . \tag{6.39}$$

As shown in Appendix B, the BdG equations decouple when the quasiparticle amplitudes are substituted by the auxiliary functions

$$\psi_i^{(\pm)}(\mathbf{r}) = u_i(\mathbf{r}) \pm v_i(\mathbf{r}) . \tag{6.40}$$

These are related by (B.11)

$$\left(\hat{h}_{\mathrm{GP}} - \mu\right) \psi_i^{(+)}(\mathbf{r}) = E_i \psi_i^{(-)}(\mathbf{r}) . \tag{6.41}$$

Using the above, the BdG equations take the form

$$\begin{aligned} \left(\hat{h}_{\mathrm{GP}} - \mu\right)^2 \psi_i^{(+)}(\mathbf{r}) + 2\,g n_c(\mathbf{r}) \left(\hat{h}_{\mathrm{GP}} - \mu\right) \psi_i^{(+)}(\mathbf{r}) &= E_i^2\, \psi_i^{(+)}(\mathbf{r}) \\ \left(\hat{h}_{\mathrm{GP}} - \mu\right)^2 \psi_i^{(-)}(\mathbf{r}) + 2\,g \left(\hat{h}_{\mathrm{GP}} - \mu\right) n_c(\mathbf{r})\, \psi_i^{(-)}(\mathbf{r}) &= E_i^2\, \psi_i^{(-)}(\mathbf{r}) . \end{aligned} \tag{6.42}$$

The inverse transformation to (6.40) is given by

$$u_i(\mathbf{r}) = \frac{\psi_i^{(+)}(\mathbf{r}) + \psi_i^{(-)}(\mathbf{r})}{2} \quad \text{and} \quad v_i(\mathbf{r}) = \frac{\psi_i^{(+)}(\mathbf{r}) - \psi_i^{(-)}(\mathbf{r})}{2} . \tag{6.43}$$

6.3.2. Expanding into the Hartree-Fock basis

We consider the decoupled form of the BdG equations (6.42), that was derived in the preceding section. In order to obtain an eigenvalue equation, we expand the auxiliary

functions (6.40) into the basis states *of the condensate*

$$\begin{aligned} \psi_i^{(+)}(r) &= \sum_\alpha c_\alpha^i \phi_\alpha(r) \\ \psi_i^{(-)}(r) &= \sum_\alpha d_\alpha^i \phi_\alpha(r) \end{aligned} \tag{6.44}$$

and refer to the basis $\{\phi_\alpha(r)\}$ as the *Hartree-Fock basis*.[8] The choice of this basis has the great advantage that the quasiparticle amplitudes, and with them the non-condensate, are orthogonal to the condensate. If choosing a different basis, the orthogonality must be ensured by projecting out the condensate part from each u_i, v_i.

We now explain how to obtain the functions $\{\phi_\alpha(r)\}$. The GPE has an infinite number of eigenvalues $\tilde{\varepsilon}_\alpha$ and eigenvectors ϕ_α,

$$\left(\hat{h}_{\mathrm{GP}} - \mu\right) \phi_\alpha(r) = \varepsilon_\alpha \, \phi_\alpha(r) \ , \tag{6.45}$$

where the Hamiltonian of the GPE was defined in (6.39). Since n_c is known from solving the GPE for the ground state, and $\tilde{n}$ is known from solving the BdG equations from the previous iteration, the solution to equation (6.45) is a linear problem in the $\phi_\alpha(r)$. The eigenvalues in this equation are measured relative to the chemical potential of the condensate, $\varepsilon_\alpha = \tilde{\varepsilon}_\alpha - \mu$. The eigensolution with the lowest eigenvalue we refer to as the condensate ground state, or the condensate wave function $\phi_0 \equiv \Psi_0$. Its eigenvalue is the condensate eigenvalue, which is approximately the chemical potential[9], $\mu \simeq \tilde{\varepsilon}_0$, so that the lowest eigenvalue in (6.45) is $\varepsilon_0 \simeq 0$. The condensate state is the only *physically* important state, and the HF basis should rather be looked at as a mathematical aid to solve the decoupled BdG equations.

In order to calculate the eigenfunctions of (6.45), we expand the solutions $\phi_\alpha(r)$ in the basis of the harmonic oscillator, i. e.

$$\phi_\alpha(r) = \sum_i a_i^\alpha \, \chi_i(r) \ , \tag{6.46}$$

where, as mentioned before, the quantum numbers $\{n, m\}$ in (C.21) are summarized in the index i. To calculate the coefficients in (6.46), we insert the expansion into the GPE (6.45), multiply with $\chi_j(r)$ and integrate over $\mathbf{r}$, which gives

$$\sum_i \int \mathrm{d}^2 r \, \chi_i(r) \Big[\hat{h} + g\left(n_c(r) + 2\,\tilde{n}(r)\right)\Big] a_\alpha^i \, \chi_j(r) = \sum_i \int \mathrm{d}^2 r \, \varepsilon_\alpha \, a_i^\alpha \, \chi_i(r)\chi_j(r) \ . \tag{6.47}$$

[8] These ϕ_α are not to be mixed up with the iterative solution $\phi_0(r) = \sum_i \phi_i \, \chi_i(r)$ of the GPE in Section 6.2.4.

[9] c. f. Sections 3.5 and 3.3

With the orthonormality relation of the oscillator basis (C.23), and with (C.10), (C.19), we get

$$\sum_i \left[A_{ij} + \epsilon_i\,\delta_{ij}\right] a_i^\alpha = \varepsilon_\alpha\, a_j^\alpha \ , \tag{6.48}$$

where the ϵ_i are the energies of the harmonic oscillator, ε_α is the energy of an eigenstate of the GPE relative to the condensate eigenvalue, and the matrix elements of A are given by

$$A_{ij} = g \int \mathrm{d}^2 r\ \chi_i(r) \left[n_c(r) + 2\,\tilde{n}(r)\right] \chi_j(r) \ . \tag{6.49}$$

Therefore, the states (6.45) of the HF basis can be obtained by simply solving the eigenvalue problem (6.48) for the coefficients in (6.46).
From the linear independence of the coefficient vectors a^α follows the orthonormality relation

$$\int \mathrm{d}^2 r\ \phi_\alpha(r)\phi_\beta(r) = \delta_{\alpha\beta} \ , \tag{6.50}$$

since they are the representation of the $\phi_\alpha(r)$ in the orthonormal basis set of the harmonic oscillator.

6.3.3. Solution of the Bogoliubov-de Gennes equations

Inserting the expansion of the auxiliary functions (6.44) into the first equation of the decoupled BdG equations (6.42) yields

$$\sum_\alpha \left[\left(\hat{h}_{\mathrm{GP}} - \mu\right)^2 c_\alpha^i\,\phi_\alpha(r) + 2\,g n_c(r)\left(\hat{h}_{\mathrm{GP}} - \mu\right) c_\alpha^i\,\phi_\alpha(r)\right] = \sum_\alpha E_i^2\, c_\alpha^i\,\phi_\alpha(r) \ . \tag{6.51}$$

Multiplying with $\phi_\beta(r)$ and integrating over $\mathbf{r}$, we get with (6.45)

$$\sum_\alpha \int \mathrm{d}^2 r\ \left(\varepsilon_\alpha^2 c_\alpha^i + 2\,g n_c(r)\,\varepsilon_\alpha c_\alpha^i\right) \phi_\alpha(r)\phi_\beta(r) = \sum_\alpha \int \mathrm{d}^2 r\ E_i^2\, c_\alpha^i\,\phi_\alpha(r)\phi_\beta(r) \ . \tag{6.52}$$

Using (6.50), this expression simplifies to

$$\sum_\alpha \left[M_{\alpha\beta} + \varepsilon_\alpha \delta_{\alpha\beta}\right] \varepsilon_\alpha c_\alpha^i = E_i^2\, c_\beta^i \ , \tag{6.53}$$

where the matrix M is defined as

$$M_{\alpha\beta} = 2\,g \int \mathrm{d}^2 r\ \phi_\alpha(r)\, n_c(r)\, \phi_\beta(r) \ . \tag{6.54}$$

Analogous to the calculation of the HF basis in (6.48), the solution of the BdG equations can be obtained by solving the eigenvalue problem (6.53) for the coefficient vectors c^i

in the basis expansion (6.44) of the functions $\psi_i^{(\pm)}(r)$.
The coefficients of $\psi_i^{(-)}(r)$ can be obtained from the c^i by using

$$d_\alpha^i = \frac{\varepsilon_\alpha}{E_i}\, c_\alpha^i \ . \tag{6.55}$$

This follows immediately with (6.45) from inserting (6.44) into (6.41).
The quasiparticle amplitudes can then be retained by the inverse transformation (6.43).

6.4. Numerical techniques

Some important aspects of the implementation in Matlab shall finally be mentioned in the end of this chapter.

6.4.1. Discretization

We use an equidistant grid with 250 – 700 grid points to discretize the basis functions in which the condensate density and all other functions of interest are expanded in. Depending on the number of basis functions that are used, the range of the grid has to be adapted. This is, on the one hand, because the oscillator wave functions with higher eigenvalues spread out further from the origin, so that a wider range must be regarded to ensure orthogonality. On the other hand, their oscillatory character becomes stronger with increasing quantum number n, so that a finer grid is needed in order to represent the functions well. The determination of the right condensate population requires a calculation with many basis functions, whereas for the mere extraction of low-lying excitation frequencies, a calculation with less basis states on a smaller grid is sufficient.

6.4.2. Integration

For the discrete integration, we use an extended version of *Simpson's rule*, as explained in [96, §4.1]. It is given by

$$\int_{x_1}^{x_N} \mathrm{d}x\ f(x) = \frac{\Delta x}{3}\Big[f(x_1) + 4\,f(x_2) + 2\,f(x_3) + 4\,f(x_4) + \\ \cdots + 2\,f(x_{N-2}) + 4\,f(x_{N-1}) + f(x_N)\Big] + O\left(\frac{1}{N^4}\right)\ , \tag{6.56}$$

with the spacing Δx of the grid. In MATLAB, this formula can very easily be realized by defining a vector

$$\mathbf{S} = \frac{2\pi\Delta x}{3}\,\mathbf{s}\cdot\mathbf{x}\;, \tag{6.57}$$

where $\mathbf{s}$ contains the Simpson weights, $\mathbf{s} = (1, 4, 2, 4, \ldots, 4, 2, 1)^T$, and $\mathbf{x}$ is the grid vector. This form accounts for the cylindrical symmetry in two dimensions, i. e. $\int \mathrm{d}^2 r = 2\pi \int \mathrm{d}r\, r$.

The advantage of Simpson's integration rule is its easy usage and its speed. More sophisticated methods, like Gaussian Quadrature, which leads to a minimization of required grid points while giving exact results, were not necessary since computation time does not constitute an issue in our numerical one-dimensional treatment, even though an implementation for the Laguerre polynomials would have been feasible and, admittedly, more elegant.

The energy integrals (4.43), (4.44) and (6.59) that arise from the semi-classical expressions of the non-condensate density and the anomalous average must be treated differently, since the integration variable is not the spatial grid vector. Because the integrand is nevertheless spatially dependent, we use MATLAB's `quadl`-function to evaluate these integrals at each grid point.

6.4.3. Basis set

The oscillator wave functions $\chi_{n,m}(r)$ (C.21) are used, since they are the solutions of the non-interacting case of the GPE. Thus, they form a convenient basis that incorporates the symmetry of the system and avoids the use of finite difference operators that would arise from the discretization of the Laplace operator. Both the GPE and the BdG equations are solved in this basis representation. Two important points are worth of discussion:

1. Numerical implementation requires the distinction between basis states with different angular momenta, defined through the quantum number m. Therefore, we solve the BdG equations separately in subspaces of a distinct angular momentum and add the contributions from all subspaces together.[10] Naturally, the ground state solution has no angular momentum and is, thus, to be calculated solely in the $m = 0$ subspace.

[10] Since the oscillator basis states are orthogonal in n and m, c. f. (C.23), these subspaces are independent of each other and can, therefore, be treated separately.

2. There exists a basis cutoff, since it is not possible to sum over an infinite amount of basis states. This is not only due to the number of terms to add up, but also since the basis functions $\chi_{n,m}$ have n nodes. As mentioned before, in order to represent them on a discrete grid, an increasing number of grid points is needed for more and more nodes of the basis state. Normally, a calculation is done with 64–400 basis states, depending on temperature and wanted quantity.
   The basis cutoff is an important feature and is discussed in the following section.

6.4.4. Basis cutoff

The basis cutoff that has been mentioned before constitutes the limit of the fully quantum mechanical, discrete treatment. Since subspaces with different angular momentum are dealt with separately, the cutoff has to be consistently introduced in all the subspaces.

Introducing the energy cutoff. In order to do so, the maximal energy of the basis functions is a defined parameter of the program, defined by declaring the maximum n and m value for the basis states. Then, the energy cutoff is given by

$$\epsilon_{\mathrm{cut}} = 2\left[2\,n_{max} + m_{max} + 1\right] , \tag{6.58}$$

where (C.19) has been used. As a consequence, the number of basis states within a subspace decreases with increasing angular momentum.

Above the energy cutoff. We apply the method described in [101] to use a semi-classical approximation (see Section 3.4.4) above the energy cutoff. Up to ϵ_{cut}, the non-condensate density and the anomalous average are calculated quantum mechanically. The upper end of the spectrum is then added by evaluating the semi-classical equations. We can write this as

$$\tilde{n}(r) = \sum_i \tilde{n}_i^{\mathrm{qm}}(r) \times \Theta(\epsilon_{\mathrm{cut}} - E_i) + \int_{\epsilon_{\mathrm{cut}}}^{\infty} \mathrm{d}E\; \tilde{n}^{\mathrm{sc}}(E, r) \tag{6.59}$$

$$\widetilde{m}(r) = \sum_i \widetilde{m}_i^{\mathrm{qm}}(r) \times \Theta(\epsilon_{\mathrm{cut}} - E_i) + \int_{\epsilon_{\mathrm{cut}}}^{\infty} \mathrm{d}E\; \widetilde{m}^{\mathrm{sc}}(E, r) \ , \tag{6.60}$$

where

$$\tilde{n}_i^{\mathrm{qm}}(r) = f_{\mathrm{B}}(E_i)\left(|u_i(r)|^2 + |v_i(r)|^2\right) + |v_i(r)|^2 \tag{6.61}$$

$$\widetilde{m}_i^{\mathrm{qm}}(r) = \left(2f_{\mathrm{B}}(E_i) + 1\right) u_i(r)\, v_i(r) \tag{6.62}$$

from (3.30) and (3.31), respectively, and $\tilde{n}_{\mathrm{sc}}(E,r)$, $\widetilde{m}_{\mathrm{sc}}(E,r)$ are the integrands with the scalar pre-factors of (3.55) and (3.59).
The details of the calculation for $\widetilde{m}$ is rather involved and is discussed in detail in Section 4.4.

6.4.5. Correlation function

In Section 5.2.3 we define the first order correlation function in terms of the average over the pair product of two Bose field operators. As discussed in Section 5.2.2, the term $\langle\hat{\psi}^\dagger(\mathbf{r})\hat{\psi}(\mathbf{r}')\rangle$ corresponds to the off-diagonal density matrix. To calculate this average, we make use of the decomposition (3.13) and the off-diagonal expressions for (3.14), (3.18), i. e. in the cylindrical symmetric case

$$n_c(r,r') = \Psi_0^*(r)\Psi_0(r') \tag{6.63}$$

$$\tilde{n}(r,r') = \langle\delta\hat{\psi}^\dagger(r)\delta\hat{\psi}(r')\rangle\ . \tag{6.64}$$

The off-diagonal non-condensate density in terms of the quasiparticle amplitudes is explicitly given by

$$\tilde{n}(r,r') = \sum_i \left[f_B(E_i)\, u_i^*(r)u_i(r') + \left(f_B(E_i)+1\right) v_i^*(r)v_i(r')\right]\ . \tag{6.65}$$

Using the above for the correlation function (5.11) gives

$$g^{(1)}(r,r') = \frac{n_c(r,r') + \tilde{n}(r,r')}{\sqrt{n(r)\, n(r')}}\ , \tag{6.66}$$

where $n(r) = n_c(r) + \tilde{n}(r)$.

6.4.6. Convergence

With increasing temperature, it becomes harder to reach a convergent solution. At high temperatures ($> 0.6\, T_c$), the non-condensate density might grow larger that the condensate density within the first iterations. This leads to the unphysical phenomenon

of a negative condensate density. Therefore, only a part p of the non-condensate density (and the anomalous average, if G1 or G2 is used) is mixed with $(1-p)$ of the solution of the previous iteration. The value of p is determined dynamically and adapts in order to achieve quick convergence.
Up to $0.6\,T_c$, this does not constitute an issue, but for $T > 0.9\,T_c$, values of $p < 0.1$ might be necessary to reach convergence. This is sensible, since the condensate fraction goes down to less than 2% at such high temperatures.

There are different indicators to tell whether convergence has been reached:[11]

- the change in the excitation frequencies between two iterations, preferably those of the Kohn mode and the breathing mode.
- the change in the chemical potential.
- the change in particle number of the condensate or non-condensate.

6.5. Implementation of the gapless theories G1 and G2

So far in this chapter, we have spared out the usage of different coupling parameters for notational simplicity. None of the previous discussions is altered in principal by the introduction of the many-body T-matrix or the unlike treatment of collisions with the condensate or the thermal cloud in the case of the G1 theory. We now go back to the general form of the Gross-Pitaevskiĭ equation (3.36) and the Bogoliubov-de Gennes equations (3.37) that were introduced in Chapter 3 and show how to replace the mutual coupling constant g with separate, spatial dependent coupling parameters.

6.5.1. Calculation of the many-body T-matrix

In gapless HFB, the many-body T-matrix can be introduced by replacing

$$g \quad \rightarrow \quad T_{\mathrm{MB}}(r) \equiv U_0 \left(1 + \frac{\widetilde{m}^R(r)}{\Psi_0(r)^2 + \varepsilon}\right) , \tag{6.67}$$

[11] They are shown in the order of occurrence of convergence. This means, the change in the Kohn mode becomes small faster than the change in the chemical potential.

as derived in Chapter 4 and is thus calculated self-consistently. Here, $\widetilde{m}^R$ refers to the renormalized anomalous average. The renormalization can be done in different ways, as explained in Section 4.4. When numerically calculating the fraction in (6.67), problems arise as the condensate wave function drops to zero. Therefore, a correction of $\varepsilon = 10^{-4}$ is added to the denominator. This value has been found to be small enough not to adulterate the result in the region which is important for interactions, i. e. where the condensate density and the anomalous average are not zero, but also to be large enough large enough to suppress oscillations when both go to zero and two very small numbers are divided.

In three dimensions, the factor U_0 is simply the first order approximation of the two-body T-matrix. Since this is zero in two dimensions, we use to first order the coupling parameter which is valid in the quasi-3D regime, given by (4.6). In order to obtain a better approximation in the quasi-2D regime, the homogeneous limit of the zero-temperature many-body T-matrix, which can be obtained from the two-body T-matrix, can be used.

6.5.2. Implementation of the many-body T-matrix

For the different kinds of approximations, the coupling parameters g_{con} and g_{exc}, introduced in (3.36) – (3.39), must be replaced as described in Section 3.4. This is done in a straightforward way, once the many-body T-matrix is calculated according to (6.67).

Part III.

Results

7. HFB Results for the 2D Bose Gas within the Popov Approximation

In this Chapter, if not stated differently, we study a sample of 2000 Na atoms confined in a cylindrical trapping potential with characteristic parameters equal to those in the experiment of Görlitz [39]. Namely, $\omega_\perp/2\pi = 20\,\mathrm{Hz}$, which is the average of the anisotropic frequencies in x and y-direction, and $\omega_z/2\pi = 790\,\mathrm{Hz}$.[1] These trapping frequencies correspond to the oscillator lengths $l_\perp = 4.7\,\mu\mathrm{m}$ and $l_z = 0.8\,\mu\mathrm{m}$, respectively, and the energy spacing in the tightly confined direction is $\hbar\omega_z/k_\mathrm{B} \approx 38\,\mathrm{nK}$. All energies and lengths are scaled with respect to the energy spacing and the oscillator length $l_{\perp/z} = \sqrt{\hbar/m\omega_{\perp/z}}$ in the radial direction, if not stated differently. For these parameters, the critical temperature of the non-interacting gas is given by $T_c \approx 34\,\mathrm{nK}$, which corresponds to a dimensionless temperature of $\widetilde{T} \approx 70$.

7.1. General comments

The number of atoms in the trap is naturally limited in lower dimensions to [27, 39]

$$N_{2D}^{\max} = \sqrt{\frac{32\,\hbar}{225\,ma^2}\,\frac{\omega_z^3}{\omega_\perp^4}}\,. \tag{7.1}$$

For the parameters given above, this predicts the crossover regime from 3D to 2D for an atom number of $N_{2D}^{\max} \sim 16,000$ atoms. We studied atom numbers in the range from 200–5000 atoms.

In this chapter, the trapping frequency in the axial direction is chosen to represent that of the experiment of Görlitz. Therefore, the condensate is approximately in the two-dimensional regime with three-dimensional scattering and the coupling parameter we use is given by (4.6).[2] For the above parameters, $g'_{3\mathrm{D}} \approx 0.038$.

[1] In the experiment, the radial frequencies $\omega_{\perp x}$ and $\omega_{\perp y}$ were not equal. We chose the median to determine $\omega_\perp$ for our calculations.

[2] c. f. Section 8.3.1

7.2. Zero temperature results

The results presented in this section concern the ground state of a Bose-Einstein condensate in two dimensions. The full solution of the Gross-Pitaevskiĭ equation is compared to the Thomas-Fermi approximation and the harmonic oscillator ground state. Both of these states may serve as an initial guess for the numerical solution of the Gross-Pitaevskiĭ equation.

7.2.1. Eigenstates of the GPE

Figure 7.1 shows in the left panel the Thomas-Fermi density profile and the density profile of the ground state of the GPE (6.11) at zero Kelvin for different numbers of atoms. For large atom numbers, the TF wave function is closer to the solution of the GPE, since the kinetic energy term becomes negligible.
For very small values of the coupling parameter, the condensate wave function approaches the eigenstate of the trap, which is the ground state of the harmonic oscillator. Hence, in the non-interacting case or for $gNc \lesssim 5$, the TF wave function is not suited as an initial guess, as discussed in Section 6.2.4.3. The right panel in Figure 7.1 shows this case for $gN_0 = 4$. Depending on the regime (weak or strong coupling), either the TF or the oscillator ground state serves as an initial guess for the optimization algorithm.

7.2.2. Zero temperature depletion

Arising from the temperature independent part in expression (3.30) for the non-condensate density, there exists a small fraction of excited atoms even at zero temperature, referred to as *quantum-* or *zero-temperature depletion*. It is driven out of the condensed phase due to interactions. The classical analogy is the dynamical equilibrium between the thermal and condensed phases. In the case of strong interactions, as in the superfluid ^{4}He system, this depletion makes 90% of the total atom number, whereas in the non-interacting gas, there is no quantum depletion. For a weakly interacting BEC with our parameters, the contribution is only about 1% of the total atoms. It is the same order of magnitude as has been found in the 3D case [48]. The effect on the ground state is generally negligible. The quantum depletion for 2000 atoms is shown in Figure 7.2.

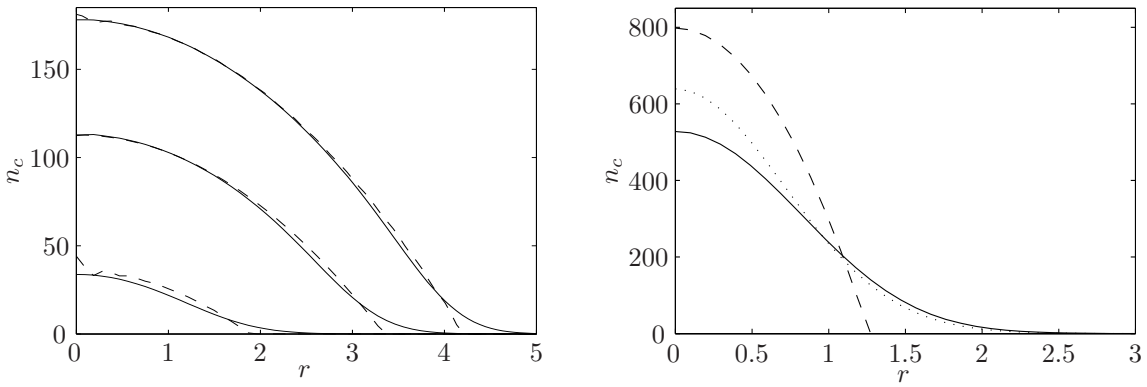

Figure 7.1.: Zero temperature behaviour of the density profile. **Left:** $N = 5000$, 2000 and 200 atoms from top to bottom. The dashed line corresponds to the TF-profile, the full line to the solution of the GPE. The TF profile is represented through a limited basis set, too, and the shown functions differ slightly from the true TF profile on the edges. **Right:** $N = 2000$ atoms, $g = 0.002$. The dashed line corresponds to the TF-profile, the dotted to the ground state of the trap and the full line to the solution of the GPE.

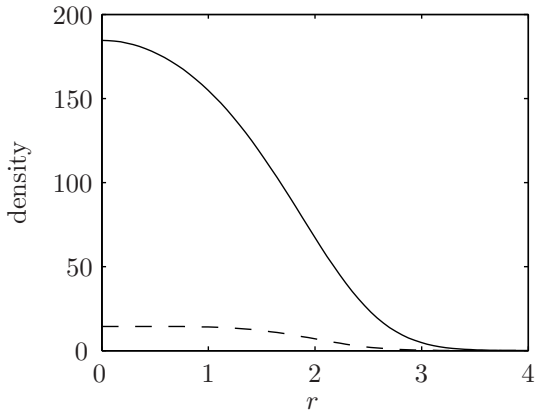

Figure 7.2.: Quantum depletion of the condensate: The solid line shows the condensate density at zero temperature, the dashed line is the quantum depletion, scaled by a factor of 100.

7.3. Finite temperature results

The finite temperature results require the self-consistent solution of the Gross-Pitaevskiĭ equation and the Bogoliubov-de Gennes equations. The iterative solution scheme converges at all temperatures without difficulty. However, above $0.8\,T_c$ the ratio of old to new solution in each iteration must be chosen carefully to prevent the non-condensate density from growing larger than the total atom number, which is kept fixed.

We present the density profile of the non-condensate, the temperature dependent condensate population and analyze the coherence properties of the condensate.

The presented results are based on the Popov approximation. In three dimensions, the zero-momentum and low-energy limit of the two-body T-matrix is used to parameterize scattering processes within the pseudo-potential approximation (4.1). In two dimensions this limit vanishes which leads to the unphysical phenomenon of zero interaction strength for the interacting gas. Thus, many-body effects must be considered already to first order. The implications for the Popov approximation and the gapless theories G1 and G2 are discussed in the next chapter. The results in this chapter are obtained by using the homogeneous limit of the zero-temperature many-body T-matrix for the coupling parameter. This can be obtained from the off-shell two-body T-matrix, as explained in Section 4.3.2.1. In dimensionless units, it is given by

$$g_{\mathrm{q2D}}^{\mathrm{hom}} = -\frac{8\pi}{\ln(\mu a_{\mathrm{2D}}^2/8)}\,, \tag{7.2}$$

c. f. also the next chapter.

7.3.1. Non-condensate density

Figure 7.3 shows the thermal density at different temperatures. The temperature dependent term in (3.30) leads to the formation of the characteristic off-center peak of the non-condensate density. It is located at the edge of the condensate due to the repulsion of the thermal atoms by the condensate. This is depicted in Figure 7.4, where the two densities n_c and $\tilde{n}$ are plotted next to each other. In comparison to the rapidly decaying condensate density, the thermal density has a long tail. Thus, the condensate is a dense and sharp peak within the diffuse thermal cloud. The tail of the thermal cloud becomes longer as the temperature increases (Fig. 7.3) while the condensate

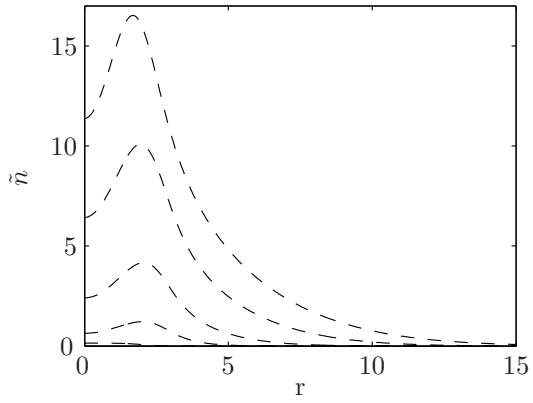

Figure 7.3.: Non-condensate density at $T/T_c = 0$, 0.1, 0.25, 0.5 and 0.75 (from bottom to top). The lowest line corresponds to the quantum depletion, shown in Figure 7.2.

radius does not change much even if the number of condensate atoms drops by an order of magnitude. Note that the long tail contains a large number of atoms despite its low density because the spatial integral is weighted by a factor of r (r^2 in three dimensions). The slight change in the size of the condensate can also be seen in the shift of the non-condensate peak towards the trap center with increasing temperature, remaining located at the edge of the condensate (Fig. 7.4).

7.3.2. Ground state population

In Figure 7.5 the condensate population is shown as a function of temperature. The result is compared to the case of the trapped ideal gas, where the population is determined by a power law expression, i. e. (2.24). To fit the data, we allow for two fitting parameters α, β:

$$\frac{N_0}{N} = 1 - \left(\frac{T}{\overline{T}_c}\right)^{\beta}, \quad \text{where} \quad \overline{T}_c = \alpha T_c \ . \tag{7.3}$$

In the case of the ideal gas, $\beta = 2$ and $\alpha = 1$, c. f. (2.39). In the fit the critical temperature is reduced due to interactions by a factor of $\alpha \approx 0.95$. This shift has two contributions: The finite size of the system reduces the critical temperature [34], but the interactions also modify the temperature. This second contribution as been extensively discussed in the literature, see [61] and references therein.
For the exponent we find $\beta \approx 1.70$, which is 15% smaller than for the ideal trapped gas. With these values, (7.3) parameterizes our data very well.

The right panel in Figure 7.5 focuses on the region close to the transition temperature $\overline{T}_c$. We see a *finite temperature tail* in the population of the interacting condensate.

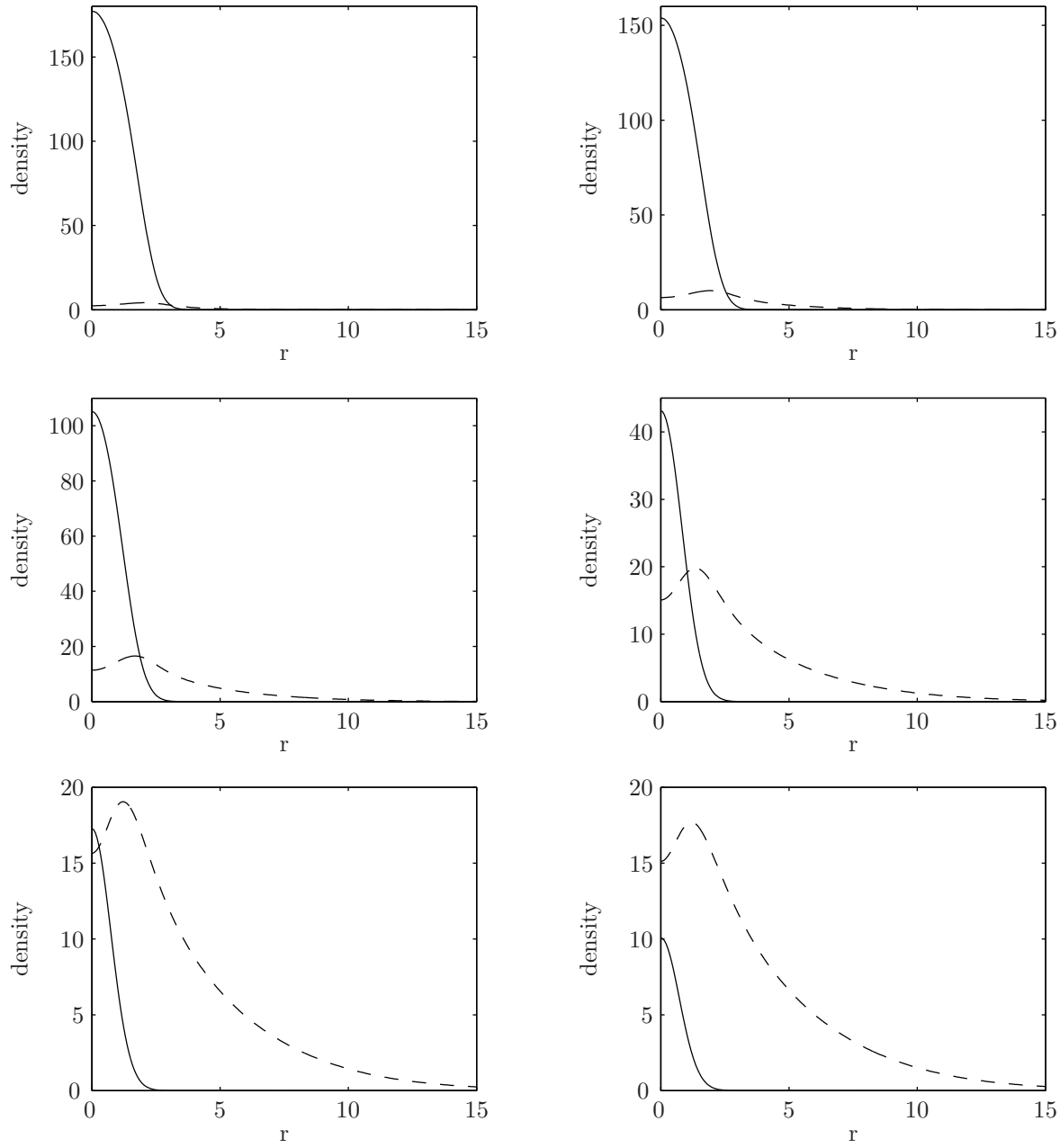

Figure 7.4.: Shown is the condensate (solid) and non-condensate density (dashed) at various fractions of the critical temperature: 0.25, 0.5, 0.75, 0.9, 0.95, 0.975 (from upper left to lower right). The peak of the thermal cloud sits right at the edge of the condensate.

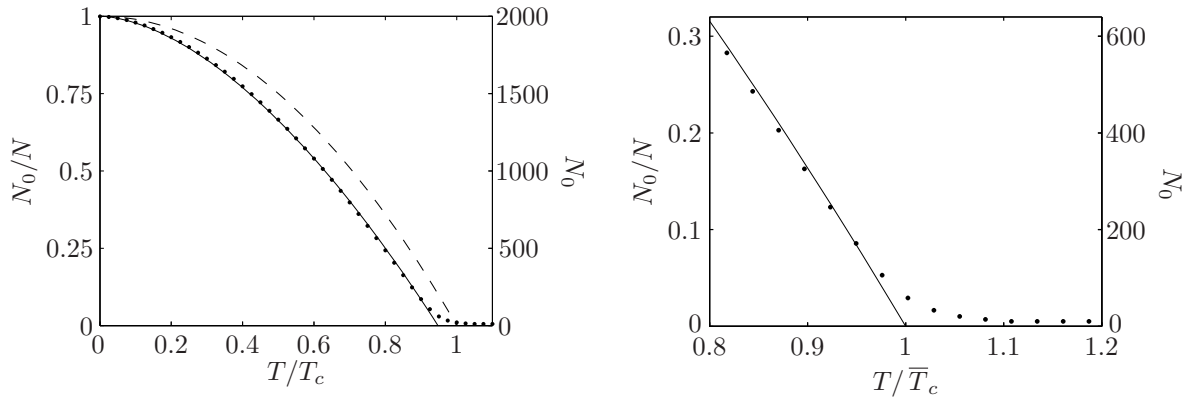

Figure 7.5.: Condensate population versus the critical temperature. The solid line corresponds to a fit (7.3) to the ideal gas equation, the dotted line shows the ideal gas power law dependence with an exponent $\beta = 2$. The points are results from the HFB-Popov calculation. **Right:** Magnified region around the critical temperature. The data from the calculation shows a smooth finite temperature tail while the power law abruptly ends at the critical temperature. In this plot the x-axes has been scaled by α^{-1} to represent the critical temperature $\overline{T}$ from this fit.

Physically this is a finite size effect. In the ideal gas the chemical potential is zero at the point of the phase transition, and therefore the transition point is strictly defined. In the interacting gas, the chemical potential depends implicitly on the non-condensate [48] and, when this becomes large, the transition point becomes smeared out. Technically, the occurrence of the finite temperature tail can be explained through the fugacity term in the quasiparticle distribution function (3.32), which is explicitly given by (3.34). The term $\propto 1/N_0$ prevents the condensate population from becoming negative. However, this expression for the fugacity is only approximate and the shape of the tail and the speed with which it approaches zero depends on the explicit choice of the fugacity term at temperatures $T > \overline{T}_c$.

Furthermore, when the condensate population drops to very small numbers, e. g. 1.6% at $T/T_c = 0.975$, one cannot really speak of a condensate anymore. For these reasons, the results for the region very close to the critical temperature are strongly influenced by numerical techniques, e. g. the explicit choice of the fugacity, and most likely do not correspond to real physics in this regime. Still, the results at and above the transition temperature are given for completeness and because they give further insight into how the theory works in this regime.

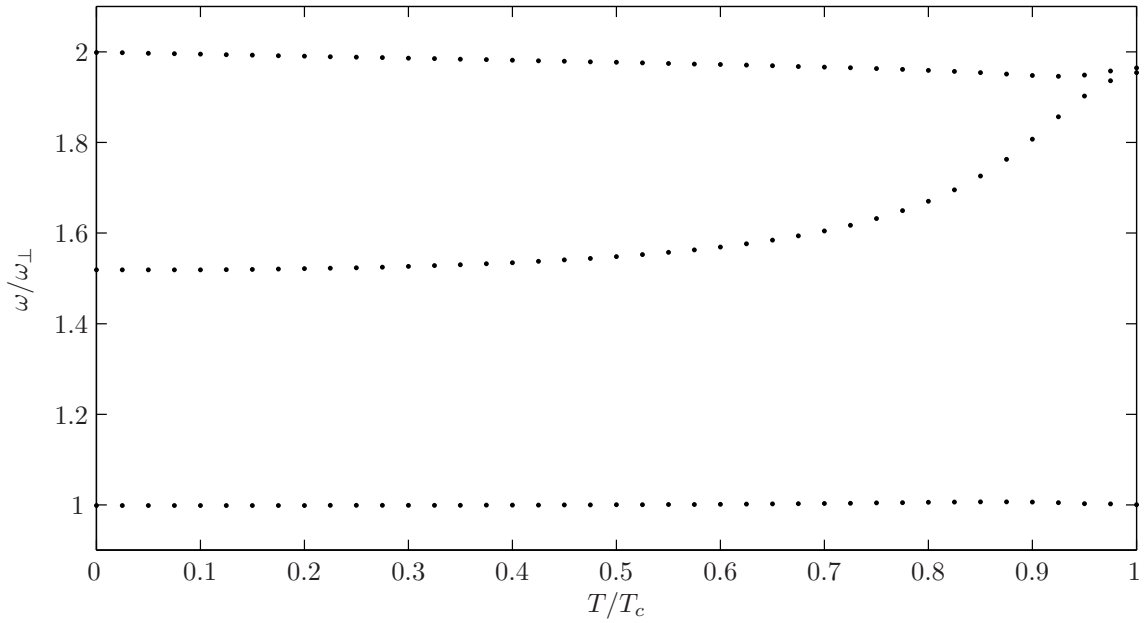

Figure 7.6.: Low-lying excitation modes of the condensate as a function of temperature. The uppermost line corresponds to the *breathing mode* with angular momentum quantum number $m = 0$, the middle line to the *quadrupole mode* with $m = 2$. The lowest line is the *Kohn mode*, $m = 1$, which lies constantly at the trapping frequency.

7.3.3. Excitation spectrum

The low-lying collective or elementary excitation modes of the condensate are important results because they reflect certain fundamental properties of the system. Furthermore, they are easily accessible to experiments. The nomenclature describing the different excitation modes was discussed in Section 3.7.
Figure 7.6 shows the modes with angular momentum $m = 0, 1, 2$ as a function of temperature. Each of the three branches corresponds to the lowest quasiparticle energy eigenvalue in the lowest three, separated, angular momentum subspaces, in which the BdG equations are solved (c. f. Section 6.4.3).

Breathing mode. It is crucial that we observe the breathing mode to lie at a frequency that is twice the trapping frequency. As introduced in Section 3.7.1, this is due to a special symmetry of the many-body Hamiltonian with a $\delta^{(2)}$-interaction potential in two dimensions. As the temperature increases, the non-condensate density increases and starts to constitute a deviation from the harmonic oscillator potential in the Gross-Pitaevskiĭ equation so that the frequency moves away slightly from $2\omega_\perp$. The effective potential becomes weaker so that the frequency decreases.

Kohn mode. Less affected by the perturbation to the harmonic potential, the Kohn mode remains very constant at the trapping frequency, as is predicted by the generalized Kohn theorem, c. f. Section 3.7. However, looking closer at Figure 7.6 one may see a slight increase in the frequency near the critical temperature as the effective potential becomes less harmonic and, therefore, breaks the Kohn theorem. Physically, the Kohn mode is a translative oscillation of the whole condensate. In our calculation we treat the thermal cloud as stationary. The condensate atoms are oscillating against this constant background, which increases the frequency of the oscillation. An inclusion of the full dynamics of the thermal cloud would ensure the Kohn mode to be constant at all temperatures [48, 82, 98].

With increasing temperature, all three frequencies smoothly approach the frequencies of the non-interacting gas and the breathing and quadrupole mode become degenerate. The reason for this is that, as the extension of the condensate shrinks, the non-condensate becomes locally uniform in the region that matters for the low-lying excitations (see Fig. 7.4). Using a local density approximation, we can use the relation $\mu = g(n_c + 2\tilde{n})$ for the uniform gas in the Hartree-Fock approximation [87, §8.3] to show that the BdG equations for $n_c = 0$, given by

$$\Big(\hat{h}_0 - \mu + 2g\tilde{n} - E_i\Big)u_i = 0 \ , \tag{7.4}$$

recover the energies of the harmonic oscillator. In the case that there is still a condensate, the total density in the region where $n_c \neq 0$ is approximately constant just below the critical temperature, so that the mean-field energy constitutes merely a constant shift to the trapping potential and, hence, only slightly alters the eigenfrequencies of the trap.

Comparison to the three-dimensional case

We would briefly like to mention the three-dimensional case where the frequency spectrum looks very similar. The striking difference is the breathing mode which is temperature dependent, whereas it is a feature of the two-dimensional system to have breathing oscillations with a universal energy of $2\hbar\omega$. Calculations for the isotropic three-dimensional case can be found in [48, 49].

7.3.4. Coherence properties

The quantitative analysis of coherence within the condensate is the key-issue in lower-dimensional BECs. As opposed to the three-dimensional gas, phase fluctuations can destroy the global phase of the condensate well below the critical temperature, leading to the formation of a quasicondensate with a coherence length which is smaller than its spatial extension. This quasicondensate still shows long range order and is, therefore, a superfluid phase. We present the first order correlation function and extract a measure of the coherence length that decreases as a function of temperature. Based on this, we suggest a Bragg spectrum in analogy to [102] (Section 5.4.1). Finally, our code is tested against exactly known results for the non-interacting gas.

7.3.4.1. Correlation function

In Figure 7.7 the correlation function $g^{(1)}(0,r)$ is depicted in the left panel at various temperatures. The x-axis has been scaled by the extent of the condensate r_{con}. This is here determined not by the Thomas-Fermi radius, but in such way that at zero temperature the coherence function drops to zero exactly at the edge of the condensate.[3]

The correlation functions at very low temperatures show some unphysical oscillations that are purely numerical noise. At low temperatures $n(r) \approx n_c(r)$. In the limit $\tilde{n} \equiv 0$ the correlation function is given by the Heaviside function $\Theta(1-r/r_{\mathrm{con}})$. However, there is a small contribution from the quantum depletion of the condensate that smoothes the sharp corner as $g^{(1)}$ drops to zero. The unphysical wiggles in the plot occur as the quantum depletion drops to zero and we divide two very similar small numbers in (6.66), hence losing numerical accuracy.

In order to compare the coherence length of the condensate at different temperatures, we extract the lengths at which the correlation function drops to half its value. Looking at the right hand graph in Figure 7.7, we can distinguish three different regimes. Close to zero Kelvin, the slope is very steep and the coherence length decreases to a third of the condensate size below $0.1\,T_c$. Then, up to about $0.8\,Tc$, the coherence length l_ϕ decreases monotonically, but much more slowly. From there up to the critical temperature, the coherence length drops again rapidly.

[3] Explicitly, the coherence length at 0 K is set to $1\,r/r_{\mathrm{con}}$.

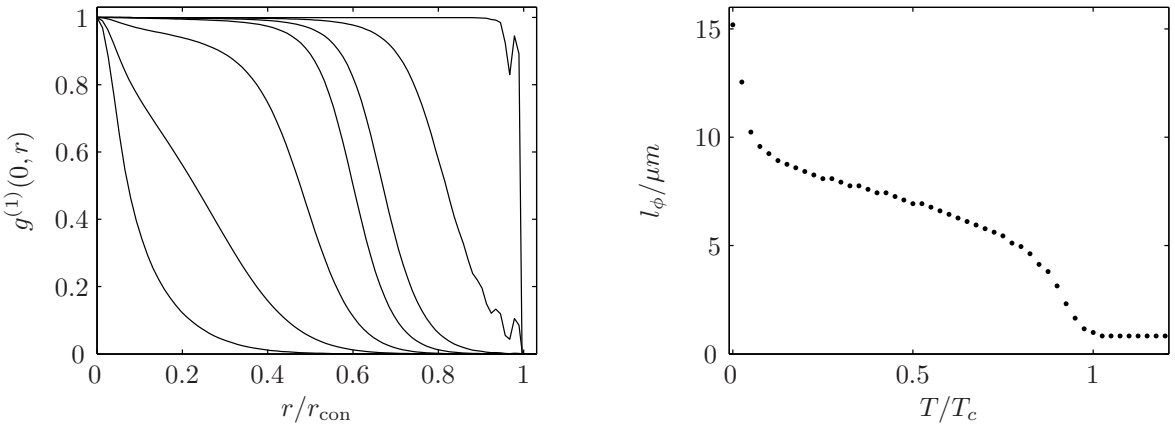

Figure 7.7.: Left: Correlation function $g^{(1)}$ for the non-interacting Bose gas at different temperatures T/T_c: 0, 0.025, 0.05, 0.1, 0.5, 0.9 and 1 f. r. t. l. The scaling of the radius is explained in the text. **Right:** An estimate for the coherence length within the condensate is the extracted full width at half maximum from the correlation function in the left panel.

A decreasing coherence length directly implies a loss in the global phase coherence of the superfluid phase. The Bose-Einstein condensate is destroyed when the phase of the order parameter fluctuates on a length scale which is reasonably smaller than the extent of the condensate. From Figure 7.7 we see that the coherence length drops smoothly. Therefore, it is not possible to determine an exact point on the temperature scale where the transition from a true condensate to a quasicondensate takes place. At about $0.5\,T_c$ the coherence length has dropped to about half of the maximal value, which we can use to determine the spatial extent of the condensate (indicated in the right panel of Figure 7.12). The treatment in [88] predicts a value of approximately $0.4\,T_c$, obtained by evaluating (5.24) for our parameters, for the onset of phase fluctuations. Our result is, therefore, consistent with [88], although the phase coherent phase seems to persist at slightly higher temperatures. Rather than doing a quantitative prediction for the destruction of the true condensate, we compare our results with results calculated for the one-dimensional Bose gas.

Comparison to 1D. The same behaviour has been observed in calculations[4] for the one-dimensional Bose gas at finite temperatures [31]. Their results are depicted for convenience in Figure 7.8. In the one-dimensional case the coherence length drops even more quickly than in the two-dimensional case, showing that phase fluctuations become

[4]The calculation in the reference is based on the hydrodynamic approach within the TF-approximation. The measure used for the coherence length is $1/\sqrt{e} \approx 0.6$ of the correlation function, rather than 1/2 as we choose.

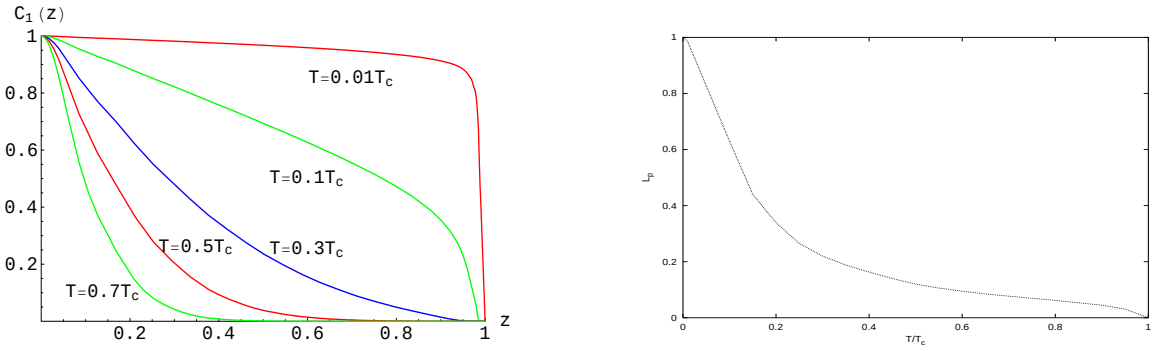

Figure 7.8.: Left: Correlation function calculated for the 1D Bose gas. **Right:** Extracted coherence length ($1/\sqrt{e}$ in left panel). Both plots taken from the reference cited in the text.

much more dominant as the dimension is reduced further. In 1D, the temperature range between 0.3 and $0.5\,T_c$ has about the same coherence properties as the range around $0.9\,T_c$ in our 2D calculation. The author (Ghosh) identifies the 1D condensate at even $0.1\,T_c$ as a quasicondensate with large phase fluctuations. From looking at Figure 7.7, we see that in the 2D case, even if the coherence length has decreased slightly, there is still a large proportion of the condensate where $g^{(1)}$ is constantly 1, indicating that the system is essentially a phase coherent BEC.

Non-interacting case. The off-diagonal density matrix is known in closed analytical form for the non-interacting gas. In can be determined by means of the inverse Laplace transform of the zero-temperature Bloch density matrix [120, 121]. Its explicit form in two dimensions is given by

$$g^{(1)}(\mathbf{r},\mathbf{r}',T) = \sum_{j=1}^{\infty} \frac{e^{j\mu/T}}{\pi(1-e^{-2j/T})} \times \exp\left(-\frac{|\mathbf{r}+\mathbf{r}'|^2}{4}\tanh(j/2T) - \frac{|\mathbf{r}-\mathbf{r}'|^2}{4}\coth(j/2T)\right) . \tag{7.5}$$

We find the chemical potential $\mu = \mu(T)$ for the trapped non-interacting gas by optimizing $\sum_{n=0}^{\infty} f_{\mathrm{B}}(E_n = n+1, \mu, T)\,(n+1) - N = 0$ with respect to μ, $f_{\mathrm{B}} = \left[(1+N_0^{-1})e^{\beta(E_n-\mu)} - 1\right]^{-1}$ is the Bose-Einstein distribution function *with the fugacity factor* that takes into account the number of condensate particles from the HFB calculation. Without this fugacity factor, finite size effects, taken into account in the HFB calculation, would be neglected and, therefore, the comparison would be between two approaches based on different assumptions. The expression (7.5) for the correlation function is exact at all temperatures. Numerically, the infinite sum can be calculated up to any required accuracy.

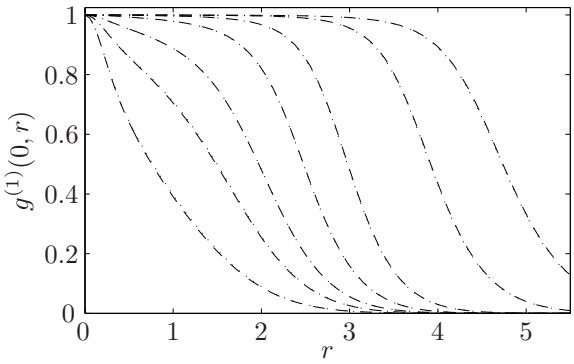

Figure 7.9.: Correlation function $g^{(1)}$ for the non-interacting Bose gas at different temperatures T/T_c: 0.02, 0.03, 0.1, 0.34, 0.75, 0.9 and 1 f. r. t. l. The dashed lines correspond to the HFB results at zero interaction strength, the dotted lines represent the exact result (7.5).

We seek comparison with the non-interacting gas for two reasons: Firstly, we can run the HFB-Popov calculation with the coupling parameter set to zero and verify that the results agree with the exact results for the non-interacting gas. Secondly, the differences that emerge when interactions are included lead to conclusions about the role of interactions and the validity of our calculation in the high-temperature regime.

In Figure 7.9 we compare our code against the exact known results for the non-interacting gas. At all temperatures the HFB results agree perfectly with the correlation function calculated from (7.5). This implies that the numerics works well even at high temperatures and the results obtained can be reliably assumed to represent the physics up to the order of approximation the theory uses. Deviations would indicate an insufficiency in the basis set or an inaccuracy due to a wrong spacing or range in the computational grid.

The influence of the interactions can be seen in Figure 7.10. The dashed lines show the coherence function for the interacting gas, compared to the exact non-interacting gas equation (dotted line). We see that interactions increase the coherence length in a large part of the temperature regime. At $0.8\,T_c$ and above, however, the coherence length of the interacting gas is decreased relative to the non-interacting gas. This can be explained by the effect of the mean-field interaction on the condensate radius. At high temperatures (N_c small) the radius of the interacting condensate is approximately the same as the radius of the non-interacting condensate, given by the size of the lowest harmonic oscillator state. At low temperatures, however, the condensate population is large and mean-field effects broaden the condensate. Correspondingly, the coherence function of the interacting condensate is broader. If the spatial coordinate would be

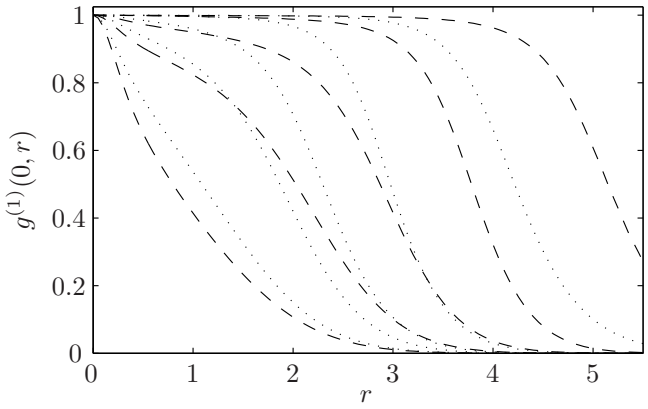

Figure 7.10.: Correlation function $g^{(1)}$ for the non-interacting Bose gas at different temperatures T/T_c: 0.025, 0.1, 0.5, 0.8 and 0.95 f. r. t. l. The dashed lines correspond to the HFB-Popov results for the interacting gas, the dotted lines represent the non-interacting gas (7.5).

scaled by the size of the condensate, interactions would always reduce the coherence.

7.3.4.2. Momentum spectrum

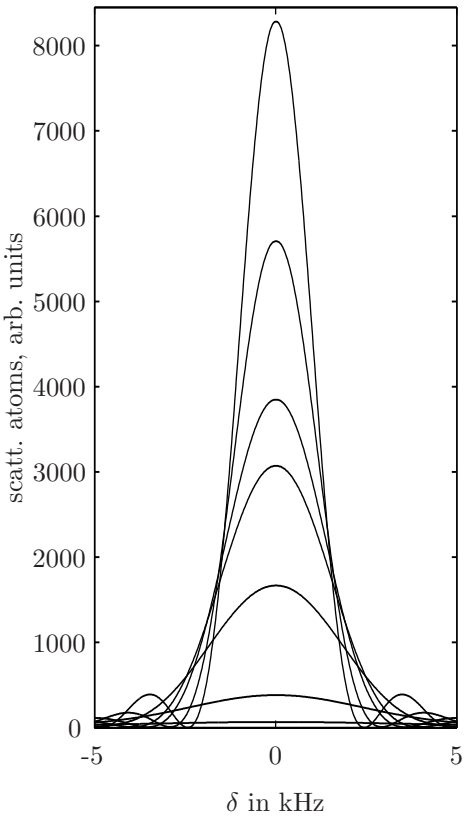

The plot on the left side shows the momentum spectrum, as it could be measured by means of Bragg spectroscopy. Corresponding to (5.7), it has been calculated by Fourier transforming the correlation function in Figure 7.7, c. f. Chapter 5. On the ordinate is the detuning of the Bragg laser beams, which we take in accordance with (5.25) to be directly proportional to the momentum of the atoms, c. f. Section 5.4.1. The highest peak corresponds to the lowest temperature where the momentum distribution of the atoms is narrowest. With increasing temperature the spectrum is broadened, as it can be seen clearly in the left panel in Figure 7.12. An experimental setup is limited by its resolution at low temperatures, because of the decrease of the spectral width.

Figure 7.11.: Momentum spectrum, intensity corresponding to the fraction of scattered atoms as function of the detuning δ. Temperatures T/T_c from top: 0, 0.025, 0.05, 0.1, 0.5, 0.9 and 1.

The right panel in Figure 7.12 shows the coherence length which has been calculated by fitting the momentum spectra in Figure 7.11 and extracting the half widths of the fits. A Gaussian provides a good fit to the momentum spectrum at temperatures $\lesssim 0.9\,T_c$. Above a small crossover regime, the momentum profile at temperatures higher $0.925\,T_c$ fits more closely to a Lorentzian. This is demonstrated in Figure 7.13. Thus, the data points in the right panel of Figure 7.12 correspond to the full width at half maximum (fwhm) of a Gauß or a Lorentz fit, depending on which gives better agreement with the data.

In the same plot the lengths are compared to the previously shown results from the right panel of Figure 7.7. Qualitatively the results agree with each other, although the fwhm of $g^{(1)}$ leads to somewhat smaller values for the coherence length. However, the coherence length is to some extent a matter of personal definition. For example we

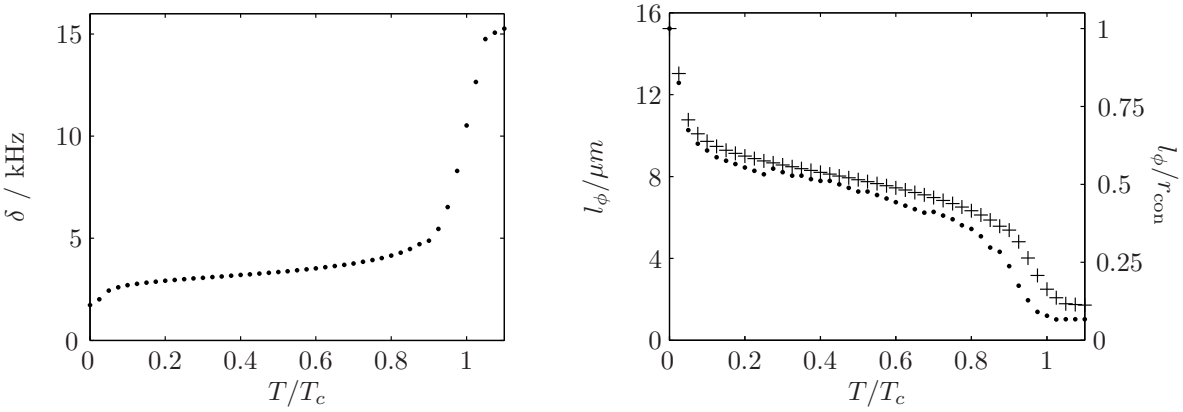

Figure 7.12.: Left: Bragg width as a function of temperature, calculated from fits to the spectra in Figure 7.11, as described in the text. **Right:** Coherence length of the condensate, shown in real units and scaled by the extension of the condensate. The upper line (+) has been calculated from the momentum spectrum (left panel), the lower line (·) is the data from Figure 7.7.

could have chosen $1/e$ rather than fwhm and, within this freedom, the results are in agreement.

In 1D the case of a Lorentzian momentum profile has been found to be characteristic for a phase-fluctuating quasicondensate [30] and has even been used as an identification for such [102]. However, we are convinced that the shape change we observe is not a signature of a phase fluctuating condensate, but the kick-in of the fugacity term as N_0 goes to zero. Furthermore, from looking at the correlation function in Figure 7.7, we would expect the phase fluctuations to become important already at about $0.5\,T_c$.

7.4. Reliability of the results

We briefly comment on the validity of our results. In three dimensions, the Popov theory is known to agree with experimental results (i. e. excitation frequencies) up to $0.6\,T_c$ in the anisotropic trap. To go further, either G2 [49] or even a full second order treatment [82] must be invoked.

When looking at the phase fluctuating regime, we are interested in the region close to the critical temperature. The correctly calculated correlation functions for the non-interacting case and the fact that the results, e. g. the frequencies, are completely smooth do not indicate a general failure of the method we employ. However, the

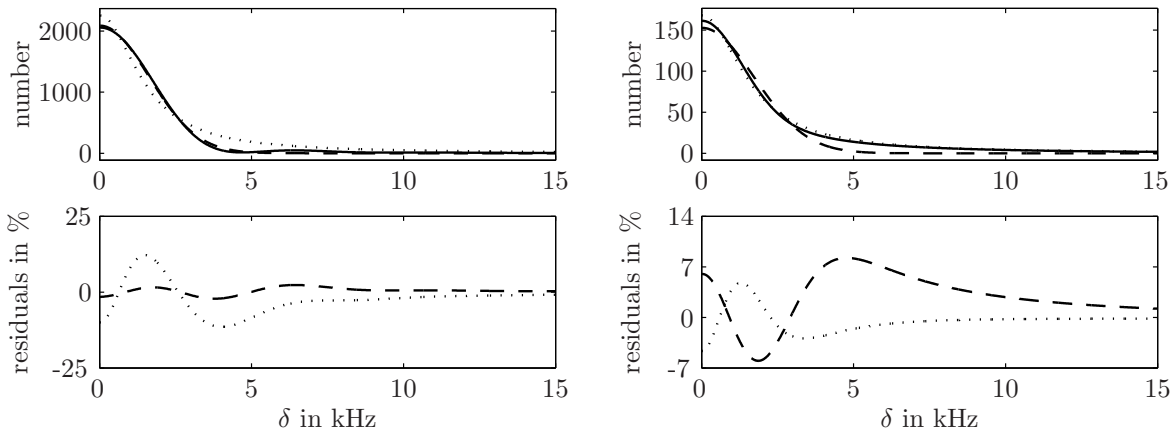

Figure 7.13.: Fit to the momentum profile at 0.35 (**left**) and 0.95 T_c (**right**). Solid line: data. Dashed line: Gauß fit. Dotted line: Lorentz fit. The upper graphs show the fits in comparison to the original curve, the lower graphs show the residuals to each fit. The residuals are shown as a percentage of the maximum of the data.

decomposition of the field operator relies on the existence of a macroscopic order parameter. At high temperatures when phase fluctuations dominate the condensate, we still expect the overall density still to be well represented by the condensate wave function, even though the order parameter does not describe the actual physical state correctly. For example it is not possible to gain any information about the nature of the condensate in the regime where phase fluctuations dominate, e. g. unordered state or regular vortex/antivortex lattice (Kosterlitz-Thouless (KT) phase).

Thus, a fundamental problem constitutes mean-field theory itself. Replacing the local order parameter by its mean value is only a good approximation if the fluctuations to this mean are small. It can be shown that, in general, mean-field theory always breaks down in $D < 4$ dimensions at a temperature sufficiently close from below to the critical phase transition temperature, because phase fluctuations become dominant. The criteria for the internal consistency of the mean-field approximation can be formulated as [33]

$$\frac{1}{V_\xi} \int_{V_\xi} \mathrm{d}^D x \; G^{(1)}(\mathbf{0}, \mathbf{x}) < \langle \Psi_0(\mathbf{x}) \rangle \; , \tag{7.6}$$

where $G^{(1)}(\mathbf{0}, \mathbf{x})$ is the first order correlation function defined in (5.9), $\Psi_0(\mathbf{x})$ is the mean of the order parameter, defined in (3.13) and $V_\xi \sim l_\phi^D$ denotes the coherence volume in that the order parameter does not deviate considerably from its mean value. The regime where (7.6) is violated is termed the *Ginzburg region*, as he introduced the criteria. To extract the physics in the regime where mean-field theory breaks down, other methods have to be employed, such as Quantum-Monte-Carlo or renormalization

groups. Renormalization group theory is a powerful method which has been used by Kosterlitz and Thouless to study the critical properties of an ideal two-dimensional system (XY-model) [68, 69]. The possibility of a phase transition of the Kosterlitz-Thouless type as well as the occurrence of an universal jump, predicted for the KT transition, has been verified for the dilute, weakly interacting Bose gas by Stoof [109]. For further discussion, we refer to the textbook [18].

When interpreting the results close to the critical temperature, we have to keep in mind that mean-field theory is supposed to break down in this regime and that our results may rather show this aspect than corresponding to real physics in the Ginzburg-region of the system.

Accuracy

In general, the accuracy of our results depends on the convergence criteria for the self-consistent solution. At temperatures below $0.95\,T_c$ results can be obtained to any required accuracy without difficulties. Thus, in the plots the numerical error is smaller than the point size unless stated differently.
As the condensate fraction drops to very small values, convergence might become more difficult to achieve, since only a small fraction of the solution of each iteration can be mixed into results of the previous iteration in order to keep the number of condensate atoms positive. Close to the transition temperature it can happen that the program is trapped in an oscillatory solution where no better convergence can be achieved even if the number of iterations is increased. We have already pointed out that the results in this regime are strongly dependent on the numerical methods. Furthermore, because of the expected breakdown of mean-field theory, the results should not be considered to represent the actual physics in this regime.

8. Beyond the Popov Approximation – Results using Gapless HFB

In the previous chapter we looked at the results from the Hartree-Fock-Bogoliubov theory within the limitations of the Popov approximation. Now we go beyond the Popov approximation and include many-body effects in the collisions. This enables us to compare the gapless HFB many-body T-matrix to its approximation by the off-shell two-body T-matrix. In gapless HFB, many-body effects are introduced through the anomalous average. The thermal properties of this quantity and different renormalization methods are topic of the first section.

In the three-dimensional anisotropic case the excitation frequencies predicted from the Popov theory disagree with the results known from experiment [49]. An inclusion of the many-body T-matrix by using the G2 theory has been shown to resolve this problem partially. However, complete agreement between theory and experiment has only recently been achieved by including the dynamics of the thermal cloud in a second order treatment [82]. In the symmetrical case the shifts in the frequencies in G1 and G2 to the Popov results are not substantial. We show the results of our calculation in Section 8.2 and discuss the modified spectrum of the low-lying excitations.

The main part of this chapter is concerned with the study of scattering in two dimensions. As explained in Chapter 4, the Bose-Einstein condensed system goes through different regimes as dynamics in the third dimension is eliminated. In Section 8.3 we discuss how the treatment of collisions and the choice of the coupling parameter is altered as the axial trapping frequency is increased, based on the gapless HFB and the off-shell two-body T-matrix approach for the coupling strength. At finite temperatures the off-shell two-body T-matrix approach introduced in [73] for finding an analytic expression for the many-body T-matrix becomes invalid. We discuss an extension to finite temperatures in the last Section of this chapter.

The determination of the many-body T-matrix is of particular interest for the use of the Popov approximation in two dimensions, too. Normally, in three dimensions, the

bare interaction potential is approximated by a contact interaction pseudo potential where the interaction strength is given by the lowest order of the zero-momentum and low-energy limit of the two-body T-matrix. In two dimensions, however, the two-body T-matrix vanishes in this limit. Thus, the choice of an appropriate coupling parameter in the Popov theory must take many-body effects on scattering into account. If this is not done via the anomalous average by using the gapless theories G1 and G2, finding an analytic expression for the many-body T-matrix at finite temperatures is of fundamental interest.

8.1. The anomalous average

The Popov approximation corresponds to setting $\widetilde{m} \equiv 0$. This avoids problems contained in the full HFB theory, such as the ultra-violet divergences and not producing a gapless spectrum, c. f. Section 3.4.1. However, the anomalous average incorporates many-body effects on interactions and the many-body T-matrix can be found in terms of $\widetilde{m}$ if these are introduced consistently, c. f. Section 4.3.3. In order to avoid divergences, we must use a renormalization scheme when calculating $\widetilde{m}$, c. f. Section 4.4. We use the semi-classical renormalization scheme, introduced in Section 4.4.2.1, to estimate the contribution towards $\widetilde{m}$ in the limit that there is no condensate. By subtracting this, we ensure that vacuum contributions which are part of $\widetilde{m}$ are not accounted for twice, since they are already included in the scattering length.

In the left panel of Figure 8.1 the renormalized anomalous average, denoted with the superscript R, is plotted at various temperatures. Often $\widetilde{m}$ is renormalized by dropping the '1' in the term $2f_{\mathrm{B}} + 1$ in (3.31). Then $\widetilde{m}$ is negative at all times. At zero temperature, however, this implies $\widetilde{m} \equiv 0$. Utilizing the semi-classical or perturbative renormalization, c. f. Section 4.4.2.2, the anomalous average becomes positive at low temperatures. This can also be seen in Figure 8.2 where we compare the latter two renormalization schemes at two different temperatures.

As the temperature is increased towards the critical temperature, the condensate becomes highly depleted and the anomalous average vanishes. This is shown in the right panel of Figure 8.1.

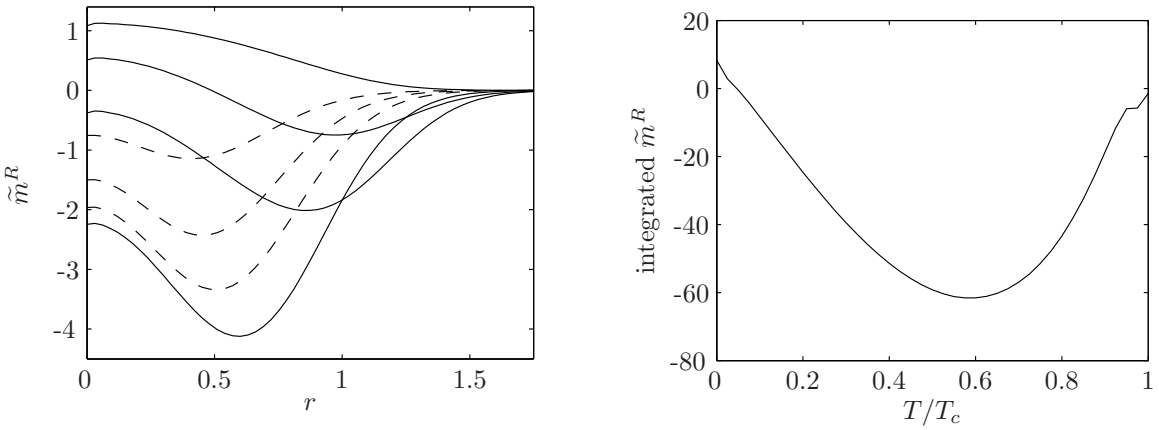

Figure 8.1.: Renormalized anomalous average. **Left:** Shown is $\widetilde{m}^R$ at the temperatures T/T_c: 0, 0.15, 0.3, 0.75 (solid lines from top to bottom), 0.85, 0.9 and 0.975 (dashed lines from bottom to top). The renormalization makes $\widetilde{m}^R$ positive at low temperatures. **Right:** Spatially integrated anomalous average. As pair interactions are reduced due to the decrease in the condensate fraction, the anomalous average must go to zero at the critical temperature. The kink indicates a not completely converged solution in the run for this temperature ($0.975\,T_c$).

8.2. Excitation modes

In Figure 8.3 we plot the frequencies of the $m = 0, 1, 2$ modes calculated in within G1, G2 and the Popov approximation. Interestingly, in the high temperature regime, all three modes show an increase in frequency in the G1 theory and a decrease in the G2 theory towards the Popov results. For the Kohn mode, the shift can be explained as follows: In the Popov approximation, the effective potential the condensate is in is given by $U_{\text{trap}} + 2g\tilde{n}$. Through the additional high density of thermal atoms, the effective trapping potential becomes steeper so that the frequency increases. If we now consider the G2 theory where the coupling parameter for the condensate–non-condensate interactions is replaced by the many-body T-matrix, there is an additional term $\propto \widetilde{m}$ which reduces the effective potential (since $\widetilde{m}$ is always negative at high temperatures). The effective trapping potential becomes wider and the frequency decreases. In the G1 theory, many-body effects for interactions with the non-condensate are not accounted for.

In the anisotropic case, the Popov theory has been found to overestimate the frequency of the breathing mode [98, 114].

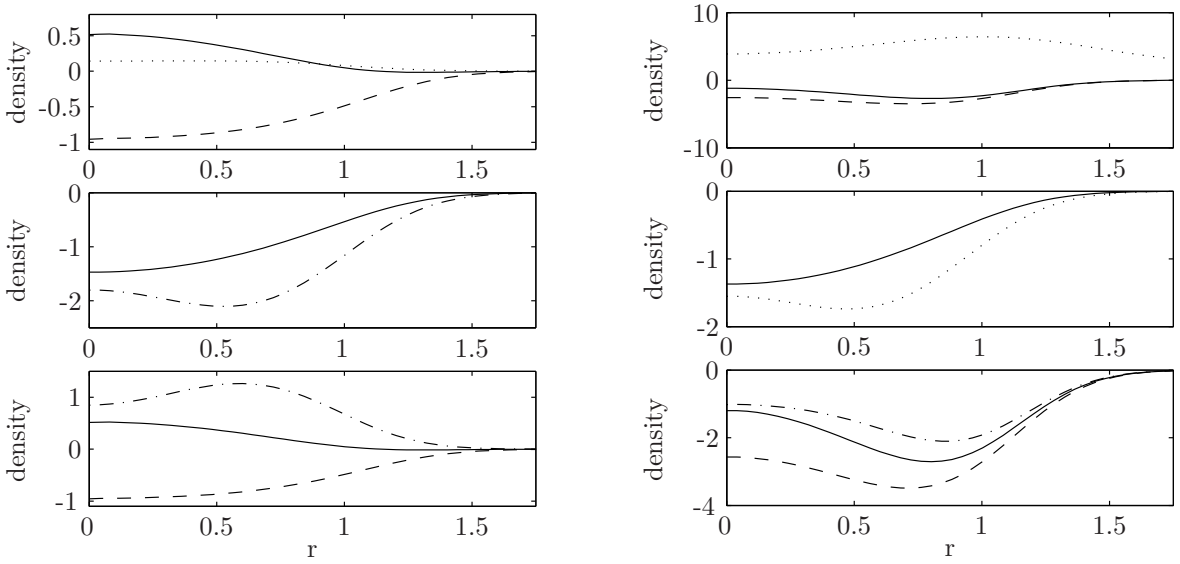

Figure 8.2.: Renormalization of the anomalous average, **left** at $0.01\,T_c$, **right** at $0.35\,T_c$. The upper plot shows the renormalized (solid line) and unrenormalized (dashed line) anomalous average in comparison the non-condensate density (dotted line). The middle plot shows the renormalized part of $\widetilde{m}$ due to the semiclassical (solid line) and perturbative (dash-dotted/dotted line) calculation. Since it is calculated in the zero temperature limit, the plot in the left and the right panel are identical. In the lowest plot, we compare these two renormalization methods: The dashed line is the unrenormalized anomalous average, the solid line is $\widetilde{m}$ within the semiclassical renormalization, the dash-dotted line shows $\widetilde{m}$ within the perturbative renormalization (see text). Note that at sufficiently low temperature the anomalous average changes its sign due to the renormalization.

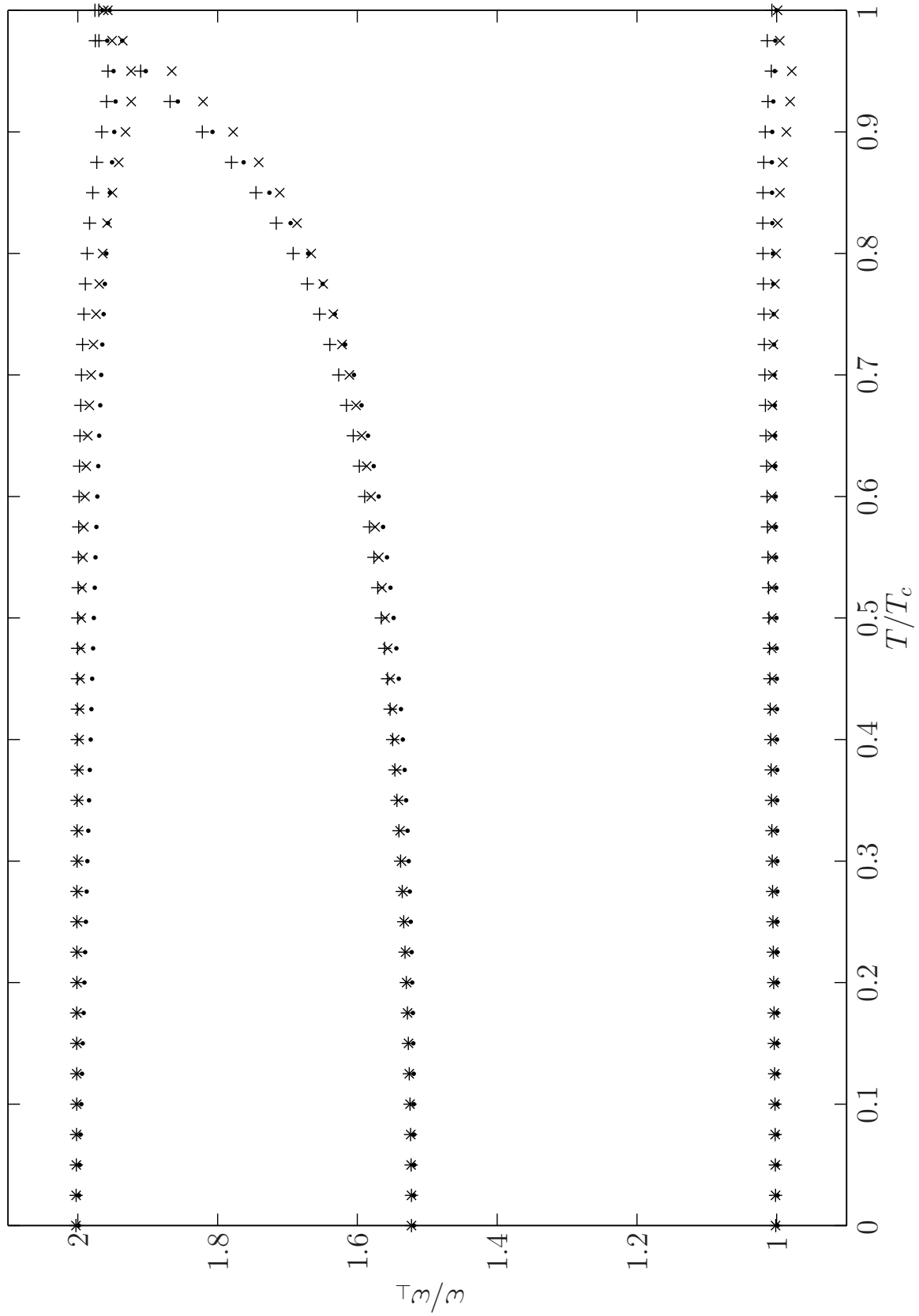

Figure 8.3.: Low lying excitation frequencies. Compared are the Popov approximation (·), G1 (+) and G2 (×).

8.3. Interactions and coupling parameter

When discussing the two-dimensional BEC, we introduced three different regimes in Chapter 4, regarding to which extent the third dimension has been eliminated from the system. This is characterized by the parameter $l_z/a_{3\mathrm{D}}$.

This section is divided into two parts. First, we compare the two versions of the many-body T-matrix, introduced in Sections 4.3.2.1 and 4.3.3, at zero temperature for different values of this parameter. From this, in the second part we suggest a choice of the parameter U_0 in the gapless HFB many-body T-matrix (4.36) at finite temperatures, where the approach from Section 4.3.2.1 is not valid anymore.

To avoid confusion, we refer to the many-body T-matrix that is approximated by the off-shell two-body T-matrix, evaluated at the off-shell negative energy $-\mu$, and used with the specific quasi-two-dimensional scattering length (4.9), as the *quasi-2D coupling parameter*. The other form of the T-matrix (4.36) that originates from the gapless theories and incorporates the anomalous average is referred to as the *gapless HFB many-body T-matrix*. Both forms are approximations to the many-body T-matrix that is defined in (4.16).

8.3.1. Zero temperature

Figure 8.4 shows the coupling parameter for the conditions of the experiment of Görlitz [39], as it is calculated self-consistently from the off-shell two-body T-matrix, evaluated at the negative energy $-\mu$. The dotted line is the homogeneous expression for the many-body T-matrix (4.14), evaluated at $E = -\mu$, i. e.

$$g_{\mathrm{q2D}}^{\mathrm{hom}} = -\frac{8\pi}{\ln(\mu a_{2\mathrm{D}}^2/8)} \tag{8.1}$$

in dimensionless units. If, for simplicity, a constant coupling parameter is being used in the calculation, it should be this value. The dashed line is the approximate solution (4.27) which we use as an initial guess for solving (4.26). This form of the many-body T-matrix, where $a_{2\mathrm{D}}$ is given by (4.9), is valid in the crossover regime from quasi-2D, where scattering is still three-dimensional, to purely quasi-2D. With a ratio of $l_z/a_{3\mathrm{D}} \approx 270$, the regime investigated in Fig. 8.4 lies in this crossover section.

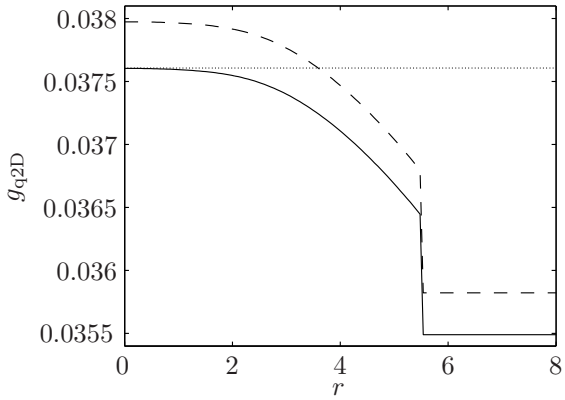

Figure 8.4.: Many-body T-matrix at zero temperature, as it is valid in the quasi-two-dimensional regime. The full line corresponds to the spatially dependent, self-consistent solution of (4.26), the dashed line is the approximate solution (4.27). The dotted line is the homogeneous limit (4.24) in (4.14). The trapping parameters are those of the previous chapter, $l_z/a_{3\mathrm{D}} \approx 270$.

The many-body T-matrix has only physical relevance in the region where the condensate density is not negligible. Thus, the ordinate in the right panel of Fig. 8.5 and the following figures displays only the regime where $n_c > 10^{-5}$. Note that, for the parameters from [39], between 3 and 3.5 in trap units the condensate density has already dropped down to 1% of its peak value. The plots show a larger region in order to display the behaviour of the coupling parameters. Nevertheless, discrepancies between the two coupling strengths away from the bulk of the condensate have only little effect.

In Figure 8.5 we compare the self-consistent result from Figure 8.4 with the result from gapless HFB, using the coupling parameter (4.6) $U_0 = g'_{3\mathrm{D}}$ in the calculation of the gapless HFB many-body T-matrix. This parameter is valid in the quasi-2D regime where collisions take place in three dimensions. As can be seen in the left panel, the gapless HFB result lies above the quasi-2D coupling parameter. The choice of $U_0 = g'_{3\mathrm{D}}$ is an upper limit to the quasi-2D expression for the case that the ratio $l_z/a_{3\mathrm{D}}$ reaches a maximal value while the dynamics in the tightly confined dimension is still suppressed. Thus, a better choice for U_0 in the quasi-2D regime is given by the homogeneous coupling parameter (8.1), since it accounts for the modifications in the scattering length due to the reduction of dimensionality. This choice leads to very good agreement between the two many-body T-matrices in the region where interactions take place, as can be seen in the right panel of Figure 8.5.

At the edge of the condensate, where $\widetilde{m}$ and Ψ_0 go to zero, the gapless HFB many-

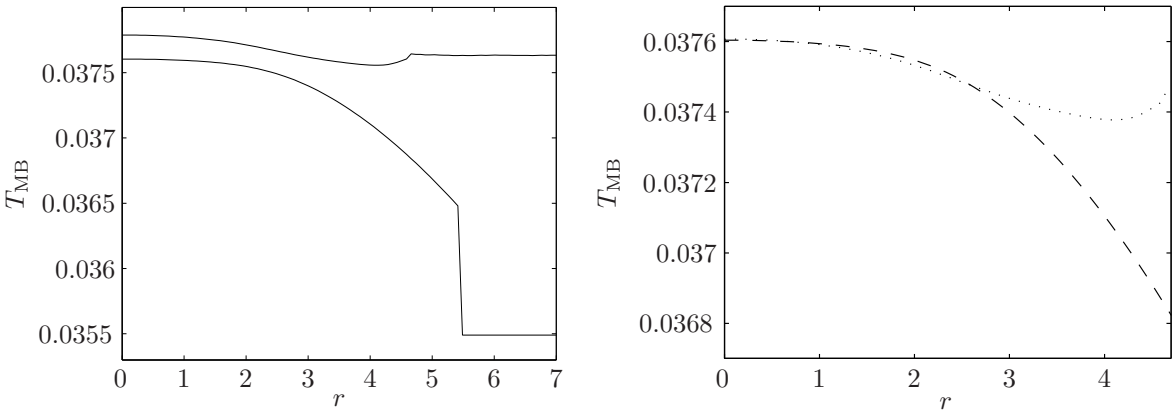

Figure 8.5.: Comparison of the quasi-2D coupling parameter (lower line in the left panel, dotted line in the right panel) and the gapless HFB many-body T-matrix (upper line, dashed line respectively) at zero temperature. The result from gapless HFB is based on the coupling parameter $U_0 = g'_{\mathrm{3D}}$. In the **right panel** the gapless HFB result has been calculated with $U_0 = g^{\mathrm{hom}}_{\mathrm{q2D}}$. The trapping parameters are those of the previous chapter, $l_z/a_{\mathrm{3D}} \approx 270$.

body T-matrix returns to the value of U_0, which would be the two-body T-matrix in the three-dimensional case. The quasi-2D coupling parameter approaches zero in the case that $n_c = 0$. However, it remains finite due to the logarithmic dependence on the condensate density, which numerically never becomes exactly zero.

Figure 8.6 shows the same as the right panel in Figure 8.5, but the axial trapping frequency is increased up to a factor of 10^4, $l_z/a_{\mathrm{3D}} \approx 3$ correspondingly, which brings the condensate close to the genuine 2D limit. As the frequency increases, the gap between the gapless HFB many-body T-matrix, based on the g'_{3D} coupling parameter (dotted line), and the quasi-2D coupling parameter (solid line) becomes larger. As explained, this is because the confinement of the trap becomes relevant for the length scale on that interactions take place. This is not taken into account in the derivation of g'_{3D}. The dashed line shows the gapless HFB many-body T-matrix where $U_0 = g^{\mathrm{hom}}_{\mathrm{q2D}}$ has been used, which shifts the gapless HFB result to overlap with the quasi-2D coupling parameter as the trapping frequency is increased. The agreement between the off-shell coupling parameter and the gapless HFB many-body T-matrix improves the more 'two-dimensional' the system becomes.

Density profile. It is worth pointing out that, despite all the considerations about the correct treatment of scattering in the quasi-two-dimensional regime, the shape of the condensate is only negligibly altered. We compared the condensate density for the

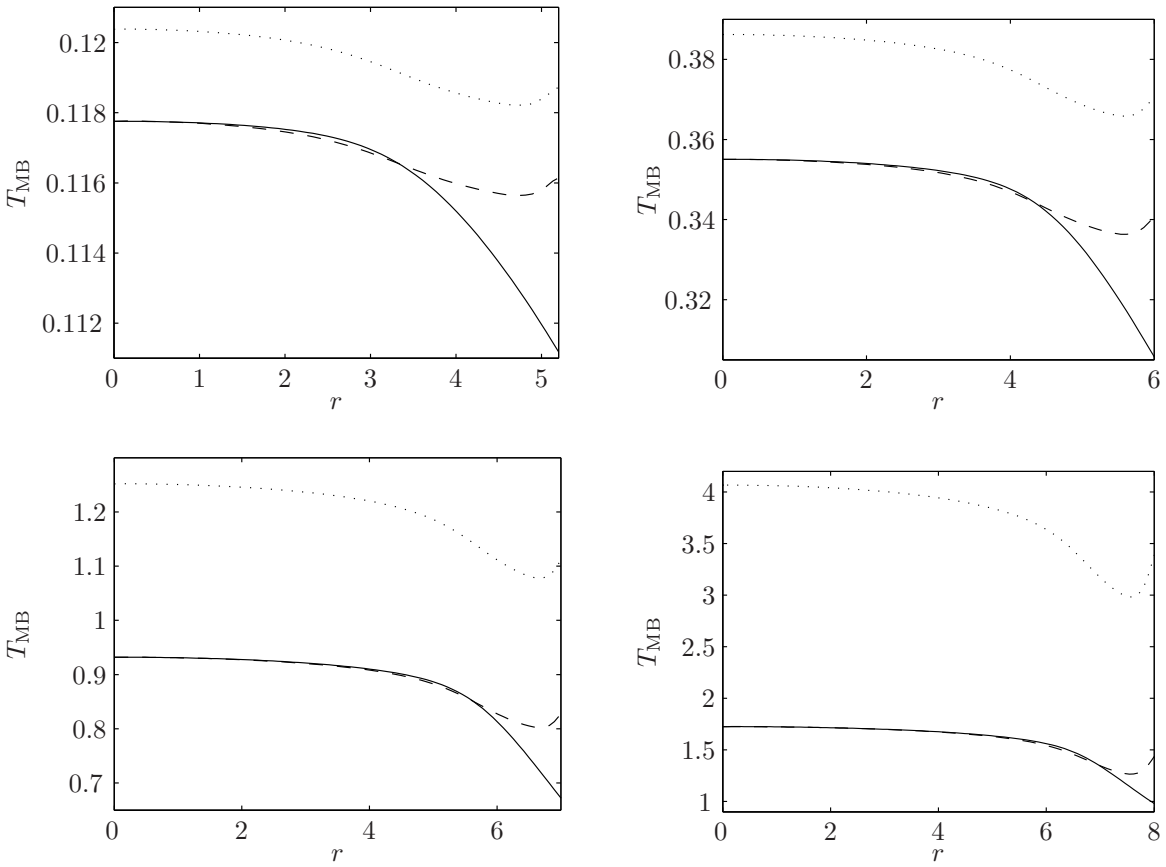

Figure 8.6.: Comparison of the quasi-2D coupling parameter (solid line) and the gapless HFB many-body T-matrix at zero temperature for different axial trapping frequencies. The dotted line corresponds to the choice of $U_0 = g'_{\mathrm{3D}}$, the dashed line to $U_0 = g^{\mathrm{hom}}_{\mathrm{q2D}}$, see text. With increasing trapping frequency, the condensate approaches the purely two-dimensional regime. In comparison to Fig. 8.5, the ratio l_z/a_{3D} is decreased to 84, 27 in the first row, and 8, 3 in the second row. This corresponds to trapping frequencies of 10^1, 10^2, 10^3 and 10^4 times the original frequency of $\omega_z = 2\pi\,790\,\mathrm{Hz}$. Note that the radius of the condensate increases with increasing ω_z.

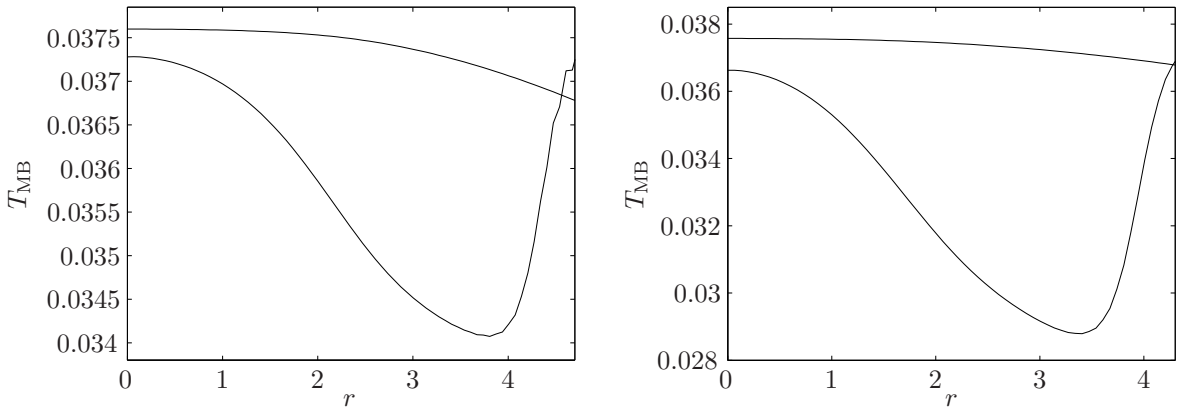

Figure 8.7.: Gapless HFB many-body T-matrix (lower line) and quasi-2D coupling parameter (upper line) at finite temperatures, **left** at $0.35\,T_c$, **right** at $0.75\,T_c$. The trapping parameters are those from the previous chapter, i. e. $l_z/a_{3\mathrm{D}} \approx 270$. Shown is only the regime that is relevant for condensate interactions. Note the different scale on the y-axes.

homogeneous quasi-2D coupling parameter (8.1), the self-consistent solution (4.26) and the gapless HFB many-body T-matrix (4.36) and the difference in the shape is of the order of 0.1%.

8.3.2. Finite temperature

As the temperature and the non-condensate fraction increase, many-body effects cause the coupling strength to drop throughout the condensate size down to about 70% of its maximal value. Figure 8.7 shows this for two different temperatures. The approximation of the many-body T-matrix via the off-shell two-body T-matrix in the zero-temperature limit cannot represent the behaviour of the gapless HFB result, which incorporates finite temperature contributions naturally through the anomalous average and the condensate density.

Therefore, we suggest the following method to determine the coupling parameter at finite temperatures. The quasi-2D coupling parameter for the uniform gas (8.1) is calculated at zero temperature, where (4.26) is used in the self-consistent calculation. This is then taken to be the parameter U_0 in the gapless HFB many-body T-matrix which is utilized in the finite temperature calculation.
This method relies on the agreement of the quasi-2D coupling parameter and the gapless HFB many-body T-matrix at zero temperature. In the previous section we have shown that these do agree in the quasi-2D limit in the spatial regime where

condensate interactions take place. Furthermore, the parameter U_0 can be expected to be independent of temperature, since in gapless HFB many-body effects are accounted for via the anomalous average and the condensate wave function.

A recent publication treats the problem of determining the many-body T-matrix at finite temperatures approximated through the off-shell two-body T-matrix within the Thomas-Fermi approximation for a homogeneous coupling parameter [99]. The influence of temperature has been found to be rather small and negligible for the effect on the condensate wave function. Comparison with the results from gapless HFB implies, however, that the shape of the condensate must be taken into account. We found that using a local density approximation in the theory described in this publication leads to partial agreement with the gapless HFB many-body T-matrix. This will be subject of further study independent of this thesis.

9. Conclusion and Future Prospects

We have used the Hartree-Fock-Bogoliubov (HFB) formalism to investigate the finite-temperature physics of a Bose-Einstein condensate confined to a two-dimensional geometry. This formalism has been proven successful in the three-dimensional case. However, in the lower dimensional system phase fluctuations must be taken into consideration at comparatively lower temperatures. In a regime below the critical temperature they destroy the global coherence of the condensate and the superfluid state is best described as a quasicondensate. In the HFB formalism phase fluctuations are included via the contribution to the non-condensate density from low-energy quasiparticles. We showed that the formalism is not only applicable in the two-dimensional case, but also that the quantities obtained, such as the single-particle off-diagonal density matrix, allow for a quantitative analysis even in the phase fluctuating regime. Our work is consistent with [88] and goes beyond the treatment in this publication, although we find that, within the HFB treatment, the pure condensate phase persists to higher temperatures.

Our work [32] is the first HFB treatment of the two-dimensional Bose gas undertaken in the literature. Previous work was based on the semi-classical or the Thomas-Fermi approximation. Due to modifications in the density of states, the semi-classical approximation fails in two dimensions. This has led to confusion in previous work [5, 27, 110], among it the assumption that BEC cannot occur because the condensate is destabilized by long wavelength phonons [27]. In conclusion, we have shown that the presence of the trap stabilizes the condensate against long wavelength fluctuations if the quantum mechanical character of the trap is properly accounted for, and BEC exists in a large regime below the critical temperature.

The coherence length of the condensate can be determined from its momentum profile. Based on the experimental and theoretical results presented at the ICOLS conference in 2003 for the one-dimensional case [4], we have calculated the Bragg spectrum for a condensate in two dimensions. We found the values extracted for the coherence

length to be in qualitative agreement with those calculated for the one-dimensional Bose gas, although a true BEC with global phase coherence still exists at much higher temperatures than in the 1D case.

We have compared our results against exact theoretical predictions, such as the off-diagonal density matrix for the non-interacting gas and the excitation frequencies. Our calculation shows a breathing mode with a constant frequency of twice the trapping frequency. This is in agreement with [93] and a characteristic of the two-dimensional problem. Hence, it is critical that our calculation renders this result. The correlation function calculated for the non-interacting gas agrees perfectly with the exact theoretical result, showing that the chosen basis set represents the occupation of states well at all temperatures.

We have also studied collisions in the regime of reduced dimensionality. The common way to treat interactions in the mean-field description of BEC is to neglect many-body effects by considering the low-energy low-momentum limit of the two-body T-matrix, which describes collisions in a vacuum. However, this limit of the T-matrix vanishes in two and one dimensions and, a consistent treatment of collisions must include many-body effects even in the first order approximation. At zero temperature, the many-body T-matrix can be approximated through the off-shell two-body T-matrix, evaluated at a negative energy. We found agreement between this approximation and results obtained using gapless HFB, where the many-body T-matrix is introduced through the anomalous average. It is well-known that this quantity suffers an ultra-violet divergence, which must be renormalized. However, the most commonly used way to do this is rather approximate [48, 98] and, in two dimensions, does not lead to agreement between the two approaches to calculate the many-body T-matrix. We invoked two other, more justifiable, methods to renormalize the anomalous average and found better agreement if the renormalization term is calculated within a semi-classical or perturbative renormalization scheme. Physical considerations led to the result that the semi-classical method is the most appropriate way to remove the ultra-violet divergence.

The off-shell two-body T-matrix approximation, as introduced in [73], is valid only at zero temperature, where the finite-temperature Bose-enhancement on scattering can be neglected. We calculated the many-body T-matrix at finite temperatures by means of the anomalous average within gapless HFB to obtain self-consistent solutions for $T > 0$. However, in the gapless theories G1 and G2, the choice of the coupling strength U_0

depends on the regime of dimensionality. We investigated the regimes where collisions are unaffected or partially affected by the reduction of dimensions and proposed a corresponding choice for the coupling strength by comparison of the two many-body T-matrix approaches at zero temperature.

Finally, results from the three different gapless theories, Popov, G1 and G2, have been compared. We found changes in the low-lying excitation frequencies due to the effect of the anomalous average. However, when comparing the correlation functions and the momentum spectra, as well as the condensate wave function itself, we found the differences to be negligible.

Future work

In the context of this thesis we have worked on a finite temperature extension to the off-shell two-body approximation of the many-body T-matrix. The calculation of the many-body T-matrix within the gapless HFB approach is rather involved and requires the self-consistent solution of the Gross-Pitaevskiĭ equation and the Bogoliubov-de Gennes equations. Therefore, a closed equation for the spatial dependent coupling parameter at finite temperatures would be considerably more convenient, as well, as allowing a mutual confirmation for the validity of both approaches. Work regarding a finite temperature expression for the many-body T-matrix in closed form for a condensate within the Thomas-Fermi approximation has already been undertaken [99], but only for a coupling parameter in the homogeneous limit, i. e. without explicit dependence on the condensate shape. Comparison of this work with our results using gapless HFB implies that the shape of the condensate cannot be neglected. Further study of this problem is currently being undertaken.

Of great interest is also the physical nature of the phase-fluctuating condensate. It is a well-known result that vortex/antivortex pairs destroy the long-range order in two-dimensional systems [26, 63, 68, 69, 109]. At high enough temperatures, these pairs can even unbind in a phase transition of the Kosterlitz-Thouless-Berezinski type. Currently, we are investigating the effect of a single vortex/antivortex pair on the free energy of the condensate ground state at finite temperatures. Comparison to the state without vortices and variation of the vortex separation will give us a deeper insight into the phase-fluctuating regime of the quasicondensate.

Part IV.

Appendices

A. Properties of the Generalized Zeta-Function

We defined the generalized ζ-function in Chapter 2 as

$$\zeta_\nu(z) = \frac{1}{\Gamma(\nu)} \int_0^\infty \mathrm{d}x \frac{x^{\nu-1}}{z^{-1}e^x - 1} \ . \tag{A.1}$$

It contains the special case of the Riemann Zeta function

$$\zeta_\nu(1) = \zeta(\nu) \ . \tag{A.2}$$

The representation of (A.1) as a power series is useful and can be found by using the geometric series. It is given by

$$\zeta_\nu(z) = \sum_{k=1}^{\infty} \frac{z^k}{k^\nu} \ . \tag{A.3}$$

For (A.2), the series takes the form

$$\zeta(\nu) = \sum_{k=1}^{\infty} \frac{1}{k^\nu} \ . \tag{A.4}$$

Robinson expansion for small μ

All thermodynamical quantities for the ideal Bose gas can be defined in terms of the generalized ζ-function and the thermal de Broglie wavelength. In order to study the regime near the phase transition, the behaviour of the generalized ζ-function for small μ needs to be derived.

The subtlety of this task emerges when this is tried with a simple expansion of the exponential, i. e.

$$\zeta_\nu(e^{\beta\mu}) \overset{(A.3)}{=} \sum_{k=1}^{\infty} \frac{1}{k^\nu} \sum_{m=0}^{\infty} \frac{(\beta\mu k)^m}{m!} = \sum_{m=0}^{\infty} \frac{(\beta\mu)^m}{m!} \sum_{k=1}^{\infty} \frac{1}{k^{\nu-m}} \overset{(A.4)}{=} \sum_{m=0}^{\infty} \frac{(\beta\mu)^m}{m!} \zeta(\nu - m) \ . \tag{A.5}$$

However, the two sums cannot be interchanged [105] and this expansion turns out to be incorrect. A more careful treatment yields the correct series representation for small negative μ

$$\zeta_\nu(e^{\beta\mu}) = \Gamma(1-\nu)\,(-\beta\mu)^{\nu-1} + \sum_{k=0}^{\infty} \frac{(\beta\mu)^k}{k!}\,\zeta(\nu-k)\;. \tag{A.6}$$

A derivation in terms of the Poisson sum formula can be found in Chapter 2 of [65]. Alternatively, we refer to the original publication [103].

Limes for $\nu \longrightarrow 1$

For the case of the two-dimensional free Bose gas in Section 2.3, we need to consider the limit

$$\lim_{z\downarrow 1} \zeta_\nu(z)\;. \tag{A.7}$$

Since the ζ-function has a pole at $z=1$, we need to take the proper limit in (A.6) for $\nu \uparrow 1$. Beforehand, note the following expansions of the Gamma and Zeta function for small ϵ, which can be easily verified by looking them up looking in [40] or typing into MATHEMATICA:

$$\Gamma(\epsilon) = \frac{1}{\epsilon} - \gamma + O(\epsilon) \tag{A.8}$$

$$\zeta(1-\epsilon) = -\frac{1}{\epsilon} + \gamma + O(\epsilon)\;, \tag{A.9}$$

where $\gamma \approx 0.577$ is Euler's constant.

We now calculate the modified Robinson formula

$$\begin{aligned}
\lim_{\nu\uparrow 1} \zeta_\nu(e^{\beta\mu}) &= \lim_{\nu\uparrow 1} \left\{ \Gamma(1-\nu)(-\beta\mu)^{\nu-1} + \sum_{k=0}^{\infty} \frac{(\beta\mu)^k}{k!}\,\zeta(\nu-k) \right\} \\
&= \lim_{\epsilon\downarrow 0} \left\{ \Gamma(\epsilon)(-\beta\mu)^{\epsilon} + \zeta(1-\epsilon) + \sum_{k=1}^{\infty} \frac{(\beta\mu)^k}{k!}\,\zeta(\epsilon+1-k) \right\} \\
&= \lim_{\epsilon\downarrow 0} \left\{ \left(\frac{1}{\epsilon} - \gamma\right)\Big(1 - \epsilon\,\ln(-\beta\mu)\Big) + \left(-\frac{1}{\epsilon} + \gamma\right) + \sum_{k=1}^{\infty} \frac{(\beta\mu)^k}{k!}\,\zeta(\epsilon+1-k) \right\} \\
&= -\ln(-\beta\mu) + \sum_{k=1}^{\infty} \frac{(\beta\mu)^k}{k!}\,\zeta(1-k)\;.
\end{aligned} \tag{A.10}$$

B. The Many-Body Hamiltonian

B.1. Derivation of the Hartree-Fock-Bogoliubov Hamiltonian

In the following calculation, the explicit dependence of the field operators on space and time is, for the sake of brevity, omitted. We start from the Hamiltonian (3.7) and insert the decomposition of the Bose field operator (3.13). Writing the result in terms of the fluctuation operators (3.12), we get

$$\begin{aligned}\hat{H} = &\int \mathrm{d}\mathbf{r} \left\{ \Psi_0^* \Big(\hat{h} - \mu\Big) \Psi_0 + \delta\hat{\psi}^\dagger \Big(\hat{h} - \mu\Big) \delta\hat{\psi} + \Psi_0^* \Big(\hat{h} - \mu\Big) \delta\hat{\psi} + \delta\hat{\psi}^\dagger \Big(\hat{h} - \mu\Big) \Psi_0 \right\} \\ &+ \int \mathrm{d}\mathbf{r} \, \frac{g}{2} \Big\{ |\Psi_0|^4 + \left(\Psi_0^* |\Psi_0|^2 + \Psi_0^{*2} \Psi_0\right) \delta\hat{\psi} + \left(|\Psi_0|^2 \Psi_0 + \Psi_0^* \Psi_0^2\right) \delta\hat{\psi}^\dagger \\ &+ \Psi_0^{*2} \delta\hat{\psi}\delta\hat{\psi} + \Psi_0^2 \delta\hat{\psi}^\dagger \delta\hat{\psi}^\dagger + 4\,|\Psi_0|^2 \delta\hat{\psi}^\dagger \delta\hat{\psi} + 2\,\Psi_0^* \delta\hat{\psi}^\dagger \delta\hat{\psi}\delta\hat{\psi} + 2\Psi_0 \delta\hat{\psi}^\dagger \delta\hat{\psi}^\dagger \delta\hat{\psi} \\ &+ \delta\hat{\psi}^\dagger \delta\hat{\psi}^\dagger \delta\hat{\psi}\delta\hat{\psi} \Big\} \ . \end{aligned} \tag{B.1}$$

Now we can write the Hamiltonian in the form $\hat{H} = \hat{H}_0 + \hat{H}_1 + \hat{H}_2 + \hat{H}_3 + \hat{H}_4$, where in $\hat{H}_n$, the n denotes the number of fluctuation operators. We find

$$\hat{H}_0 = \int \mathrm{d}\mathbf{r} \, \Psi_0^* \Big(\hat{h} - \mu + \frac{g}{2} |\Psi_0|^2\Big) \Psi_0 \tag{B.2a}$$

$$\hat{H}_1 = \int \mathrm{d}\mathbf{r} \, \Psi_0^* \Big(\hat{h} - \mu + g\,|\Psi_0|^2\Big) \delta\hat{\psi} + \delta\hat{\psi}^\dagger \Big(\hat{h} - \mu + g\,|\Psi_0|^2\Big) \Psi_0 \tag{B.2b}$$

$$\hat{H}_2 = \int \mathrm{d}\mathbf{r} \, \delta\hat{\psi}^\dagger \Big(\hat{h} - \mu + 2g\,|\Psi_0|^2\Big) \delta\hat{\psi} + \frac{g}{2} \left(\Psi_0^{*2} \delta\hat{\psi}\delta\hat{\psi} + \Psi_0^2 \delta\hat{\psi}^\dagger \delta\hat{\psi}^\dagger\right) \tag{B.2c}$$

$$\hat{H}_3 = \int \mathrm{d}\mathbf{r} \, g \left(\Psi_0^* \delta\hat{\psi}^\dagger \delta\hat{\psi}\delta\hat{\psi} + \Psi_0 \delta\hat{\psi}^\dagger \delta\hat{\psi}^\dagger \delta\hat{\psi}\right) \tag{B.2d}$$

$$\hat{H}_4 = \int \mathrm{d}\mathbf{r} \, \frac{g}{2} \, \delta\hat{\psi}^\dagger \delta\hat{\psi}^\dagger \delta\hat{\psi}\delta\hat{\psi} \ . \tag{B.2e}$$

It is common to simplify the cubic and quartic products of operators by treating them within the HFB mean-field approximation [41], namely

$$\hat{a}_i^\dagger \hat{a}_j \hat{a}_k \approx \langle \hat{a}_i^\dagger \hat{a}_j \rangle \hat{a}_k + \langle \hat{a}_i^\dagger \hat{a}_k \rangle \hat{a}_j + \langle \hat{a}_j \hat{a}_k \rangle \hat{a}_i^\dagger \tag{B.3}$$

and

$$\begin{aligned}\hat{a}_i^\dagger \hat{a}_j^\dagger \hat{a}_k \hat{a}_l \approx \langle \hat{a}_i^\dagger \hat{a}_j^\dagger \rangle \hat{a}_k \hat{a}_l + \langle \hat{a}_i^\dagger \hat{a}_k \rangle \hat{a}_j^\dagger \hat{a}_l + \langle \hat{a}_i^\dagger \hat{a}_l \rangle \hat{a}_j^\dagger \hat{a}_k \\ + \langle \hat{a}_j^\dagger \hat{a}_l \rangle \hat{a}_i^\dagger \hat{a}_k + \langle \hat{a}_j^\dagger \hat{a}_k \rangle \hat{a}_i^\dagger \hat{a}_l + \langle \hat{a}_k \hat{a}_l \rangle \hat{a}_i^\dagger \hat{a}_j^\dagger \ .\end{aligned} \tag{B.4}$$

Writing this in terms of the fluctuation operators, we get for $\hat{H}_3$, with (3.12) and (3.18), (3.19)

$$\begin{aligned}\hat{H}_3 &\approx g \int \mathrm{d}\mathbf{r}\ \Psi_0^* \left(2\langle \delta\hat{\psi}^\dagger \delta\hat{\psi} \rangle \delta\hat{\psi} + \langle \delta\hat{\psi} \delta\hat{\psi} \rangle \delta\hat{\psi}^\dagger \right) + \Psi_0 \left(\langle \delta\hat{\psi}^\dagger \delta\hat{\psi}^\dagger \rangle \delta\hat{\psi} + 2\langle \delta\hat{\psi}^\dagger \delta\hat{\psi} \rangle \delta\hat{\psi}^\dagger \right) \\ &= g \int \mathrm{d}\mathbf{r}\ \left(2\tilde{n}\Psi_0^* + \widetilde{m}^* \Psi_0 \right) \delta\hat{\psi} + \left(2\tilde{n}\Psi_0 + \widetilde{m}\Psi_0^* \right) \delta\hat{\psi}^\dagger\end{aligned} \tag{B.5}$$

and for $\hat{H}_4$

$$\hat{H}_4 \approx \frac{g}{2} \int \mathrm{d}\mathbf{r}\ 4\,\tilde{n} \delta\hat{\psi}^\dagger \delta\hat{\psi} + \widetilde{m}^* \delta\hat{\psi} \delta\hat{\psi} + \widetilde{m} \delta\hat{\psi}^\dagger \delta\hat{\psi}^\dagger \ . \tag{B.6}$$

Note that there are terms omitted in the previous lines. These terms appear because the factorization in (B.4) is done *in analogy* to Wick's theorem. However, the Wick theorem is valid for time-ordered products of operator averages. The application to operators leads to extra terms which, for consistency with Wick's theorem, must be subtracted. Nevertheless, usually these terms are neglected sice they merely constitute a constant energy shift in the condensate part of the Hamiltonian (B.7) and do not affect the HFB problem. Details are discussed in Section 3.4.1 and in [79, 80].

Within the mean-field approximation, the terms (B.2d) and (B.2e) are linear and quadratic in the fluctuation operators, respectively, and the Hamiltonian (B.1) can be written approximately as

$$\begin{aligned}\hat{H} = \int \mathrm{d}\mathbf{r}\ \Big\{ &\Psi_0^* \Big(\hat{h} - \mu + \frac{g}{2} |\Psi_0|^2 \Big) \Psi_0 \\ &+ \Psi_0^* \left[\hat{h} - \mu + g \left(|\Psi_0|^2 + 2\,\tilde{n} + \frac{\Psi_0}{\Psi_0^*} \widetilde{m}^* \right) \right] \delta\hat{\psi} \\ &+ \delta\hat{\psi}^\dagger \left[\hat{h} - \mu + g \left(|\Psi_0|^2 + 2\,\tilde{n} + \frac{\Psi_0^*}{\Psi_0} \widetilde{m} \right) \right] \Psi_0 \\ &+ \delta\hat{\psi}^\dagger \Big(\hat{h} - \mu + 2g \left(|\Psi_0|^2 + \tilde{n} \right) \Big) \delta\hat{\psi} \\ &+ \frac{g}{2} \left(\left(\Psi_0^2 + \widetilde{m} \right) \delta\hat{\psi}^\dagger \delta\hat{\psi}^\dagger + \text{h.c.} \right) \Big\} \ .\end{aligned} \tag{B.7}$$

In order to eliminate the terms linear in the fluctuation operators, we demand the coefficients in the second and third line of (B.7) to vanish, i. e.

$$\begin{aligned}\left[\hat{h} - \mu + g \left(|\Psi_0|^2 + 2\,\tilde{n} + \Psi_0\, \widetilde{m}^* \right) \right] \Psi_0^* &\stackrel{!}{=} 0 \\ \left[\hat{h} - \mu + g \left(|\Psi_0|^2 + 2\,\tilde{n} + \Psi_0^*\, \widetilde{m} \right) \right] \Psi_0 &\stackrel{!}{=} 0 \ .\end{aligned} \tag{B.8}$$

In this, we recognize the generalized Gross-Pitaevskiĭ equation (3.20) and the Hamiltonian (B.7) simplifies to the form in (3.16).

B.2. Decoupling of the Bogoliubov-de Gennes equations

We show, that the auxiliary functions introduced in (6.40)

$$\psi_i^{(\pm)}(\mathbf{r}) = u_i(\mathbf{r}) \pm v_i(\mathbf{r}) \tag{B.9}$$

decouple the BdG equations (3.41)

$$\Big(\hat{h}(\mathbf{r}) - \mu + 2\,gn(\mathbf{r})\Big)\, u_i(\mathbf{r}) - gn_c(\mathbf{r})\, v_i(\mathbf{r}) = E_i\, u_i(\mathbf{r}) \tag{B.10a}$$

$$\Big(\hat{h}(\mathbf{r}) - \mu + 2\,gn(\mathbf{r})\Big)\, v_i(\mathbf{r}) - gn_c(\mathbf{r})\, u_i(\mathbf{r}) = -E_i\, v_i(\mathbf{r})\ . \tag{B.10b}$$

Adding (B.10a) and (B.10b) yields with (B.9)

$$\Big(\hat{h}_{\mathrm{GP}} - \mu\Big)\, \psi_i^{(+)}(\mathbf{r}) = E_i \psi_i^{(-)}(\mathbf{r})\ , \tag{B.11}$$

where we used the notation

$$\hat{h}_{\mathrm{GP}} \equiv \hat{h} + g\left(n_c(\mathbf{r}) + 2\,\tilde{n}(\mathbf{r})\right)\ . \tag{B.12}$$

From the difference (B.10a)−(B.10b) we get

$$\Big(\hat{h} + 2\,gn(\mathbf{r})\Big)\, \psi_i^{(-)}(\mathbf{r}) + gn_c(\mathbf{r})\, \psi_i^{(-)}(\mathbf{r}) = E_i\, \psi_i^{(+)}(\mathbf{r})\ . \tag{B.13}$$

Multiplying (B.13) once with E_i and once with $\hat{h}_{\mathrm{GP}} - \mu$ from the left side yields

$$\Big(\hat{h}_{\mathrm{GP}} - \mu\Big) E_i\, \psi_i^{(-)}(\mathbf{r}) + 2\,gn_c(\mathbf{r})\, E_i\, \psi_i^{(-)}(\mathbf{r}) = E_i^2\, \psi_i^{(+)}(\mathbf{r}) \tag{B.14a}$$

$$\Big(\hat{h}_{\mathrm{GP}} - \mu\Big)^2 \psi_i^{(-)}(\mathbf{r}) + 2\,g\Big(\hat{h}_{\mathrm{GP}} - \mu\Big)\, n_c(\mathbf{r})\, \psi_i^{(-)}(\mathbf{r}) = E_i \Big(\hat{h}_{\mathrm{GP}} - \mu\Big)\, \psi_i^{(+)}(\mathbf{r})\ . \tag{B.14b}$$

Inserting the relation (B.11) then gives the result

$$\Big(\hat{h}_{\mathrm{GP}} - \mu\Big)^2 \psi_i^{(+)}(\mathbf{r}) + 2\,gn_c(\mathbf{r}) \Big(\hat{h}_{\mathrm{GP}} - \mu\Big)\, \psi_i^{(+)}(\mathbf{r}) = E_i^2\, \psi_i^{(+)}(\mathbf{r}) \tag{B.15a}$$

$$\Big(\hat{h}_{\mathrm{GP}} - \mu\Big)^2 \psi_i^{(-)}(\mathbf{r}) + 2\,g\Big(\hat{h}_{\mathrm{GP}} - \mu\Big)\, n_c(\mathbf{r})\, \psi_i^{(-)}(\mathbf{r}) = E_i^2\, \psi_i^{(-)}(\mathbf{r})\ . \tag{B.15b}$$

C. The Harmonic Oscillator

C.1. Density of states of the *D*-dimensional harmonic oscillator

The density of states for the D-dimensional harmonic oscillator can be calculated from the integral

$$g_D(\epsilon) = \frac{1}{(2\pi\hbar)^D} \int \mathrm{d}^D r \int \mathrm{d}^D p \; \delta\left[\epsilon - \left(\frac{\mathbf{p}^2}{2m} + V(r)\right)\right] \; .$$

Both the momentum and the spatial integral are transformed due to their rotational symmetry as

$$\int_{-\infty}^{\infty} \mathrm{d}^D x \overset{(2.8)}{=} S_D \int_0^{\infty} \mathrm{d}x \; x^{D-1} \; , \tag{C.1}$$

so that we get after substituting $E = \mathbf{p}^2/2m$

$$g_D(\epsilon) = 2\left(\frac{m}{2\hbar^2}\right)^{D/2} \frac{1}{\Gamma\left(\frac{D}{2}\right)^2} \int_0^{\infty} \mathrm{d}r \; r^{D-1} \int_0^{\infty} \mathrm{d}E \; E^{\frac{D}{2}-1} \, \delta\big(\epsilon - E - V(r)\big) \; . \tag{C.2}$$

The evaluation of the energy integral yields

$$g_D(\epsilon) = 2\left(\frac{m}{2\hbar^2}\right)^{D/2} \frac{1}{\Gamma\left(\frac{D}{2}\right)^2} \int_0^{\infty} \mathrm{d}r \; r^{D-1} \left(\epsilon - V(r)\right)^{\frac{D}{2}-1} \Theta\big(\epsilon - V(r)\big) \; , \tag{C.3}$$

where the Heaviside function arises from the integration over the delta distribution. We now insert the isotropic trapping potential $V(r) = m\omega^2 r^2/2$ and substitute $x = r^2$, so that we get

$$g_D(\epsilon) = \left(\frac{m}{2\hbar^2}\right)^{\frac{D}{2}} \frac{\epsilon^{\frac{D}{2}-1}}{\Gamma\left(\frac{D}{2}\right)^2} \int_0^{\infty} \mathrm{d}x \; x^{\frac{D}{2}-1} \left(1 - \frac{m\omega^2}{2\epsilon}\, x\right)^{\frac{D}{2}-1} \Theta\Big(1 - \frac{m\omega^2}{2\epsilon}\, x\Big) \; . \tag{C.4}$$

Evaluating the Heaviside function, we finally get

$$g_D(\epsilon) = \frac{\epsilon^{D-1}}{\Gamma\left(\frac{D}{2}\right)^2 (\hbar\omega)^D} \int_0^1 \mathrm{d}x \; x^{\frac{D}{2}-1} \, (1-x)^{\frac{D}{2}-1} \; . \tag{C.5}$$

With the definition of the beta function (8.380.1) in [40]

$$B(x,y) = \int_0^1 \mathrm{d}t \; t^{x-1}(1-t)^{y-1} \tag{C.6}$$

and the relation (8.384.1) in [40]

$$B(x,y) = \frac{\Gamma(x)\Gamma(y)}{\Gamma(x+y)} \ , \tag{C.7}$$

we get the final result for the density of states of the isotropic harmonic oscillator in D dimensions

$$g_D(\epsilon) = \frac{\epsilon^{D-1}}{\Gamma(D)\,(\hbar\omega)^D} \ . \tag{C.8}$$

C.2. Eigenvalue problem of the two-dimensional harmonic oscillator

Although the solution of the harmonic oscillator Hamiltonian is rather a standard problem, it was necessary to derive its eigenstates in terms of the Laguerre polynomials for our calculation. Since we consider a cylindrical symmetric trap, the more common solution in terms of the Hermite polynomials is unsuitable, since they cannot exploit the symmetry of the system.
From the dimensionless GPE (6.11), the single particle part of the Hamiltonian is given by

$$\hat{h}_{\text{osc}} = -\Delta + r^2 \ , \tag{C.9}$$

where the quantities are to be understood dimensionless. This is just the Hamiltonian of the two-dimensional harmonic oscillator.

In order to find its eigenstates and eigenvalues, we start from the Schrödinger equation

$$\left(\hat{h}_{\text{osc}} - \epsilon\right)\chi(r,\varphi) = 0 \ . \tag{C.10}$$

Inserting the Laplacian (6.2) and executing the variable transformation $x = r^2$ leads to the following differential equation

$$\left\{ x\,\frac{\partial^2}{\partial x^2} + \frac{\partial}{\partial x} + \frac{1}{4x}\,\frac{\partial^2}{\partial \varphi^2} + \frac{1}{4}\,(\epsilon - x) \right\} \chi(x,\varphi) = 0 \ . \tag{C.11}$$

We now use the separation ansatz

$$\chi(x,\varphi) = f(x)\, x^{\frac{m}{2}} e^{-\frac{x}{2} + im\varphi} \ , \tag{C.12}$$

where the term $x^{m/2}$ dominates the behaviour for small and $e^{-x/2}$ the behaviour for large x, whereas the region in between is characterized by the function $f(x)$. Inserting this into the previous equation leads to the familiar differential equation for $f(x)$

$$x f''(x) + (1 + m - x)\, f'(x) + \frac{1}{4}\left(\epsilon - 2\,(m+1)\right) f(x) = 0 \ . \tag{C.13}$$

Laguerre Polynomials. The solution of this differential equation are the Laguerre polynomials, that are defined as

$$\begin{aligned} L_n^m(x) &= \frac{1}{n!}\, e^x x^{-m}\, \frac{\mathrm{d}^n}{\mathrm{d}x^n}\left(e^{-x}x^{n+m}\right) \\ &\equiv \sum_{i=0}^{n}(-1)^i \binom{n+m}{n-i}\frac{x^i}{i!}\ . \end{aligned} \tag{C.14}$$

They satisfy the orthogonality relation

$$\int_0^\infty \mathrm{d}x\, e^{-x}x^m\, L_n^m(x)L_{n'}^m(x) = \Gamma(1+m)\binom{n+m}{n}\delta_{nn'} \tag{C.15}$$

and in the form (C.14) they solve the differential equation for $f(x)$

$$x\,\frac{\mathrm{d}^2 f}{\mathrm{d}x^2} + (1+m-x)\,\frac{\mathrm{d}f}{\mathrm{d}x} + n\,f = 0\ . \tag{C.16}$$

In order to calculate them numerically, the following recursion formula is useful:

$$n\,L_n^m(x) = (2n+m-x-1)L_{n-1}^m(x) + (m+n-1)L_{n-2}^m(x)\ . \tag{C.17}$$

Eigenstates of the harmonic oscillator. Comparison of (C.13) and (C.16) gives for the parameter

$$n = \frac{\epsilon}{4} - \frac{1}{2}\,(m+1)\ . \tag{C.18}$$

The eigenvalues of the harmonic oscillator are therefore given by

$$\epsilon_{n,m} = 2\,(2n+|m|+1)\ , \tag{C.19}$$

or, after multiplication with the Rydberg of energy (6.4), $\epsilon\cdot E_0 = \hbar\omega_\perp(2n+m+1)$. From (C.12), (C.15), and with (C.14) being a solution of (C.13), we get for the eigenstates of the two-dimensional harmonic oscillator

$$\chi_{n,m}(r,\varphi) = \frac{1}{\sqrt{\pi\,\Gamma(1+m)\binom{n+m}{n}}}\, r^m e^{-\frac{r^2}{2}+im\varphi}\, L_n^m(r^2)\ , \tag{C.20}$$

where we have plugged the transformation $x = r^2$ back into the solution. Note that the states with angular momentum different to zero ($|m| > 0$) are two-fold degenerate, since the Hamiltonian (3.16) with a cylindrical symmetric potential does in 2D not depend on the azimuthal coordinate.

For the same reason, the phase of the wave function can be set arbitrarily to zero. That is, we are only interested in the radial part of the oscillator wave function, i. e.

$$\chi_{n,m}(r) = \frac{1}{\sqrt{\pi\,\Gamma(1+m)\binom{n+m}{n}}}\, r^m e^{-\frac{r^2}{2}}\, L_n^m(r^2)\ . \tag{C.21}$$

The wave functions (C.20) satisfy the orthogonality relation

$$\int \mathrm{d}^2 r \; \chi_{n,m}(r,\varphi)\, \chi^*_{n',m'}(r,\varphi) = \delta_{nn'}\, \delta_{mm'} \;, \tag{C.22}$$

which can be written for the case of (C.21) as[1]

$$2\pi \int \mathrm{d}r \; r \, \chi_{n,m}(r)\, \chi_{n',m'}(r) = \delta_{nn'}\, \delta_{mm'} \;. \tag{C.23}$$

[1] To remind the reader that the integration in (C.22) is actually one-dimensional, we execute the angular integral in the following expression.

D. Formulation of the Optimization Problem for the Gross-Pitaevskiĭ Equation

We derive in detail the form of the Gross-Pitaevskiĭ equation in the basis state representation of the harmonic oscillator. This form is needed to provide the `fsolve` routine with a function that can be solved via optimization. This process is done for the expansion coefficients rather than the direct function values. Details are described in Section 6.2.4. Furthermore, an approximate analytic form of the Jacobian is derived that is also needed for the optimization. The resulting equations are formulated in a vector/matrix form for convenience.

D.1. Basis state representation of the GPE

Starting from (6.32)

$$\begin{aligned}&\left[\hat{h} - \mu_\phi + g\left(\phi^2(r) + 2\,\tilde{n}(r)\right)\right]\,\phi(r)\\ &\quad + \left[\hat{h} - \mu_\phi + g\left(3\phi^2(r) + 2\,\tilde{n}(r)\right)\right]\,\delta(r) - \delta\mu\,\phi(r) = 0\ ,\end{aligned} \tag{D.1}$$

we identify the first line of (D.1) with the GPE for the guess $\phi(r)$,

$$f[\phi(r)] = \left[\hat{h} - \mu_\phi + g\left(\phi^2(r) + 2\,\tilde{n}(r)\right)\right]\,\phi(r) \equiv 0\ , \tag{D.2}$$

whereas the second line contains the information about the Jacobian, c. f. (6.18), i. e.

$$\left[\hat{h} - \mu_\phi + g\left(3\phi^2(r) + 2\,\tilde{n}(r)\right)\right]\,\delta(r) - \delta\mu_\phi\,\phi(r) \stackrel{!}{=} J(\phi)\,\delta(r)\ . \tag{D.3}$$

Although not obvious, the term $\delta\mu_\phi\,\phi(r)$ is proportional to $\delta(r)$ due to the dependence on $\delta\mu_\phi$, as we will see in (D.18).

Basis expansion. We expand the guess and the Newton step into the basis set of the two-dimensional harmonic oscillator,

$$\phi(r) = \sum_i \phi_i \, \chi_i(r) \tag{D.4}$$

$$\delta(r) = \sum_i \delta_i \, \chi_i(r) \ . \tag{D.5}$$

The eigensolutions $\{\chi_i(r), \epsilon_i\}$ of the oscillator are derived in Appendix C. They satisfy the Schrödinger equation

$$\left(\hat{h} - \epsilon_i\right) \chi_i(r) = 0 \tag{D.6}$$

and the eigenstates obey the usual orthogonality relation (C.23).

To simplify the notation, we use the Dirac notation in the remainder of this section, i. e. $|\phi\rangle = |\phi_0, \ldots, \phi_i, \ldots\rangle$, $|\delta\rangle = |\delta_0, \ldots, \delta_i, \ldots\rangle$, $\langle r|i\rangle = \chi_i(r)$, $\langle r|f_\phi\rangle = f[\phi_0(r)]$ and $\langle r|f_{\phi+\delta}\rangle = f[\phi_0(r) + \delta(r)]$.
The expansion coefficients are given by

$$\langle i|\phi\rangle = \phi_i \tag{D.7}$$

$$\langle i|\delta\rangle = \delta_i \ . \tag{D.8}$$

For the implementation in MATLAB a vector/matrix notation is more convenient, and therefore, we introduce the following notations

$$\boldsymbol{\phi} = (\phi_0, \ldots, \phi_m, \ldots)^T \tag{D.9a}$$

$$\boldsymbol{\epsilon} = (\epsilon_0, \ldots, \epsilon_m, \ldots)^T \tag{D.9b}$$

$$u_i = \int \mathrm{d}^2 r \ \chi_i(r) \, \phi(r)^3 \tag{D.9c}$$

$$v_i = \int \mathrm{d}^2 r \ \chi_i(r) \, \tilde{n}(r) \, \phi(r) \tag{D.9d}$$

$$U_{ij} = \int \mathrm{d}^2 r \ \chi_i(r) \, \phi(r)^2 \, \chi_j(r) \tag{D.9e}$$

$$V_{ij} = \int \mathrm{d}^2 r \ \chi_i(r) \, \tilde{n}(r) \, \chi_j(r) \ . \tag{D.9f}$$

In the vector notation, we denote the scalar product with a dot. Vectors are printed in boldface, while matrices are denoted with capital letters.

Gross-Pitaevskiĭ equation. We now insert (D.4) into (D.2) and project on an harmonic oscillator state $\langle i|$

$$\langle i|f_\phi\rangle = (\epsilon_i - \mu_\phi)\langle i|\phi\rangle + g\langle i|\phi^3\rangle + 2g\langle i|\tilde{n}(r)|\phi\rangle = 0 \ , \tag{D.10}$$

where we have used (D.6). In vector notation, this equation can be written as

$$(\boldsymbol{\epsilon} - \mu_\phi)\boldsymbol{\phi} + g\,\mathbf{u} + 2g\,\mathbf{v} = \mathbf{0}\ . \tag{D.11}$$

Chemical Potential. The chemical potential μ_ϕ can be found from $\langle\phi|f_\phi\rangle$

$$\langle\phi|f_\phi\rangle = \langle\phi|\hat{h}|\phi\rangle - \mu_\phi\langle\phi|\phi\rangle + g\langle\phi|\phi^3\rangle + 2\,g\langle\phi|\tilde{n}(r)|\phi\rangle = 0\ . \tag{D.12}$$

Inserting the closure relation

$$I = \sum_i |i\rangle\langle i|\ , \tag{D.13}$$

where I is the identity matrix, gives

$$\begin{aligned}\mu_\phi &= \sum_{i,j}\Big\{\langle\phi|i\rangle\langle i|\hat{h}|j\rangle\langle j|\phi\rangle + 2g\langle\phi|i\rangle\langle i|\tilde{n}(r)|j\rangle\langle j|\phi\rangle\Big\} + g\langle\phi|\phi^3\rangle \\ &= \sum_{i,j}\Big\{\epsilon_i\phi_i^2\,\delta_{ij} + 2g\langle i|\tilde{n}(r)|j\rangle\,\phi_i\phi_j\Big\} + g\int \mathrm{d}^2r\ \phi(r)^4\ .\end{aligned} \tag{D.14}$$

Using (D.9a) – (D.9f), (D.14) takes the form

$$\mu_\phi = \boldsymbol{\epsilon}\cdot(\boldsymbol{\phi}^2)^T + 2g\,\boldsymbol{\phi}^T V\boldsymbol{\phi} + g\int \mathrm{d}^2r\ \phi(r)^4\ . \tag{D.15}$$

Normalization

By using the above equations to determine the ground state, the correct normalization of the condensate wave function is assured automatically. This is because in the steps that lead to (D.10) and (D.15) we make explicit use of the orthonormality of the solution vector $\langle\phi|\phi\rangle = 1$. Therefore, the chemical potential is *not* a parameter of the optimization routine but is calculated according to (D.15). We point this out because often the chemical potential is varied explicitly to normalize the ground state to the total particle number. In this case, the solution vector of the optimization routine would be $\{\phi_0, \ldots, \phi_i, \ldots, \mu_\phi\}$.

D.2. The Jacobi matrix for the GPE

From (D.3) it is obvious that the Jacobian could be immediately calculated in the same straightforward way that leads to (D.10). Yet since the second term is not proportional

to $\delta(r)$, an expression for $\delta\mu_\phi$ must be found first. To do so, we calculate the following projection of (6.32) in analogy to (D.12)

$$\langle\phi{+}\delta|f_{\phi+\delta}\rangle = \langle\phi{+}\delta|\hat{h}|\phi{+}\delta\rangle - (\mu_\phi{+}\delta\mu_\phi) + g\langle\phi{+}\delta|(\phi{+}\delta)^3\rangle + 2\,g\langle\phi{+}\delta|\tilde{n}(r)|\phi{+}\delta\rangle = 0 \tag{D.16}$$

Keeping only terms linear in δ leads to

$$\begin{aligned}\delta\mu_\phi = {}& \langle\phi|\hat{h}|\phi\rangle - \mu_\phi + g\langle\phi|\phi^3\rangle + 2\,g\langle\phi|\tilde{n}(r)|\phi\rangle \\ & + \langle\phi|\hat{h}|\delta\rangle + \langle\delta|\hat{h}|\phi\rangle + 2\,g\big[\,\langle\phi|\tilde{n}(r)|\delta\rangle + \langle\delta|\tilde{n}(r)|\phi\rangle\,\big] + 4\,g\langle\phi^3|\delta\rangle\ .\end{aligned} \tag{D.17}$$

The first line is just the expression for μ_ϕ and vanishes due to (D.12), so that we get for $\delta\mu_\phi$

$$\delta\mu_\phi = 2\,\langle\phi|\hat{h}|\delta\rangle + 4\,g\langle\phi|\tilde{n}(r)|\delta\rangle + 4\,g\langle\phi^3|\delta\rangle\ .^{1} \tag{D.18}$$

This expression is now of the same form as the first term in (D.3). Using (D.13), (D.7) and (D.8), we express (D.18) in terms of the expansion coefficients $\boldsymbol{\phi}$, $\boldsymbol{\delta}$

$$\langle\phi|\hat{h}|\delta\rangle = \langle\delta|\hat{h}|\phi\rangle = \boldsymbol{\phi}^T\underline{\boldsymbol{\epsilon}}\boldsymbol{\delta} \tag{D.19a}$$

$$\langle\phi|\tilde{n}(r)|\delta\rangle = \langle\delta|\tilde{n}(r)|\phi\rangle = \boldsymbol{\phi}^T V\boldsymbol{\delta} \tag{D.19b}$$

$$\langle\phi^3|\delta\rangle = \mathbf{u}^T\cdot\boldsymbol{\delta}\ . \tag{D.19c}$$

Here $\underline{\boldsymbol{\epsilon}}$ is the matrix which contains the elements of the vector $\boldsymbol{\epsilon}$ on the main diagonal. The same way, we get the matrix elements of the first term in (D.3)

$$\langle i|\hat{h} - \mu_\phi|j\rangle = (\epsilon_j - \mu_\phi)\,\delta_{ij} \tag{D.20a}$$

$$\langle i|\phi^2|j\rangle = U_{ij} \tag{D.20b}$$

$$\langle i|\tilde{n}(r)|j\rangle = V_{ij}\ . \tag{D.20c}$$

[1] We used the symmetry of the matrix elements (D.19).

Bibliography

[1] Y. Aharonov and D. Bohm. "Significance of Electromagnetic Potentials in the Quantum Theory". *Phys. Rev.* **115**, 485 (Aug 1959). 1.1

[2] M. H. Anderson, J. R. Ensher, M. R. Matthews, C. E. Wieman, and E. A. Cornell. "Observation of Bose-Einstein Condensation in a Dilute Atomic Vapor". *Science* **269**, 198 (Jul 1995). 1

[3] M. R. Andrews, C. G. Townsend, H.-J. Miesner, D. S. Durfee, D. M. Kurn, and W. Ketterle. "Observation of Interference Between Two Bose-Einstein Condensates". *Science* **275**, 637 (Jan 1997). 5

[4] A. Aspect, S. Richard, F. Gerbier, M. Hugbart, J. Retter, J. Thywissen, and P. Bouyer. "Momentum Spectroscopy of Phase Fluctuations of an Elongated Bose-Einstein Condensate". *Proceedings of the International Conference on Laser Spectroscopy (ICOLS 03), Cairns, Australia* (Sep 2003). 5.4.1, 9

[5] V. Bagnato and D. Kleppner. "Bose-Einstein condensation in low-dimensional traps". *Phys. Rev. A* **44**, 7439 (Dec 1991). 2.3.2, 5, 3.4.4, 9

[6] V. L. Berezinski. *Sov. Pys. JETP* **32** (1971). [Zh. Eksp. Teor. Fiz. **59**, 907 (1970)]. 1.1

[7] M. J. Bijlsma and H. T. C. Stoof. "Variational approach to the dilute Bose gas". *Phys. Rev. A* **55**, 498 (Jan 1997). 1.2, 4

[8] J.-P. Blaizot and G. Ripka. *Quantum Theory of Finite Systems*. MIT Press, Cambridge, 1986. 3.2.1

[9] P. B. Blakie. *Optical Manipulation of Bose-Einstein Condensates*. Ph.D. thesis, University of Otago (Jul 2001). 6.2

[10] P. B. Blakie and R. J. Ballagh. "Mean-field treatment of Bragg scattering from a Bose-Einstein condensate". *J. Phys. B* **33**, 3961 (2000). 5.4.1

[11] P. B. Blakie, R. J. Ballagh, and C. W. Gardiner. "Theory of coherent Bragg spectroscopy of a trapped Bose-Einstein condensate". *Phys. Rev. A* **65**, 033602 (Feb 2002). 5.4.1

[12] N. N. Bogoliubov. "On the theory of superfluidity". *J. Phys. (U.S.S.R.)* **11**, 23 (1947). 3, 3.2

[13] N. N. Bogoliubov. "Quasi-expectation Values in Problems of Statistical Mechanics". *JINR preprint* (1961). 2.3

[14] S. N. Bose. "Plancks Gesetz und Lichtquantenhypothese". *Zeitschrift für Physik* **26**, 178 (1924). 2.2

[15] P. Bouyer, J. H. Thywissen, F. Gerbier, M. Hugbart, S. Richard, J. Retter, and A. Aspect. "One-dimensional behavior of elongated Bose-Einstein condensates". *J. Phys. IV France **1**, for the proceeding of Quantum Gases in Low Dimension, Les Houches 2003* (Jul 2003). 5.4.1, 5.4.2

[16] L. Cacciapuoti, D. Hellweg, M. Kottke, T. Schulte, K. Sengstock, W. Ertmer, J. Arlt, L. Santos, and M. Lewenstein. "Second Order Correlation Function of a Phase Fluctuating Bose-Einstein Condensate". *Preprint* `cond-mat/0308135` (August 2003). 5.2.3, 5.3, 5.4.2

[17] Y. Castin and R. Dum. "Low-temperature Bose-Einstein condensates in time-dependent traps: Beyond the $U(1)$ symmetry-breaking approach". *Phys. Rev. A* **57**, 3008 (Apr 1998). 3.5

[18] P. M. Chaikin and T. C. Lubensky. *Principles of Condensed Matter Physics*. Cambridge University Press, 1995. 2, 7.4

[19] F. Chevy, V. Bretin, P. Rosenbusch, K. W. Madison, and J. Dalibard. "Transverse Breathing Mode of an Elongated Bose-Einstein condensate". *Phys. Rev. Lett.* **88**, 250402 (2002). 3.7.1

[20] N. R. Cooper and N. K. Wilkin. "Composite fermion description of rotating Bose-Einstein condensates". *Phys. Rev. B* **60**, R16279 (Dec 1999). 1.1

[21] N. R. Cooper, N. K. Wilkin, and J. M. F. Gunn. "Quantum Phases of Vortices in Rotating Bose-Einstein Condensates". *Phys. Rev. Lett.* **87**, 120405 (Sep 2001). 1.1

[22] E. Cornell. "Very Cold Indeed: The Nanokelvin Physics of Bose-Einstein Condensation". *J. Res. Natl. Inst. Stand. Technol.* **101**, 419 (Jul-Aug 1996). Currently available at `http://physics.nist.gov/Pubs/Bec/j4cornel.pdf`. 1

[23] K. B. Davis, M.-O. Mewes, M. R. Andrews, N. J. van Druten, D. S. Durfee, D. M. Kurn, and W. Ketterle. "Bose-Einstein Condensation in a Gas of Sodium Atoms". *Phys. Rev. Lett.* **75**, 3969 (Nov 1995). 1

[24] J. F. Dobson. "Harmonic-Potential Theorem: Implications for Approximate Many-Body Theories". *Phys. Rev. Lett.* **73**, 2244 (1994). 3.7

[25] A. Einstein. "Quantentheorie des einatomigen idealen Gases. Zweite Abhandlung". *Sitzungberichte der königlich preussischen Akadademie der Wissenschaften* **XVIII–XXV**, 3 (Jan 1925). 1, 2.2

[26] P. O. Fedichev, U. R. Fischer, and A. Recati. "Zero-temperature damping of Bose-Einstein condensate oscillations by vortex-antivortex pair creation". *Phys. Rev. A* **68**, 011602(R) (2003). 9

[27] J. P. Fernández and W. J. Mullin. "The Two-Dimensional Bose-Einstein Condensate". *J. Low Temp. Phys.* **128**, 233 (Sep 2002). 1.2, 3.4.4, 3.4.4, 3.4.4, 7.1, 9

[28] A. L. Fetter. "Theory of a dilute low-temperature trapped Bose condensate". In M. Inguscio, S. Stringari, and C. E. Wieman, editors, *Proceedings of the International School of Physics - Enrico Fermi*, 263. IOS Press, 1999. 3.4.2

[29] C. W. Gardiner. "Particle-number-conserving Bogoliubov method which demonstrates the validity of the time-dependent Gross-Pitaevskii equation for a highly condensed Bose gas". *Phys. Rev. A* **56**, 1414 (Aug 1997). 3.5

[30] F. Gerbier, J. H. Thywissen, S. Richard, M. Hugbart, P. Bouyer, and A. Aspect. "Momentum distribution and correlation function of quasicondensates in elongated traps". *Phys. Rev. A* **67**, 051602(R) (May 2003). 1.2, 5.2.2, 5.3, 5.4.1, 7.3.4.2

[31] T. K. Ghosh. "Quasi-one dimensional degenerate Bose gas". *Preprint* `cond-mat/0402079` (February 2004). 7.3.4.1

[32] C. Gies, B. P. van Zyl, S. A. Morgan, and D. A. W. Hutchinson. "Finite-temperature theory of the trapped two-dimensional Bose gas". *Phys. Rev. A* **69**, 023616 (Feb 2004). 1.2, 9

[33] V. L. Ginzburg. *Fiz. Tverd. Tela.* **2**, 2031 (1960). [*Sov. Phys. Solid State* **2**, 1824 (1961)]. 7.4

[34] S. Giorgini, L. P. Pitaevskii, and S. Stringari. "Condensate fraction and critical temperature of a trapped interacting Bose gas". *Phys. Rev. A* **54**, R4633 (Dec 1996). 7.3.2

[35] M. Girardeau and R. Arnowitt. "Comment on "Particle-number-conserving Bogoliubov method which demonstrates the validity of the time-dependent Gross-Pitaevskii equation for a highly condensed Bose gas"". *Phys. Rev. A* **58** (1998). 3.5

[36] M. Gireadeau. "Relationship between systems of impenetrable bosons and fermions in one dimension". *J. Math. Phys.* **1**, 516 (1963). 4.3.2.1

[37] S. M. Girvin. "The Kosterlitz-Thouless Phase Transition". *For: Boulder School for Condensed Matter and Materials Physics – Introduction to Superconductivity: Fundamentals and Applications* (Jul 3–28 2000). Avaiable at `http://research.yale.edu/boulder/Boulder-2000/july2000-transparencies.html`. 1.1

[38] J. Goldstone. *Nuovo Cimento* **19**, 154 (1961). 2

[39] A. Görlitz, J. M. Vogels, A. E. Leanhardt, C. Raman, T. L. Gustavson, J. R. Abo-Shaeer, A. P. Chikkatur, S. Gupta, S. Inouye, T. Rosenband, and W. Ketterle. "Realization of Bose-Einstein Condensates in Lower Dimensions". *Phys. Lett.* **87**, 130402 (Sep 2001). 2, 7, 7.1, 8.3.1, 8.3.1

[40] I. S. Gradshteyn and I. M. Ryzhik. *Table of Integrals, Series and Products*. 4th edition. Academic Press, 1980. A, C.1, C.1

[41] A. Griffin. "Conserving and gapless approximations for an inhomogeneous Bose gas at finite temperatures". *Phys. Rev. B* **53**, 9341 (Apr 1996). 2, 16, 18, B.1

[42] A. Griffin. "Theory of excitations of the condensate and non-condensate at finite temperatures". In M. Inguscio, S. Stringari, and C. E. Wieman, editors, *Proceedings of the International School of Physics - Enrico Fermi*, 591. IOS Press, 1999. 3.7.2

[43] D. Hellweg, L. Cacciapuoti, M. Kottke, T. Schulte, K. Sengstock, W. Ertmer, and J. J. Arlt. "Measurement of the Spatial Correlation Function of Phase Fluctuating Bose-Einstein Condensates". *Phys. Rev. Lett.* **91**, 010406 (Jul 2003). 1.2, 1.3, 5.4.2

[44] T.-L. Ho and M. Ma. "Quasi 1 and 2d Dilute Bose Gas in Magnetic Traps: Existence of Off-Diagonal Order and Anomalous Quantum Fluctuations". *J. Low Temp. Phys.* **115**, 61 (1999). 5.3

[45] P. C. Hohenberg. "Existence of Long-Range Order in One and Two Dimensions". *Phys. Rev.* **158**, 383 (June 1967). 1.1, 2.3.1

[46] K. Huang. *Statistical Mechanics*. 2nd edition. John Wiley & Sons, New York, 1987. 3.2

[47] N. M. Hugenholtz and D. Pines. "Ground-State Energy and Excitation Spectrum of a System of Interacting Bosons". *Phys. Rev.* **116**, 489 (Nov 1959). 15

[48] D. A. W. Hutchinson, K. Burnett, R. J. Dodd, S. A. Morgan, M. Rusch, E. Zaremba, N. P. Proukakis, M. Edwards, and C. W. Clark. "Gapless mean-field theory of Bose-Einstein condensates". *J. Phys. B* **33**, 3825 (2000). 1, 3.3, 2, 3.4.3.1, 3.4.3.2, 4, 4.4, 6.3, 7.2.2, 7.3.2, 7.3.3, 7.3.3, 9

[49] D. A. W. Hutchinson, R. J. Dodd, and K. Burnett. "Gapless Finite-T Theory of Collective Modes of a Trapped Gas". *Phys. Rev. Lett.* **81**, 2198 (Sep 1998). 1, 1.2, 3.4.3.1, 3.4.3.2, 3.4.3.2, 4.1, 7.3.3, 7.4, 8

[50] D. A. W. Hutchinson and S. A. Morgan. "Finite Temperature Field Theory of Bose-Einstein Condensates". *Laser Phys.* **12**, 84 (Jul 2002). 1.2, 4.3.3

[51] D. A. W. Hutchinson and E. Zaremba. "Excitations of a Bose-condensed gas in anisotropic traps". *Phys. Rev. A* **57**, 1280 (Feb 1998). 1.2

[52] D. A. W. Hutchinson, E. Zaremba, and A. Griffin. "Finite Temperature Excitations of a Trapped Bose Gas". *Phys. Rev. Lett.* **78**, 1842 (Mar 1997). 1.2

[53] J. C. Inkson. *Many-Body Theory of Solids – An Introduction*. Plenum Press, 1984. 3.2.1

[54] A. D. Jackson, G. M. Kavoulakis, and C. J. Pethick. "Solitary waves in clouds of Bose-Einstein condensed atoms". *Phys. Rev. A* **58**, 2417 (Sep 1998). 4.2.1

[55] B. Jackson and E. Zaremba. "Transverse modes of a cigar-shaped Bose-Einstein condensate". *Preprint* `cond-mat/0208567` (2002). 3.7.1

[56] J. K. Jain. "Composite-fermion approach for the fractional quantum Hall effect". *Phys. Rev. Lett.* **63**, 199 (Jul 1989). 1.1

[57] J. K. Jain. "The Composite Fermion: A Quantum Particle and Its Quantum Fluids". *Physics Today* 39 (Apr 2000). Available at `http://chaos.ph.utexas.edu/~cmp/Jain.pdf`. 1.1

[58] D. S. Jin, M. R. Matthews, J. R. Ensher, C. E. Wieman, and E. A. Cornell. "Temperature-Dependent Damping and Frequency Shifts in Collective Excitations of a Dilute Bose-Einstein Condensate". *Phys. Rev. Lett.* **78**, 764 (Feb 1997). 3.4.3.1, 3.4.3.2

[59] S. Jochim, M. Bartenstein, A. Altmeyer, G. Hendl, S. Riedl, C. Chin, J. H. Denschlag, and R. Grimm. "Bose-Einstein Condensation of Molecules". *Science Express* **302**, 2101 (December 2003). 1

[60] Y. Kagan, E. L. Surkov, and G. V. Shlyapnikov. "Evolution of a Bose-condensed gas under variations of the confining potential". *Phys. Rev. A* **54**, R1753 (Sep 1996). 3.7.1

[61] B. Kastening. "Bose-Einstein condensation temperature of a homogenous weakly interacting Bose gas in variational perturbation theory through seven loops". *Phys. Rev. A* **69**, 043613 (Apr 2004). 7.3.2

[62] U. A. Khawaja, J. O. Andersen, N. P. Proukakis, and H. T. C. Stoof. "Erratum: Low-dimensional Bose gases [Phys. Rev. A **66**, 013615 (2002)]". *Phys. Rev. A* **66**, 059902 (2002). 3.4.3.2

[63] U. A. Khawaja, J. O. Andersen, N. P. Proukakis, and H. T. C. Stoof. "Low dimensional Bose gases". *Phys. Rev. A* **66**, 013615 (2002). 3.4.3.2, 5.2.5, 9

[64] U. A. Khawaja, N. P. Proukakis, J. O. Andersen, M. W. J. Romans, and H. T. C. Stoof. "Dimensional and temperature crossover in trapped Bose gases". *Phys. Rev. A* **68**, 043603 (2003). 3.4.3.2

[65] H. Kleinert. *Path Integrals in Quantum Mechanics, Statistics, Polymer Physics and Financial Markets*. World Scientific, Singapore, 2003. Available at `http://www.physik.fu-berlin.de/~kleinert/b3`. A

[66] E. B. Kolomeisky, T. J. Newman, J. P. Straley, and X. Qi. "Low-Dimensional Bose Liquids: Beyond the Gross-Pitaevskii Approximation". *Phys. Rev. Lett.* **85**, 1146 (Aug 2000). 1.2

[67] E. B. Kolomeisky and J. P. Straley. "Renormalization-group analysis of the ground-state properties of dilute Bose systems in d spatial dimensions". *Phys. Rev. B* **46**, 11749 (Nov 1992). 1.2

[68] J. M. Kosterlitz. "The critical properties of the two-dimensional xy model". *J. Phys. C: Solid State Phys.* **7**, 1046 (1974). 1.1, 7.4, 9

[69] J. M. Kosterlitz and D. J. Thouless. "Ordering, metastability and phase transitions in two-dimensional systems". *J. Phys. C: Solid State Phys.* **6**, 1181 (1973). 1.1, 7.4, 9

[70] L. D. Landau, E. M. Lifshitz, and L. P. Pitaevskii. *Statistical Physics – Part 2*. 2nd edition. Pergamon Press Ltd., 1980. 2.3, 5.3

[71] R. B. Laughlin. "Anomalous Quantum Hall Effect: An Incompressible Quantum Fluid with Fractionally Charged Excitations". *Phys. Rev. Lett.* **50**, 1395 (May 1983). 1.1

[72] M. D. Lee. *Interactions in Low-dimensional Bose-Einstein Condensates*. Ph.D. thesis, University of Oxford (Trinity Term 2002). 4, 4.3

[73] M. D. Lee, S. A. Morgan, M. J. Davis, and K. Burnett. "Energy-dependent scattering and the Gross-Pitaevskii equation in two-dimensional Bose-Einstein condensates". *Phys. Rev. A* **65**, 043617 (Apr 2002). 1.2, 4, 4.1, 2, 3, 4.2.1, 4.2.2, 4.2.2, 4.3, 4.3.1, 4.3.2.1, 4.3.2.1, 4.3.2.1, 4.3.2.3, 4.3.2.3, 8, 9

[74] F. London. "The λ-phenomenon of Liquid Helium and the Bose-Einstein Degeneracy". *Nature* **141**, 643 (Apr 1938). 1

[75] F. London. "On the Bose-Einstein Condensation". *Phys. Rev.* **54**, 947 (Dec 1938). 1

[76] G. D. Mahan. *Many-particle Physics*. 3rd edition. Kluwer Academics/Plenum Publishers, New York, 2000. 5.2.4, 5.2.4

[77] N. D. Mermin. "Crystalline Order in Two Dimensions". *Phys. Rev.* **176**, 250 (Dec 1968). 1.1

[78] N. D. Mermin and H. Wagner. "Absence of Ferromagnetism or Antiferromagnetism in One- or Two-Dimensional Isotropic Heisenberg Models". *Phys. Rev. Lett.* **17**, 1133 (Nov 1966). 1.1

[79] S. A. Morgan. *A Gapless Theory of Bose-Einstein condensation in Dilute Gases at Finite Temperature*. Ph.D. thesis, University of Oxford (Trinity Term 1999). 3.5, 4, 4.4.1, B.1

[80] S. A. Morgan. "A gapless theory of Bose-Einstein condensation in dilute gases at finite temperature". *J. Phys. B* **33**, 3847 (2000). 3.3, 3.4.1, 1, 2, 3.4.3.2, 3.4.3.2, 3.5, 4, B.1

[81] S. A. Morgan, M. D. Lee, and K. Burnett. "Off-shell T matrices in one, two and three dimensions". *Phys. Rev. A* **65**, 0220706 (January 2002). 4, 4.3, 4.3.1

[82] S. A. Morgan, M. Rusch, D. A. W. Hutchinson, and K. Burnett. "Quantitative Test of Thermal Field Theory for Bose-Einstein Condensates". *Phys. Rev. Lett.* **91**, 250403 (Dec 2003). 3.4.3.2, 7.3.3, 7.4, 8

[83] M. Naraschewski and R. J. Glauber. "Spatial coherence and density correlations of trapped Bose gases". *Phys. Rev. A* **59**, 4595 (June 1999). 1.2, 5.2.3

[84] P. Noziéres and D. Pines. *The Theory of Quantum Liquids, Vol. II Superfluid Bose Liquids*. Perseus Books, Cambridge, Massachusetts, 1999. 3.2.1, 3.4.4

[85] A. A. Penckwitt. *Computational Investigation of the Elementary Excitations of Bose-Einstein Condensates*. Master's thesis, University of Otago (1999). 3.2.1

[86] O. Penrose and L. Onsager. "Bose-Einstein Condensation and Liquid Helium". *Phys. Rev.* **104**, 576 (Nov 1956). 1.1, 5.2.4, 5.2.4, 5

[87] C. J. Pethick and H. Smith. *Bose-Einstein Condensation in Dilute Gases*. Cambridge University Press, 2002. 3.4.4, 25, 5.3, 7.3.3

[88] D. S. Petrov, M. Holzmann, and G. V. Shlyapnikov. "Bose-Einstein Condensation in Quasi-2D Trapped Gases". *Phys. Rev. Lett.* **84**, 2551 (Mar 2000). 1.2, 4.2.2, 5.1, 5.3, 5.3, 5.3, 5.4.1, 7.3.4.1, 9

[89] D. S. Petrov and G. V. Shlyapnikov. "Interatomic collisions in a tightly confined Bose gas". *Phys. Rev. A* **64**, 012706 (June 2001). 1.2, 2, 4.2.2, 4.3.2.3

[90] D. S. Petrov, G. V. Shlyapnikov, and J. T. M. Walraven. "Regimes of Quantum Degeneracy in Trapped 1D Gases". *Phys. Rev. Lett.* **85**, 3745 (Oct 2000). 1.2, 5.1, 5.3

[91] D. S. Petrov, G. V. Shlyapnikov, and J. T. M. Walraven. "Phase-Fluctuating 3D Bose-Einstein Condensates in Elongated Traps". *Phys. Rev. Lett.* **87**, 050404 (Jul 2001). 1.2, 5.1, 5.3, 5.4.1

[92] L. P. Pitaevskii. "Dynamics of collapse of a confined Bose gas". *Phys. Lett. A* **221**, 14 (1996). 3.7.1

[93] L. P. Pitaevskii and A. Rosch. "Breathing modes and hidden symmetry of trapped atoms in two dimensions". *Phys. Rev. A* **55**, R853 (Feb 1997). 3.7.1, 9

[94] V. N. Popov. *Functional Integrals in Quantum Field Theory and Statistical Physics*. D. Reidel Publishing Company, Holland, 1983. 1.1, 2.3, 5.3

[95] R. E. Prange and S. M. Girvin, editors. *The Quantum Hall Effect*. 2nd edition. Springer Verlag, 1990. 1.1

[96] W. H. Press, B. P. Flannery, S. A. Teukolsky, and W. T. Vetterling, editors. *Numerical Recipes in C : The Art of Scientific Computing*. 2nd edition. Cambridge University Press, 1993. 6.2, 2, 6.4.2

[97] N. P. Proukakis and K. Burnett. "Generalized Mean Fields for Trapped Atomic Bose-Einstein Condensates". *J. Res. Natl. Inst. Stand. Tech.* **101**, 457 (Jul 1996). 3.4.3.2

[98] N. P. Proukakis, S. A. Morgan, S. Choi, and K. Burnett. "Comparison of gapless mean-field theories for trapped Bose-Einstein condensates". *Phys. Rev. A* **58**, 2435 (1998). 1.2, 3.4.3.2, 4, 4.3.3, 7.3.3, 8.2, 9

[99] K. K. Rajagopal, P. Vignolo, and M. P. Tosi. "Density profile of a strictly two-dimensional Bose gas at finite temperature". *Physica B – Condensed Matter* **344**, 157 (Feb 2004). 1.2, 4.3.2.2, 8.3.2, 9

[100] J. Reidl. *Zur Theorie der Bose-Einstein Kondensation in Atomfallen*. Ph.D. thesis, Universität Gesamthochschule Essen (Februar 2002). Published by Shaker Verlag GmbH Aachen, Germany. 2

[101] J. Reidl, A. Csordás, R. Graham, and P. Szépfalusy. "Finite-temperature excitations of Bose gases in anisotropic traps". *Phys. Rev. A* **59**, 3816 (May 1999). 6.4.4

[102] S. Richard, F. Gerbier, J. H. Thywissen, M. Hugbart, P. Bouyer, and A. Aspect. "Momentum Spectroscopy of 1D Phase Fluctuations in Bose-Einstein Condensates". *Phys. Rev. Lett.* **91**, 010405 (Jul 2003). 1.2, 1.3, 5.4.1, 5.4.1, 7.3.4, 7.3.4.2

[103] J. E. Robinson. "Note on the Bose-Einstein Integral Functions". *Phys. Rev.* **83**, 678 (August 1951). A

[104] D. Rychtarik, B. Engeser, H.-C. Nägerl, and R. Grimm. "Two-dimensional Bose-Einstein condensate in an optical surface trap". *Phys. Rev. Lett.* **92**, 173003 (Apr 2004). 2, 3.7

[105] S. Schmidt. *Finite-Temperature Field Theory of Ultracold Gases*. Diplomarbeit, Freie Universität Berlin (2003). A

[106] T. F. Scott. *The Dynamics of Single and Multi-Component Bose-Einstein Condensates*. Ph.D. thesis, University of Otago (Jul 2000). 4.2.1, 2, 3

[107] R. A. Smith and N. K. Wilkin. "Exact eigenstates for repulsive bosons in two dimensions". *Phys. Rev. A* **62**, 061602(R) (Nov 2000). 1.1

[108] J. Stenger, S. Inouye, M. R. Andrews, H.-J. Miesner, D. M. Stamper-Kurn, and W. Ketterle. "Strongly Enhanced Inelastic Collisions in a Bose-Einstein Condensate near Feshbach Resonances". *Phys. Rev. Lett.* **82**, 2422 (Mar 1999). 4.2.2

[109] H. T. C. Stoof and M. Bijlsma. "Kosterlitz-Thouless transition in a dilute Bose gas". *Phys. Rev. E* **47**, 939 (1992). 1.1, 1.2, 4, 7.4, 9

[110] B. Tantar, A. Minguzzi, P. Vignolo, and M. P. Tosi. "Density profile of a Bose-Einstein condensate inside a pancake-shaped trap: observational consequences of the dimensional cross-over in the scattering properties". *Physics Letters A* **302**, 131 (Sep 2002). 1.2, 9

[111] J. R. Taylor. *Scattering Theory*. Wiley, New York, 1972. 4, 4.3, 4.3.1

[112] The MathWorks, Inc. *Optimization Toolbox User's Guide* (2002). Version 2. 6.2

[113] L. Tisza. "The λ-transition explained". *Nature* **141**, 913 (1938). 1

[114] S. M. M. Virtanen, T. P. Simula, and M. M. Salomaa. "Comparison of mean-field theories for vortices in trapped Bose-Einstein condensates". *J. Phys. Condens. Matter* **13**, L819 (2001). 3.4.3.2, 8.2

[115] N. K. Wilkin and J. M. F. Gunn. "Condensation of "Composite Bosons" in a Rotating BEC". *Phys. Rev. Lett.* **84**, 6 (Jan 2000). 1.1

[116] N. K. Wilkin, J. M. F. Gunn, and R. A. Smith. "Do Attractive Bosons Condense?" *Phys. Rev. Lett.* **80**, 2265 (Mar 1998). 1.1

[117] S. R. Wilkinson, C. F. Bharucha, K. W. Madison, Q. Niu, and M. G. Raizen. "Observation of Atomic Wannier-Stark Ladders in an Accelerating Optical Potential". *Phys. Rev. Lett.* **76**, 4512 (June 1996). 5.4.1

[118] C. N. Yang. "Concept of Off-Diagonal Long-Range Order and the Quantum Phases of Liquid He and of Superconductors". *Rev. Mod. Phys.* **34**, 694 (Oct 1962). 1.1, 5.2.4

[119] J. M. Ziman. *Elements of Advanced Quantum Theory*. Cambridge University Press, 1977. 3.2.1

[120] B. P. van Zyl. "Analytical expression for the first-order density matrix of a d-dimensional harmonically confined Fermi gas at finite temperature". *Phys. Rev. A* **68**, 033601 (Sep 2003). 7.3.4.1

[121] B. P. van Zyl, R. K. Bhaduri, A. Suzuki, and M. Brack. "Some exact results for a trapped quantum gas at finite temperature". *Phys. Rev. A* **67**, 023609 (Feb 2003). 7.3.4.1